# ADVANCES IN PET/CT IMAGING

## A TECHNOLOGISTS' GUIDE

Produced with the kind support of

SIEMENS Healthineers

# Table of contents

# Foreword

Positron emission tomography (PET) is one of the most promising areas of current medicine, considering the constant evolution of the technical equipment and the ongoing research into new and promising radiotracers for the study of human physiology and pathology. Since the advent of the hybrid imaging era, with computed tomography (CT) incorporated into the PET scanner, PET imaging has undergone a great evolution in terms of improved image quality and, consequently, better clinical output.

Nuclear medicine technologists are the professionals when it comes to the imaging process.

Acting as the link between the sciences that are the backbone of PET/CT imaging and the patient, we combine the necessary theoretical background with practical skills under the principle of best practice. To this end, an updated publication documenting the advances in this imaging technique is of major importance in order to ensure that everyone is working at the same level.

Following on from last year's edition of the Technologists' Guide, which addressed the topic of hybrid imaging in conventional nuclear medicine, the European Association of Nuclear Medicine's Technologist Committee (EANM-TC) has kept this year's focus on hybrid imaging. This time, however, we have embarked on the topic of PET-CT imaging, inviting specialists in each specific area to write about the advances in their field.

I should like to express my tremendous gratitude to all the authors who contributed their time and expertise to this project. A special thank you goes to the Physics Committee of the EANM, who have supported us throughout and made a valuable contribution to this Guide. I also gratefully acknowledge the valuable content provided by our overseas colleagues from the Society of Nuclear Medicine and Molecular Imaging – Technologist Section (SNMMI-TS). A special word of appreciation goes to the editorial team who have dedicated their time to this publication: Agata, Luca, Christelle and David – thank you! and also to Angela Parker for her editing, reviewing and support. Last but not least, I thank the EANM Board and Executive Office for their tireless efforts, which have made this series of publications possible. ***Advances in PET/CT Imaging*** was only possible thanks to the contributions of everyone mentioned above. My most sincere thanks to you all!

*Andrea Santos*
*Chair, EANM Technologists Committee*

# Introduction

Every year, the Technologists Committee publishes a Technologists' Guide to develop and improve the nuclear medicine specialists' knowledge and personal skills in various aspects of nuclear medicine. This year, together with an interdisciplinary group of specialists, we decided to address the topic of "Advances in PET/CT Imaging", outlining recent advancements in radioisotope imaging with a special emphasis on PET/CT techniques.

PET/CT study allows us to evaluate the aetiology of various diseases, and has therefore become an essential element of diagnostic management. The rapidly evolving technology of medical imaging is permitting the constant improvement of existing solutions while simultaneously eliminating the method's limitations. ***Advances in PET/CT Imaging*** aims to provide a technical and clinical overview of PET/CT principles and applications, highlighting recent innovations and the latest solutions that are improving technical and clinical study outcomes.

This extensive guide encompassing ten chapters provides the reader with a wide range of information: from hardware and software updates, PET/CT artefacts and pitfalls through radiopharmaceutical advancements to the latest solutions in oncology and the definition and applications of radiomics. The contents guide readers through the long list of specific PET/CT characteristics, advantages, utilities and applications, not forgetting the method's limitations and ways of avoiding their impact on the eventual PET/CT dataset.

We believe that hybrid imaging is not only a set of techniques and properties, but also and especially the interdisciplinary and qualified medical team, who have a significant influence on diagnostic management. The complexity of PET/CT study means that the technician's extensive knowledge and experience is vital to the success of the process. We hope that this latest edition of the Technologists' Guide will be of benefit in helping our readers update their personal skillsets.

*David Bogović, Luca Camoni, Christelle Terwinghe & Agata Pietrzak*

*Editorial team*

# 1

# HARDWARE UPDATES

*by Igor Iskra*

Positron emission tomography (PET) enables us to visualise molecular processes in the human body. Certain positron-emitting radionuclides interact with specific molecular pathways, thus giving us the opportunity of imaging physiological or pathophysiological occurrences. PET scanners use the principle of coincidence detection of annihilation photons, a method in which two photons emerging from the same annihilation process are detected on opposite sides of a detector system. Of course, like every diagnostic method, PET imaging has its own limitations and pitfalls, scattering and attenuation of photons by the tissue being the two most prominent ones. [1 2]

Coupling a PET scanner with a CT scanner is an efficient way to correct most of the imperfections of PET imaging. "Low-dose" CT can greatly improve the ability to obtain an exact anatomical localisation of pathophysiological processes in the patient. Furthermore, the correlation between the intensity of focal accumulation of radionuclide determined by the PET scanner and the degree of morphological changes ascertained by the CT scanner is important in evaluating the pathological potential of certain focal changes. Lastly, "low-dose" CT is an irreplaceable tool for correcting the attenuation of annihilation photons by the tissue. [3]

## HISTORICAL DEVELOPMENT OF PET-CT SCANNERS

Since the advent of the first PET scanners, the main developmental goals have been to improve the sensitivity and spatio-temporal resolution and to reduce the patient's exposure to radiation. The idea of using coincidence detection of positron capture was born in the early 1950s. In 1953 a first paper was published on the application of coincidence detection for localising brain tumours, describing a pair of sodium iodide detectors placed on opposite sides of the head. Then, in 1961, a ring of 32 sodium iodide-based coincidence detectors was developed and several other designs for coincidence detectors emerged in the subsequent years. [4]

The first developmental breakthrough came in the early 1970s, with the first positron camera. Its unique design enabled smaller sodium iodide crystals to be coupled with fewer and larger photomultipliers, which resulted in reduced costs and improved spatial resolution. Shortly after that, the idea of a rotating positron camera emerged, producing multiple plain images which were later back-projected onto tomographic images. In every projection a transmission image was obtained using an external source of $^{68}$Ga and enabling attenuation correction. In 1974, to reduce unwanted scattering effect, a hexagonal array of sodium iodide scintillation detectors was designed. This system was heavily shielded with the assembly rotating around a transaxial plane, hence being known as positron emission transaxial tomography (PETT). This led to a commercial version of this design, known as the ECAT I (ECAT = emission computerised axial tomograph).[4 5]

The next step towards the modern PET-CT scanner was a configuration with multi-ring geometry. This new design allowed better usage of scanners for PET quantification, but it also created some new problems, mainly by reducing the spatial resolution. First, there was the problem of size and spacing between the detector elements. Another disadvantage was the expensive and physically limiting "one-to-one" coupling between the scintillation crystal and the photodetector. Lastly, the original designs included lead or tungsten shields between the detector rings, which severely reduced the overall sensitivity. Nevertheless, the solutions to these problems yielded new designs which laid the foundations for modern PET-CT scanners. [1 4]

The problem of ineffective coupling between the crystal and detector elements was overcome by introducing the block detector concept. In this concept, an array of crystal elements was coupled with four photomultiplier tubes (PMTs). The light produced in every scintillation event, caused by the interaction between the annihilation photon and the crystal element, was shared among all four photomultiplier tubes. The information from the detector thus contained the coordinates of the scintillating element, determined from the light distribution, and the energy of the incoming photon, determined from the total amount of produced light. [1 4]

Another problem in need of solving was the small acceptance angle for coincidence photon detection due to the presence of the septa (2D mode). Retracting or totally removing the septa established a 3D mode of acquisition, improving sensitivity and enabling true 3D reconstructions. The problem with the 3D mode was an increased scatter fraction (35% or even more), but several scatter correction models were subsequently developed to compensate for this. [1]

The last and most important step towards modern PET-CT scanners was the introduction of the CT scanner itself. In the early days, a PET scanner was often equipped with some additional source of transmission scanning for the purpose of attenuation correction, as well as for regular detector checks. $^{68}$Ge and $^{137}$Cs were the main radionuclides used. As mentioned before, the introduction of CT scanners in PET acquisition not only enabled better

attenuation correction, but also paved the way for other advanced features. A main pitfall of the early CT scanners used in PET-CT acquisition was high radiation exposure, which was later remedied by the advent of modern iterative reconstruction techniques.[4 5 6]

## MODERN PET-CT SCANNERS

Although there are many specific scanner designs, every PET scanner basically consists of three main parts: scintillation detectors, photodetectors and a computer. PET detectors are based on a process called scintillation in which high-energy photons interact with scintillating crystals, creating a new electron either by Compton scatter or by photoelectric absorption. This new electron loses its energy by passing through scintillation material and exciting new electrons.[7]

The excited electrons subsequently return to their original energy state by releasing electromagnetic radiation in the form of light. This light is registered by photodetectors and transformed into an electrical signal with the specific energy and coordinates of the incident photon. All the signals are then processed by the computer, creating a final image.[1 7]

### Scintillation crystals

Scintillation crystals are the most vital part of any detector. Every scintillation material has four main characteristics: stopping power for 511 keV photons, decay constant, light output and energy resolution.

Stopping power is described as the inverse of the mean distance travelled by photons before they deposit energy in the crystal, and it is proportional to the density and effective atomic number of the material. Higher stopping power means that the electron will travel a shorter distance in a material because it will interact more often with atoms in the material, therefore indirectly enabling more effective detection of incident photons.

The decay constant is determined by the duration of the scintillation flash in the crystal. A shorter decay constant means that the scintillation material will be able to produce more individual scintillation flashes in a certain period of time, thus allowing more incident photons to be counted.

Light output can simply be described as the yield of scintillation photons produced by the incident photon. Higher light output means that the incident photon will trigger the creation of more scintillation photons, thus increasing spatial and energy resolution.

Finally, energy resolution is the ability to accurately determine the energy of the interacting photons. It depends on energy variance, which is the ratio between the range of possible values of photon energy determined by the detector and the real energy of the photons. Higher energy resolution means that the energy variance is smaller, therefore photons whose energy is different from that of the incident photons, i.e. Compton-scattered photons, will be less often detected.[1 7 8]

Sodium iodide (NaI) was the first scintillator used in PET scanners. It is cheap and has the highest light output, but it has very low effective density and a very long decay constant, so is no longer used today.

Bismuth germinate (BGO) was the main scintillator used in PET scanners throughout the 1980s and 1990s. It has the highest known effective density of all scintillators, but its low light output and long decay constant became a problem with the widespread adoption of 3D acquisition mode. This resulted in a quest to find new scintillators with a shorter decay constant, better light output and improved energy resolution.

Then came lutetium oxyorthosilicate (LSO), a component originally used for nuclear well logging. It has a high light output and high efficient density, but its main advantage is a very short decay constant. LSO's superior time resolution has given PET scanners the ability to measure the time difference between the arrivals of the two annihilation photons. This is called "time of flight" (TOF), and it provides otherwise unavailable positioning information which enables us to determine an annihilation point to within a few centimetres. Lutetium yttrium orthosilicate (LYSO), a derivate of LSO with a small percentage of yttrium, is currently being used in the newest TOF-PET scanners since it has slightly better light output and energy resolution compared to LSO.

Instead of using LSO, some manufacturers opted to replace BSO with gadolinium orthosilicate (GSO), the main advantage of which is better energy resolution. Other materials such as lanthanum (III) bromide (LaBr3) or LuAP (lutetium aluminium perovskite, $LuAlO_3$:Ce) are currently being evaluated as possible new scintillators in PET scanners.[1 4 7 9]

### Block detectors

As mentioned before, a block detector setup was one of the major breakthroughs in the development of modern PET scanners. Instead of using "one-to-one" coupling between scintillators and photodetectors, this concept proposed using a block of scintillation crystals divided into an array of single-functioning smaller elements, a few millimetres in size. This was achieved by mechanical incision of channels in the primary crystal block, with channels being filled with opaque material. This opaque material prevents so-called "cross-talk", i.e. a scatter of light between the elements. A block is then usually coupled with four photomultiplier tubes. The sharing of light between the PMTs is converted to their relative signal output, which is then

used to determine the crystal element involved in interaction with the photon. There are also improved versions of block detectors constructed from two different scintillation materials with different decay constants (photoswitch), enabling better determination of the depth of photon interaction with the detector material. [4 7]

### Photodetectors

Photomultiplier tubes were the most commonly used photodetectors in PET scanners. PMTs are glass-enveloped vacuum tubes with three main parts: a photocathode, dynodes and an anode. Their functioning is based on the photoelectric effect, in which an emission of electrons is caused by interaction of light with photoelectric material. In PMTs, the photoelectric component is called the photocathode. When electrons are emitted from the photocathode, induced by scintillation photons, they are pulled towards the anode by the electric potential generated. On their way to the anode, electrons collide with the dynodes, creating secondary electron emissions from the collision. The resulting electrical current is proportional to the number of initial scintillation photons, and is translated into an electrical signal. PMTs are therefore considered as analogue photodetectors, their main advantage being their lower sensitivity to temperature variations. [1 10]

The development of modern solid-state detectors started in the 1990s with analogue versions called avalanche photodiodes (APDs) and silicon photomultipliers (SiPMs). APDs, working in Geiger mode, are generally not considered an effective choice for TOF-PET scanners due to their significantly slower response time. Analogue SiPMs use single photon avalanche diode (SPAD) arrays to detect single scintillation photons, subsequently turning all the generated pulses into one analogue output signal. Like APDs, SiPMs initially didn't have TOF capability.[10 11]

In recent years a new group of solid-state detectors has emerged, called digital photon counters (DPCs). In this version of detectors, every detector module consists of a 4 x 5 array of SiPM detector tiles, additionally divided into a 4 × 4 matrix of silicon sensor chips. Each chip is a 2 × 2 matrix of digital photon counter detectors called silicon pixels. In every pixel there are 3200 SPADs or microcells, with every microcell functioning as an individual detector. The total count of all photon–microcell interactions detected in a certain interval of time, initiated by the arrival of the very first scintillation photon, is translated into a digital number proportional to the energy of the photon that induced the scintillation event. PET scanners equipped with DPCs show better image quality, improved lesion detectability, and are reported to perform faster acquisitions with lower radiation exposure.[11]

The main advantage of SiPMs is their exceptional light collection capability, which is due to their compact structure. Unlike the circular shape of PMTs, which was responsible for the significant gaps between them, SiMPs are square in shape, which allows them to be packed more tightly together. SiPMs mainly use "one-to-one" coupling to crystals, which provides a much higher count rate capability and improved spatial resolution.[9]

### PET-CT scanner geometry

Most of the modern PET scanners have "full-ring" geometry, with their detectors covering a full 360° around the patient. This setup provides optimum sensitivity, fewer image artefacts due to tracer, organ or patient motion, and excludes the need for additional calibrations since there are no moving components.[5]

Additionally, there are three different types of detector surface structure. The first type is the common block detector concept, in which there is a cylindrical assembly of crystal blocks in a ring structure several blocks deep. The second option is a curved crystal structure, in which 6 bigger blocks of NaI crystals, coupled with 48 PMTs each, are placed side by side to achieve ring geometry. Finally, there is the PIXELAR module, consisting of a curved matrix made up of 628 (22 x 29) GSO crystals attached to a continuous light guide, in which ring geometry is achieved by placing 28 of these modules side by side and coupling them with 420 PMTs.[12]in terms of physical performance and technical features. Particular attention has been given to evaluate the whole-body performance by sensitivity, spatial resolution, dead time, noise equivalent counting rate (NECR

An alternative type of scanner geometry is the "partial-ring" setup, in which two opposing matrices of crystal blocks rotate around the patient. They are not perfectly opposed, thus achieving a better transversal field of view during the rotation, but their general sensitivity is lower compared to "full-ring" scanners. [12]in terms of physical performance and technical features. Particular attention has been given to evaluate the whole-body performance by sensitivity, spatial resolution, dead time, noise equivalent counting rate (NECR

Axially, PET scanners today consist of 2 to 5 rings of detector elements, compared to several dozen in the earlier days. These rings can be separated by thin annular rings or septa made of photon-absorbing material like tungsten and used for collimation. The presence or absence of septa determines the type of acquisition. If septa are present, then so-called "2D acquisition" is performed, since the septa shield "out of plane" coincidence photons. Since the septa block a fairly large number of true coincidences from ever reaching the detector, this type of acquisition is characterised by reduced scattered and random coincidences, but it also has lower

sensitivity. Another type of acquisition is so-called "full 3D acquisition", performed with or without retracted septa. In this situation coincidences are accepted from all angles, thus providing higher sensitivity. However, that also implies an increase in random coincidences, higher scatter fraction and loss of events due to an increased count rate, and subsequently increased dead time. It is worth mentioning that today's commercial PET scanners are not equipped with septa and thus acquire data in this second acquisition mode. [14] [12]in terms of physical performance and technical features. Particular attention has been given to evaluate the whole-body performance by sensitivity, spatial resolution, dead time, noise equivalent counting rate (NECR).

### PET-CT coupling

The first PET-CT scanner prototype emerged in 1998. The PET scanner was placed on the rear end of the CT scanner, creating a single integrated assembly. The scanners rotated together at 30 rpm and the patient bed could be moved axially from the CT to the PET scanner so the corresponding images were accurately registered. However, the acquisition, reconstruction and operating systems were separate and image fusion was performed by software. [5]

Nowadays, PET and CT scanners are coupled through hardware fusion. The characteristics of scanners vary depending on the vendor, although the basic elements of design are largely similar. PET scanners have "full-ring" geometry and are integrated with CT scanners in a single device. The patient is positioned only once and the scans are acquired in close sequence, enabling improved registration accuracy and a single integrated scan. [4] [5]

### Additional hardware for PET-CT studies

FDG PET-CT has an important role in evaluation of pulmonary lesions and detection of occult intrathoracic metastases. In contrast to CT, which covers only a part of one breathing cycle, PET acquisition lasts substantially longer through multiple breathing cycles. Respiratory motion can thus cause a lot of motion and attenuation correction artefacts on PET images. To eliminate this negative effect, respiratory gating is performed. In this process, data collected in each respiratory cycle is divided into "bins", either by detecting a certain respiratory amplitude (amplitude-based gating) or a phase of the respiratory cycle (phase-based gating).

Gating is usually performed using external sensors which track respiratory motion. This can be accomplished in several ways:

- by monitoring the displacement of the abdominal wall using an elastic chest belt;
- by monitoring the displacement of two infrared markers positioned on the patient's thorax;
- by measuring the changes in air temperature during respiration, either with a sensor placed inside an oxygenation mask or with a sensor placed close to the patient's nostrils: this mode of respiratory gating uses the fact that the air is warmer during exhalation;
- by using a spirometer placed close to the patient's nostrils or mouth: this mode of respiratory gating has not yet been used in clinical practice.

It is worth mentioning that nowadays, in view of the significant practical limitations of hardware-based respiratory gating, the emphasis is on software gating, Bayesian penalised likelihood (BPL) PET reconstruction, and texture analysis. [13] [14]follow-up, and treatment planning. For cancers located in the thorax or abdomen, the patient's breathing causes artifacts and errors in PET and CT images. Many different approaches for artifact avoidance or correction have been developed; most are based on gated acquisition and synchronization between the respiratory signal and PET acquisition. The respiratory signal is usually produced by an external sensor that tracks a physiological characteristic related to the patient's breathing. Respiratory gating is a compensation technique in which time or amplitude binning is used to exclude the motion in reconstructed PET images. Although this technique is performed in routine clinical practice, it fails to adequately correct for respiratory motion because each gate can mix several tissue positions. Researchers have suggested either selecting PET events from gated acquisitions or performing several PET acquisitions (corresponding to a breath-hold CT position

Cardiac PET-CT scanners also use an external ECG device for gating and detecting certain phases of the cardiac cycle, in the same way as in gSPECT.

## CT SCANNER IMPROVEMENTS

Over the years, the two main goals of CT scanner development have been better image resolution and lower radiation exposure to the patient. Alongside better software solutions and image reconstruction algorithms, upgrades in hardware have been the main drivers of CT scanner improvement. Nowadays, PET-CT systems are equipped with up to 128-slice CT scanners, compared to the 16-slice scanners in use as little as 15 years ago. [4] [5] [15]

One other important area of improvement is the development of new acquisition modes. Conventional PET-CT studies are performed in so-called "step-and-shoot" mode, in which the patient bed is moved between every step of image acquisition outside the initial axial FOV range. An alternative mode is "continuous table motion" mode, in which the patient table moves continuously throughout the whole scanning process. Data is acquired uninterruptedly while the patient is being

moved through the gantry, resulting in increased uniformity and sensitivity of acquisition. [16]

## FUTURE INNOVATIONS

Improved ratio of deposited energy to light output of scintillators. Current Lu-based scintillation crystals have a somewhat non-linear light output in response to the energy deposited by the interacting photon. In particular, this light yield ratio decreases with decreasing energy of photons. LuAP (lutetium aluminium perovskite, LuAlO3) and LuYAP (lutetium-yttrium aluminium perovskite) scintillator crystals have a superior light yield ratio and hence superior energy resolution. [9]

Semiconductor detectors. These non-scintillating detectors use dense crystals which are capable of directly absorbing the interacting photon energy and converting it into electrical charge detected by previously placed electrodes. The materials used in these detectors are CdZnTe (CZT) and TlBr. [9]

Using Cherenkov light to improve time resolution. Cherenkov light is produced instantaneously when a 511 keV photon interacts with detector material, emitting a small number of transient, high-energy, faster-than-light electrons. Lead-based crystals, such as PbF2, show an excellent time resolution of 70–90 ps. Also, it seems that BGO scintillators could be used effectively for this type of detection. [9]

Monolithic detector. One thin block of crystal coupled with multiple photodetectors can improve light transduction because of the larger crystal volume and absence of inter-crystal boundaries. [9]

## EXPLORER – A WHOLE-BODY PET-CT SCANNER

Current PET-CT scanners only capture a small portion of the patient's body inside the field of view (FOV). What is more, only 3–5% of the available signal is detected by scanners. These are the two main reasons for the poor sensitivity of current whole-body PET-CT scanners.

EXPLORER is a PET-CT scanner prototype which can perform a whole-body PET scan up to 40 times better than the currently available scanners. It has 40 rings and is able to scan the whole body within 30 seconds. Its 564,480 LYSO crystals, 2.76 x 2.76 x 18.1 mm each, are arranged in 7 x 6 arrays and coupled with SiPM. This PET scanner has a diameter of 78.6 cm and an axial length of 194 cm. EXPLORER is also equipped with an 80-row, 160-slice CT scanner.

This setup allows EXPLORER to significantly increase acquisition sensitivity in whole-body scans and to produce more reliable images along with rapid scanning and lower radiation exposure. However, its main disadvantages are expensive components and ambiguities regarding the indications for whole-body scans, which are still unclear. [17 18]

## CONCLUSION

Modern PET-CT scanners are currently undergoing rapid development. New designs and software improvements are aimed at ensuring better image resolution with lower radiation exposure to the patient. New detector technologies using digital photon counters are set to significantly improve the acquisition process, enabling faster and more reliable diagnostics.

| PET-CT SCANNER | EXPLORER | VEREOS (PHILLIPS HEALTH-CARE) | BIOGRAPH VISION 600 (SIEMENS HEALTHINEERS) | DISCOVERY MI (GE HEALTHCARE) |
|---|---|---|---|---|
| crystals | LYSO | LYSO | LSO | LYSO |
| crystal size | 2.76 x 2.76 x 18.1 $mm^3$ | 3.86 × 3.86 × 19 $mm^3$ | 3.2 x 3.2 x 20 $mm^3$ | 3.95 × 5.3 × 25 $mm^3$ |
| photon detectors | SiPM | SiPM | SiPM | SiPM |
| number of crystals | 564 480 | 23 040 | 60 800 | 19 584 |
| number of detectors | 53 760 | 23 040 | 304 | 9 792 |
| CT slices | 160 | 128 | 128 | 128 |

*Table 1. Comparison of some of the currently available PET-CT scanners [11 17 19 20 21]*

## REFERENCES


1. Schmitz RE, Alessio AM, Kinahan PE. 1 The Physics of PET/CT Scanners. ***PET PET/CT***. Published online 2019:1-16. doi:10.1055/b-0039-166611
2. Shukla AK, Kumat U. Positron emission tomography: An overview. ***J Med Phys***. 2006;31(1):13-21.
3. Vaquero JJ, Kinahan P. Positron Emission Tomography: Current Challenges and Opportunities for Technological Advances in Clinical and Preclinical Imaging Systems. ***Annu Rev Biomed Eng***. 2015;17:385-414.
4. Jones T, Townsend D. History and future technical innovation in positron emission tomography. ***J Med Imaging***. 2017;4(1):011013. doi:10.1117/1.jmi.4.1.011013
5. Townsend DW, Carney JPJ, Yap JT, Hall NC. PET / CT Today and Tomorrow. 2019;45(1):4-15.
6. Alessio AM, Kinahan PE, Cheng PM, Vesselle H, Karp JS. PET/CT scanner instrumentation, challenges, and solutions. ***Radiol Clin North Am***. 2004;42(6):1017-1032. doi:10.1016/j.rcl.2004.08.001
7. Authors G of. ***PET/CT- Klinička Primjena***. Markulin d.o.o.; 2015.
8. Kapoor V, McCook BM, Torok FS. An Introduction to PET-CT Imaging. ***RadioGraphics***. 2004;24:523-543.
9. Berg E, Cherry SR. Innovations in instrumentation for positron emission tomography. ***Semin Nucl Med***. 2018;48(4):311-331.
10. Spanoudaki VC, Levin CS. Photo-Detectors for Time of Flight Positron Emission Tomography (ToF-PET). ***Sensors***. 2010;10:10484-10505.
11. Zhang J, Maniawski P, Knopp M V. Performance evaluation of the next generation solid-state digital photon counting PET/CT system. ***EJNMMI Res***. 2018;8(97).
12. Tarantola G, Zito F, Gerundini P. PET Instrumentation and Reconstruction Algorithms in Whole-Body Applications Continuing Education. ***J Nucl Med***. 2003;44(5):756-769. http://www.snm.org/education/ce_online.html
13. Frood R, McDermott G, Scarsbrook A. Respiratory-gated PET/CT for pulmonary lesion characterisation—promises and problems. ***Br J Radiol***. 2018;91.
14. Pépin A, Daouk J, Bailly P, Hapdey S, Meyer ME. Management of respiratory motion in PET/computed tomography: The state of the art. ***Nucl Med Commun***. 2014;35(2):113-122. doi:10.1097/MNM.0000000000000048
15. Mccollough CH, Chen GH, Kalender W, et al. Achieving routine submillisievert CT Scanning : Report from the Summit on Management of Radiation Dose. ***Radiology***. 2012;264(2):567-580.
16. Rausch I, Cal-gonzález J, Dapra D, et al. Performance evaluation of the Biograph mCT Flow PET / CT system according to the NEMA NU2-2012 standard. ***EJNMMI Phys***. 2015;2(26). doi:10.1186/s40658-015-0132-1
17. Cherry SR, Jones T, Karp JS, Qi J, Moses WW, Badawi RD. Total-Body PET: Maximizing Sensitivity to Create New Opportunities for Clinical Research and Patient Care. ***J Nucl Med***. 2018;59(1):3-12. doi:10.2967/jnumed.116.184028
18. EXPLORER PET-CT scanner: a total body experience. Accessed March 5, 2021. https://openmedscience.com/explorer-pet-ct-scanner-a-total-body-experience/#:~:text=EXPLORER PET%2FCT scanner design and features,-Design&text=The EXPLORER combines positron emission,images with high temporal resolution.&text=40 Rings are present in,inclu
19. Oddstig J, Leide Svegborn S, Almquist H, et al. Comparison of conventional and Si-photomultiplier-based PET systems for image quality and diagnostic performance. ***BMC Med Imaging***. 2019;19(1):1-9. doi:10.1186/s12880-019-0377-6
20. No Title. Accessed March 10, 2021. https://www.philips.co.uk/c-dam/b2bhc/gb/resource-catalog/landing/brightontender/vereos-petct-product-specification-lr.pdf
21. No Title. Accessed March 10, 2021. https://www.siemens-healthineers.com/en-us/molecular-imaging/pet-ct/biograph-vision

# 2

# UPDATES IN RECONSTRUCTION ALGORITHMS

*by Dimitris Visvikis*
*Michel Koole*
*Ian Armstrong*
*Christian Vanhove*

Image reconstruction generates a volume of image data that reflects the distribution and quantities of the injected radiopharmaceutical within the patient. A reconstructed image typically consists of a 3-dimensional array of discrete elements referred to as voxels. When all appropriate corrections have been applied, the value for each voxel typically indicates the radioactive concentration of the radiopharmaceutical within this voxel volume in units of Bq/ml. Since reconstruction starts from the raw or acquired PET data, a short overview of the process for PET data acquisition is given below.

## PET DATA ACQUISITION

For PET imaging, positron-emitting radioisotopes are required. When the positron is emitted, it travels for a few millimetres through the body until it interacts with a free electron, resulting in an annihilation event which produces two back-to-back gamma photons with energy of 511 keV each. These photons are emitted in almost opposite directions, defining a line along which the annihilation event must have occurred. Since PET is based on the coincident detection of these two opposite gamma photons along this line of response (LOR), a pair of detectors is needed. Clinical PET systems use a full ring of detectors surrounding the patient, which also explains the superior sensitivity of PET. If the two back-to-back gamma photons are detected within a certain short time window (typically 4 ns depending on the PET system settings), it is assumed that they originate from the same annihilation event. These coincidence events are stored in a matrix which represents the number of detected events along different angles of a transaxial section through the patient. This matrix is called a sinogram, since all LORs passing through a point at different angles correspond to a sinusoid curve. This also explains the term sinogram. However, before the detected events are stored in a sinogram, coincidence events can also be stored in a list as individual events in the order in which they are detected (1). This is called list mode, but it should be noted that list-mode acquisition is not always available on the PET system, or it needs to be deliberately selected as the acquisition mode. List-mode acquisition provides more flexibility, however, as additional information such as photon energy, detection timing and detection location can be stored as well (2). Based on this information, list-mode data can then be used to generate sinograms. In addition, list-mode data also allow for retrospective rebinning of dynamic raw PET data into sinograms corresponding to different time frames, where the frame duration can be chosen after data acquisition is completed.

Once generated, sinogram data are used to reconstruct the 3D distribution of the PET tracer in the body of the patient.

## TIME OF FLIGHT (TOF)

In TOF-PET the difference in time between the coincidence photons' arrival is measured and stored. For list-mode acquisition the time difference (Δt) is stored event by event, while in sinogram mode the sinogram is divided into several TOF-bins, each corresponding to a time difference. In conventional PET image reconstruction, the probability of an annihilation event is constant along the LOR (see Figure 1a), while in TOF-PET it depends on the time difference between the arrival of two coincidence photons, as well as detector characteristics, and it is applied as a Gaussian distribution on the LOR (see Figure 1b). The centre of this Gaussian distribution along the LOR is the length equivalent of the time difference between the arrival of the two coincidence photons, computed as $s = c \cdot \Delta t$, with c representing the speed of light. The full width at half maximum (FWHM) of the Gaussian distribution is related to the time resolution of the detector.

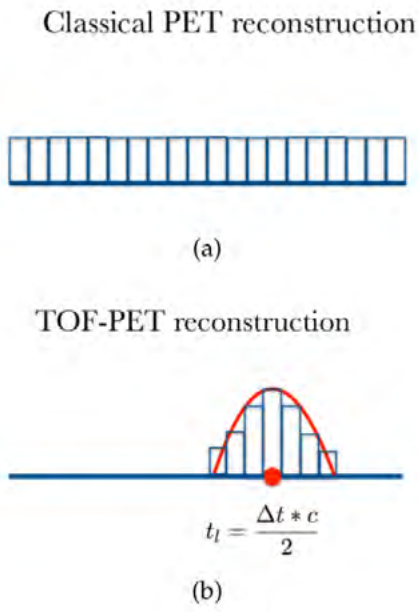


*Figure 1: Probability distributions during (a). conventional image reconstruction, (b). TOF-PET image reconstruction*

## RECONSTRUCTION

After acquisition of PET data, the next step is to reconstruct an estimate of the ***in vivo*** tracer distribution. There are different approaches to reconstruct the PET data. On the one hand, there is an analytical approach with filtered back-projection (FBP), which consists in back- projecting the sinogram data across the imaging matrix. However, simple back-projection of the measured data results in a blurred version of the original image. The blurring is minimised by applying a filter to sinogram data before back-projection to amplify the high frequencies representing fast-varying intensity changes such as edges, hence the name filtered back-projection. Although FBP is a very fast technique with limited memory requirements, it does not take into account the statistical nature of radioactive decay, nor does it make allowance for the characteristics of the PET system (3).

For these reasons, along with the general increase in memory and computation power, FBP is no longer the reconstruction technique of choice, and iterative methods represent the current state of the art in clinical PET reconstruction. The most widely-used iterative reconstruction algorithm is maximum likelihood expectation maximisation (MLEM) (4). The principle behind MLEM is to estimate the activity distribution that would most likely produce the sinograms that have been acquired by the PET system. As such, it takes into account the Poisson statistics of radioactive decay and the statistical nature of the measurement process. Since this approach is iterative, it starts from an initial estimate and updates the previous estimate of the reconstructed image until the new estimate is very close the previous one, meaning that the reconstruction is no longer improved and convergence is reached. To update the previous estimate, iterative reconstruction utilises a probability matrix, commonly referred to as the system matrix. This matrix defines the probability that a 511 keV gamma-ray pair originating from a particular voxel location within the reconstructed image would give rise to a particular line of response in a sinogram. An initial estimate of the reconstructed image is created and, from here, estimated sinograms are generated from the system matrix values – a process referred to as forward projection. These estimated sinograms are compared with the acquired sinograms and a ratio is calculated at each sinogram pixel. The ratios are then transposed back into the reconstructed image – a process referred to as back-projection – and the estimate of the reconstructed image is updated. This process repeats in a series of loops referred to as iterations, and the estimate of the activity distribution in the reconstruction image converges until it represents the real activity distribution within the patient. In MLEM, the number of updates also corresponds to the number of iterations.







An accelerated variant of MLEM, ordered subsets expectation maximisation (OSEM) (5), is currently the most commonly used iterative reconstruction algorithm in PET clinical imaging. OSEM accelerates the convergence of MLEM by performing updates based on part of the measured data only, so that it approximates the MLEM solution but in a much shorter computation time and with less memory requirement. This technique divides the measured PET data into several subsets, following a specific order. During reconstruction, each update is based on the projection data belonging to a specific subset only, while a different subset is selected for the next update. This accelerated convergence using subsets allows the OSEM algorithm to generate PET images in clinically relevant times (6). Unlike MLEM, where one iteration corresponds to one update, one OSEM iteration corresponds to a cycle in which all subsets have been used to update the reconstruction. In OSEM, the number of updates therefore corresponds to the number of iterations multiplied by the number of subsets.

The system matrix is the critical component in iterative reconstruction, as this is where most of the physical aspects of the PET measurement are modelled. This includes modelling of the geometric efficiency of the PET detector, the position-dependent spatial resolution, the calibration factor used to convert a measured count rate to activity concentration, and the attenuation and time-of-flight differences of the two 511 keV gamma rays. The exceptions are corrections for scattered and random coincidences; these are typically added on to the estimated sinograms that are generated using the forward projection.

Since accurate modelling of the PET system response during iterative reconstruction results in a reconstructed PET image with much better quantitative properties and homogeneous resolution, iterative reconstruction provides clear advantages over the older method of FBP reconstruction. However, it is not without disadvantages. Due to computational limitations, the system matrix is unlikely to perfectly model the system response for the forward and back projection operations. This may place data in erroneous locations, which manifests as noise. What is more, PET measurements are generally very noisy. This in combination with the discrete spatial sampling of both sinograms and the reconstructed image volume means that the process is ill-conditioned, the main consequence being that the noise in the reconstructed image increases as more iterations are performed. Noise in an image that is fully converged will be so significant that the image is unlikely to be of any clinical use.

There are three mitigating strategies to reduce noise in reconstructed images. The first strategy is to stop the reconstruction

process before convergence in order to prevent excessive image noise amplification. Although the degree of noise is kept to an acceptable level, this approach can produce an image with reduced quantitative properties as convergence is not fully reached and not all necessary corrections are fully applied. The second approach is to perform a sufficient number of updates to ensure that the full image is close to convergence and all appropriate corrections have been applied. A filter is then applied to the reconstructed PET image to reduce the noise levels (7). A Gaussian full width half maximum (FWHM) filter is generally used for this purpose. The FWHM determines how many neighbouring voxels are used to calculate the smoothed image, so that a larger FWHM corresponds to a higher degree of smoothing.

The final approach is to constrain the amplification of noise during the reconstruction process using the maximum a posteriori approach (8). This approach basically assumes that not all reconstructions are equally likely, but that prior assumptions can be made about the reconstructed image. These prior assumptions correspond to a penalty term which is taken into account when updating the image – a process referred to as penalisation or regularisation, which results in a Bayesian penalised likelihood (BPL) reconstruction algorithm. In general, this penalty term is used to reduce noise amplification in the image by penalising highly varying activity values between neighbouring voxels. More recently, the approach was introduced as a clinical reconstruction approach which makes use of a prior relative difference to reduce noise amplification during image reconstruction (9). Basically, it penalises small relative differences between neighbouring activity values as these are assumed to be noise, while larger differences are attributed to edges and are therefore preserved. Unlike a conventional OSEM reconstruction, which needs the number of iterations and subsets to be specified, a BPL reconstruction only needs one tuneable parameter to be set which controls the strength of the penalty to preserve edges. Furthermore, no filter for post-smoothing the reconstructed image and increasing image quality is necessary as full convergence is reached without increasing noise (10).

## RESOLUTION MODELLING

In recent years, there have been multiple hardware and software advances in PET/CT to improve image quality, small lesion detectability and quantification accuracy. However, the two main limitations of PET compared to CT and MRI are its relatively low spatial resolution and generally low signal-to-noise ratio. In this section we will focus on advances in reconstruction algorithms to improve spatial resolution.







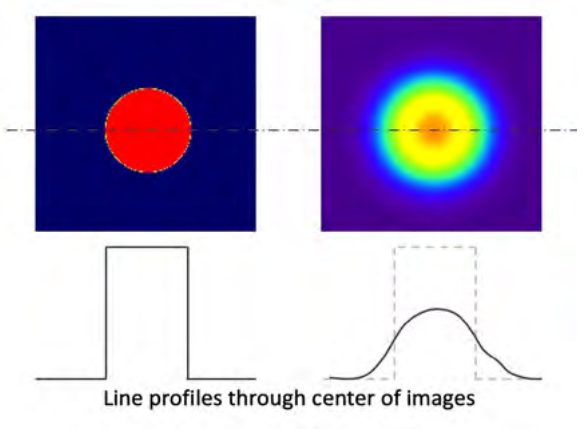


*Figure 2. Partial volume effects. On the left there are no partial volume effects, resulting in sharp representation of a lesion. On the right, partial volume effects due to the limited spatial resolution of a PET system cause signal spread.*

A limited spatial resolution leads to partial volume effects, which, as pointed out by Soret et al (11, 12), are a major confounding factor in PET imaging that cannot be ignored because it can severely affect image quality and image quantification. Partial volume effects typically refer to two different phenomena: (1) the image blurring introduced by the finite spatial resolution of the PET imaging system, and (2) image sampling into voxels so that individual voxels contain different tissue types where the measured voxel intensity is mostly a weighted average of different tissue intensities included in each voxel (13). It is important to note that even imaging systems with perfect spatial resolution would still be hampered by partial volume effects due to image sampling into voxels. For this reason, partial volume effects not only affect PET, but are also of concern in image modalities with better spatial resolution, such as MRI or CT (11). As a result of partial volume effects, small tumour lesions (typically < 15mm) will look larger but less aggressive in PET imaging because partial volume effects will spread the signal of a small hot lesion, resulting in voxel values that will be lower than the actual maximum value (Figure 2). Because these voxel values (i.e. radioactive concentration) are often used to follow up treatment response, these partial volume effects can lead to misinterpretation of the measured data. Furthermore, the apparent larger lesion size can lead to problems when lesion contouring is derived from the PET data, resulting in a lesion that is larger than the real metabolically active lesion. The spatial resolution in the reconstructed images determines how far the signal of small hot lesions spreads. A better spatial resolution will result in less spread, whereas a lower spatial resolution will introduce a larger amount of spread. Consequently, a better spatial resolution will result in fewer partial volume effects.

The spatial resolution in PET is partly determined by physical effects such as crystal size, positron travel, non-collinearity and crystal depth of interaction (14), but it is also important to note that the spatial resolution in the reconstructed images can be controlled to some extent by a good choice of reconstruction parameters, such as number of iterations and subsets (15). If the number of iterations is too low, the spatial resolution in the reconstructed images will be reduced, while increasing the number of iterations improves the spatial resolution in the reconstructed images. A sufficient number of iterations therefore needs to be used to obtain maximum spatial resolution in the reconstructed images.

To further improve spatial resolution in PET, different vendors have considered the idea of correcting for the physical effects that degrade the spatial resolution in PET (16-18). These resolution modelling algorithms incorporate a-priori knowledge of the PET/CT system during the reconstruction process. In these algorithms, the so-called point spread function is modelled during the reconstruction process to correct for image degrading effects such as crystal size, positron travel, non-collinearity and crystal depth of interaction. Resolution modelling can be done using measured data (19) or simulation data (18) and is based on measurements of a point source positioned in different parts of the field of view of the PET/CT scanner.

The application of resolution recovery in clinical PET/CT imaging is very attractive, since it can improve diagnostic performance. It has been reported that resolution modelling in PET leads to higher and more uniform spatial resolution across the transaxial field of view, which can be beneficial in improving the detection of small lesions (20, 21). Although resolution modelling was primarily developed and evaluated for $^{18}$F-FDG imaging, it has also been demonstrated to improve the detectability of small lesions using $^{68}$Ga-based tracers (20). Recently, the impact of resolution recovery on PET/CT scanners was investigated by multi-centric comparison of the recovery coefficient using a $^{68}$Ge phantom (22). The authors concluded that resolution modelling provides a noticeable gain in activity recovery compared to traditional iterative reconstruction algorithms. However, the recovery gain provided by the advanced reconstruction algorithms vanishes on the smaller spheres (6 mm and 10 mm diameter) where it is of greater importance. This study also demonstrates that resolution modelling has a significant impact on quantification, which highlights the need for harmonisation across multicentre networks or collaborations (23, 24).







## REFERENCES


1. Matej S, Karp JS, Lewitt RM, Becher AJ. Performance of the Fourier rebinning algorithm for PET with large acceptance angles. Phys Med Biol. 1998;43(4):787-95.
2. Colsher JG. Fully three-dimensional positron emission tomography. Phys Med Biol. 1980;25(1):103-15.
3. Pelt DM, Batenburg KJ. Improving filtered backprojection reconstruction by data-dependent filtering. IEEE Trans Image Process. 2014;23(11):4750-62.
4. Shepp LA, Vardi Y. Maximum likelihood reconstruction for emission tomography. IEEE Trans Med Imaging. 1982;1(2):113-22.
5. Hudson HM, Larkin RS. Accelerated image reconstruction using ordered subsets of projection data. IEEE Trans Med Imaging. 1994;13(4):601-9.
6. Lantos J, Mittra ES, Levin CS, Iagaru A. Standard OSEM vs. regularized PET image reconstruction: qualitative and quantitative comparison using phantom data and various clinical radiopharmaceuticals. Am J Nucl Med Mol Imaging. 2018;8(2):110-8.
7. Boellaard R, Krak NC, Hoekstra OS, Lammertsma AA. Effects of noise, image resolution, and ROI definition on the accuracy of standard uptake values: a simulation study. J Nucl Med. 2004;45(9):1519-27.
8. Sangtae A, Fessler JA. Globally convergent image reconstruction for emission tomography using relaxed ordered subsets algorithms. IEEE Transactions on Medical Imaging. 2003;22(5):613-26.
9. Nuyts J, Beque D, Dupont P, Mortelmans L. A concave prior penalizing relative differences for maximum-a-posteriori reconstruction in emission tomography. IEEE Transactions on Nuclear Science. 2002;49(1):56-60.
10. Tong S, Alessio AM, Kinahan PE. Image reconstruction for PET/CT scanners: past achievements and future challenges. Imaging Med. 2010;2(5):529-45.
11. Soret M, Bacharach SL, Buvat I. Partial-volume effect in PET tumor imaging. J Nucl Med. 2007;48(6):932-45.
12. Soret M, Riddell C, Hapdey S, Buvat I. Biases affecting the measurements of tumor-to-background activity ratio in PET. IEEE Transactions on Nuclear Science. 2002;49(5):2112-8.
13. Tomasi G, Turkheimer F, Aboagye E. Importance of quantification for the analysis of PET data in oncology: review of current methods and trends for the future. Mol Imaging Biol. 2012;14(2):131-46.
14. Moses WW. Fundamental Limits of Spatial Resolution in PET. Nucl Instrum Methods Phys Res A. 2011;648 Supplement 1:S236-s40.
15. Jaskowiak CJ, Bianco JA, Perlman SB, Fine JP. Influence of reconstruction iterations on 18F-FDG PET/CT standardized uptake values. J Nucl Med. 2005;46(3):424-8.
16. Rahmim A, Qi J, Sossi V. Resolution modeling in PET imaging: theory, practice, benefits, and pitfalls. Med Phys. 2013;40(6):064301.
17. Alessio AM, Kinahan PE, Lewellen TK, editors. Modeling and incorporation of system response functions in 3D whole body PET. IEEE Symposium Conference Record Nuclear Science 2004; 2004 16-22 Oct. 2004.
18. Alessio AM, Kinahan PE, Lewellen TK. Modeling and incorporation of system response functions in 3-D whole body PET. IEEE Trans Med Imaging. 2006;25(7):828-37.
19. Panin VY, Kehren F, Michel C, Casey M. Fully 3-D PET reconstruction with system matrix derived from point source measurements. IEEE Transactions on Medical Imaging. 2006;25(7):907-21.
20. van der Vos CS, Koopman D, Rijnsdorp S, Arends AJ, Boellaard R, van Dalen JA, et al. Quantification, improvement, and harmonization of small lesion detection with state-of-the-art PET. Eur J Nucl Med Mol Imaging. 2017;44(Suppl 1):4-16.
21. Rogasch JM, Steffen IG, Hofheinz F, Großer OS, Furth C, Mohnike K, et al. The association of tumor-to-background ratios and SUVmax deviations related to point spread function and time-of-flight F18-FDG-PET/CT reconstruction in colorectal liver metastases. EJNMMI Res. 2015;5:31.
22. Chauvie S, Bergesio F, De Ponti E, Morzenti S, De Maggi A, Ragazzoni M, et al. The impact of time-of-flight, resolution recovery, and noise modelling in reconstruction algorithms in non-solid-state detectors PET/CT scanners: - multi-centric comparison of activity recovery in a 68Ge phantom. Phys Med. 2020;75:85-91.
23. Armstrong IS, Thomson KE, Rowley LM, McGowan DR. Harmonizing standardized uptake value recovery between two PET/CT systems from different manufacturers when using resolution modelling and time-of-flight. Nucl Med Commun. 2017;38(7):650-5.
24. Munk OL, Tolbod LP, Hansen SB, Bogsrud TV. Point-spread function reconstructed PET images of sub-centimeter lesions are not quantitative. EJNMMI Physics. 2017;4(1):5.

# 3

# DIAGNOSTIC CT IN THE ONCOLOGICAL PET APPLICATIONS AND PROTOCOLS

*by Ivana Zagar*

In the vast majority of cases, the CT component of PET/CT scans is performed according to a »low-dose, contrast-free protocol«, aiming to provide attenuation-weighted reconstruction of PET sinograms and anatomical correlation of radiotracer distribution. This protocol is usually guided by the need to keep the radiation burden as low as reasonably achievable, to reduce patient discomfort and increase daily scanner output in the department. Additionally, if enhanced CT image quality is required, PET/CT studies should utilise diagnostic quality CT scans that improve delineation of anatomical structures, increase sensitivity for detection of pathological lesions and improve accuracy in lesion characterisation [1–6].

Indications for diagnostic quality CT implementation in PET/CT studies may arise from equivocal or insufficient results of previous examinations, suspicion of hepatocellular or cholangiocarcinoma, hypervascular liver lesions with neuroendocrine tumours and other malignancies. Enhanced CT image quality is also necessary for precise assessment of tumour extent before local radiation therapy and post-therapy assessment of an inpatient in whom restaging with diagnostic CT and PET/CT is required [3,5].

| PET/CT INDICATION | DIAGNOSTIC (FULL-DOSE) CT WITH INTRAVENOUS AND ORAL CONTRAST* | LOW-DOSE CT WITHOUT CONTRAST |
|---|---|---|
| **Staging and restaging** | | |
| Tumour staging | recommended | not appropriate for indication |
| Tumour restaging | recommended | not appropriate for indication |
| **Therapy planning** | | |
| RT planning: | | |
| Head and neck, abdomen, pelvis | recommended | not appropriate for indication |
| Thorax | recommended if tumour invasion into mediastinum is suspected | recommended |
| | | not appropriate for indication |
| Surgical planning: | recommended | |
| | | recommended |
| Interventional planning: | | |
| separate contrast-enhanced CT available | not appropriate for indication | not appropriate for indication |
| no contrast-enhanced CT available | recommended | |
| **Therapy control** | | |
| Chemotherapy/irradiation | not appropriate for indication | recommended |
| Surgical/interventional | not appropriate for indication | recommended |

*Table 1. Indications for a full-dose diagnostic contrast-enhanced FDG PET/CT vs. low-dose FDG PET/CT*
*Oral contrast applicable when abdomen in the field of view.







## THE VALUE OF ENHANCED QUALITY CT IMAGING

Lesion detection is enhanced by increasing attenuation differences between anatomical structures; the pattern of contrast enhancement can help lesion characterisation. On non-enhanced CT scans, differentiation of anatomical structures with similar density is often demanding or compromised, especially in the head and neck region and in the abdominal-pelvic region. The interpretation of PET/CT findings in the head/neck region is demanding because of the complex anatomy, and because numerous areas of physiological uptake are present. Intravenous (i.v.) contrast agents enable differentiation of malignant lesions adjacent to blood vessels, thyroid, salivary glands, muscles, and FDG uptake in the fatty brown tissue. They additionally help delineate centrally necrotic lymph nodes, which may be associated with squamous cell carcinoma, but may be missed by low-dose PET/CT (due to the low metabolic activity). In the abdominal-pelvic region, i.v. and oral (p.o.) contrast agents help to visualise lesions adjacent to bowel loops, stomach, parenchymal organs, and mesenteric and iliac blood vessels. This is especially the case with hypervascular liver lesions, with small metastases located within the liver parenchyma, with millimetric peritoneal metastatic spread or with small peritoneal lesions. In the abdominal-pelvic region, diagnostic CT has proved helpful for differentiating between residual tumour and abscess after gastric surgery, splenosis vs. metastases, malignant vs. benign adrenal lesions, and bladder uptake vs. rectal tumour recurrence. Moreover, it is superior for identification of small lesions with size below PET image resolution (Figure 1) and other incidental findings that might not have been detected due to the limitations of low-dose PET/CT scan (vascular complications – aneurysms,

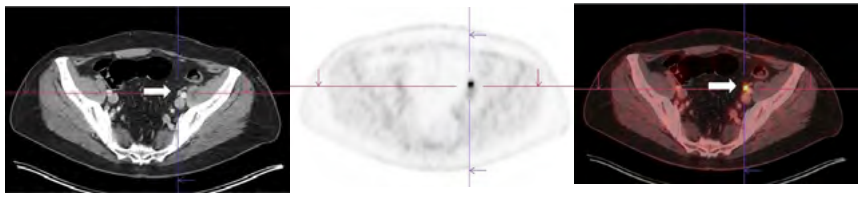

*Figure 1. [18F]FDG PET/diagnostic contrast-enhanced CT in a patient with a diffuse large cell B lymphoma – focally increased metabolic activity (SUV max 9.7) in a less than 0.5 cm lymph node just adjacent to the left external iliac vessels (arrows), which could not have been clearly delineated by a »low-dose« PET/CT scan.*

thrombi; unstable fractures due to osteolytic metastases, complicated/ multiple cysts, ileus, etc.) (Figure 2) [2,3,5].

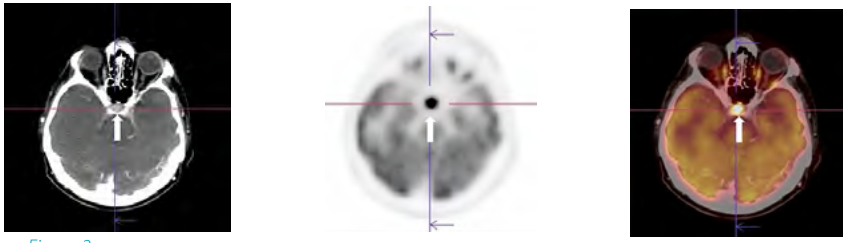

*Figure 2.*

*[$^{18}$F]FDG PET/diagnostic contrast-enhanced CT in a patient with diffuse large cell B lymphoma. Incidental finding of a focal lesion in the pituitary with contrast medium enhancement (arrow), suspected pituitary adenoma – for additional diagnostic (CT, MRI) imaging according to the »pituitary acquisition protocol«.*

Changes in image interpretation may impact clinical management as follows: modifications to diagnostic approach (guiding or eliminating the need for further procedures – biopsy, endoscopy, other diagnostic imaging, etc.); modification of surgical or chemotherapeutic approach, as it is based on accurate TNM staging; modification of radiotherapy (optimisation of the radiation field as an accurate delineation of tumour from the adjacent organs helps to prevent inclusion of radiation-sensitive organs in the planning of target volume) (**Figure 3**) and therapy in cases of clinically significant additional findings [2,3,5].

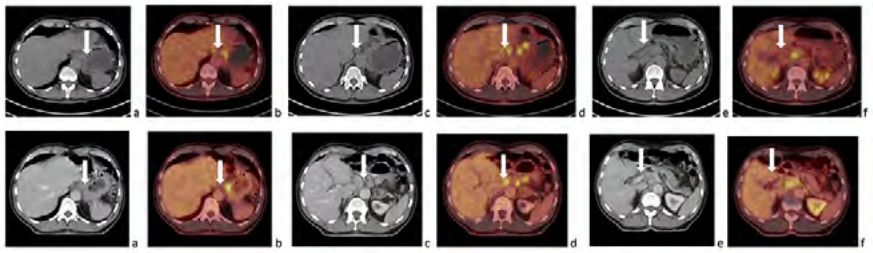

*Figure 2.*

*[$^{18}$F]FDG PET/CT in a patient with a moderately differentiated gastric adenocarcinoma at the level of cardia. Top row, a-f: a »low-dose« staging PET/CT; Bottom row, a-f: radiotherapy planning, contrast-enhanced CT, more clearly delineating (hypermetabolic) lymph nodes in the gastrohepatic ligament and at the level of celiac truncus (arrows).*







## WORKFLOW SPECIFICS

For CT imaging of the abdomen or pelvis, an intraluminal gastrointestinal contrast agent may be administered to improve visualisation of the gastrointestinal tract on CT (unless it is unnecessary for the clinical indication or medically contraindicated). When a diagnostic CT scan with i.v. contrast agent enhancement is to be performed as part of the PET/CT study, indications, contraindications and restrictions have to be assessed by a qualified physician. A previous reaction to a contrast agent is the most important of all the risk factors. Life-threatening reactions are rare. In patients with a history of severe reaction, an unenhanced CT examination is preferred. First-line emergency drugs and equipment should be in the examination room when a diagnostic CT scan with an intravenous contrast agent is to be performed. Emergency devices and drugs are to be available according to national and hospital procedures. When an i.v. contrast agent (iopamidol 61%, 30% organically bound iodine) is given, the timing of the i.v. contrast bolus can be optimised using automated, programmable fluid injector triggering with serial low-dose CT. I.v. contrast material is usually injected at 2.5 – 3 mL/s for a catheter of 20G×1.16″, if located in the elbow, and is followed by a 30 mL saline flush. If the catheter is placed in other locations, the diameter of the catheter and/or the speed of infusion and delay may need to be adjusted [1,4,7].

CT imaging within the framework of PET/CT studies typically consists of a topogram and single or multiple helical CT scans, followed by PET acquisition. CT acquisition parameters (e.g. tube current, voltage, slice thickness, rotation time and pitch) should be chosen with regard to the goals of the CT examination, i.e. CT for attenuation correction, anatomical localisation or CT-derived additional diagnosis. General recommendations, as listed by the IAEA (International Atomic Energy Agency), are shown in **Table 2**.

If the CT examination was optimised for diagnosis, then a more complete, detailed description of the CT protocol and anatomical findings (primary tumour size, volume, growth pattern, density, structure homo-/heterogeneity, relation to the adjacent anatomical structures, infiltration of vascular or other structures, contrast enhancement and washout, lymph node involvement, distant metastases) should be provided. Criteria for visual interpretation need to be defined for each study protocol and may vary according to the type of cancer and for different tumour locations. For response evaluation in oncology, a decrease in tumour size in response to therapy, measured on CT, is one of the most important parameters in the Response Evaluation Criteria in Solid Tumours (RECIST). However, CT may be inaccurate in differentiating viable tumour from surrounding necrotic or fibrotic tissue; consequently, the degree of

| PARAMETER | PARAMETERS FOR CT SCAN FOR ATTENUATION CORRECTION AND ANATOMICAL LOCALISATION, 3-D PET/CT | PARAMETERS FOR CT SCAN FOR ATTENUATION CORRECTION AND ANATOMICAL LOCALISATION FOR PATIENTS WITH HEAD AND NECK TUMOURS, 3-D PET/CT | | PARAMETERS FOR CT SCAN FOR ATTENUATION CORRECTION AND DIAGNOSTIC PARAMETERS, 3-D PET/CT |
|---|---|---|---|---|
| Protocol | Standard body study | Standard body study | Neck | Standard body study |
| Coverage | From base of the skull to upper thighs | From base of the skull to upper thighs | From base of the skull to upper thighs | From base of the skull to upper thighs |
| Patient positioning | Arms up | Arms up | Arms down | Arms up |
| Scout | 120 mV – 10 mA | 120 mV – 10 mA | 120 mV – 10 mA | 120 mV – 10 mA |
| Scan type | helical | helical | helical | helical |
| Rotation time | 0.6 s | 0.6 s | 0.5 s | 0.5 s |
| Rotation length | Full | Full | Full | Full |
| Detector coverage | 40 mm | 40 mm | 40 mm | 40 mm |
| Helical thickness | 3.75 mm | 3.75 mm | 3.75 mm | 3.75 mm |
| Pitch | 0.984:1 | 0.984:1 | 0.984:1 | 0.984:1 |
| Table speed | 39.37 mm/rotation | 39.37 mm/rotation | 39.37 mm/rotation | 39.37 mm/rotation |
| Coverage speed | 65.62 mm/s | 65.62 mm/s | 78.74 mm/s | 65.62 mm/s |
| Tube potential | 120 kV | 120 kV | 120 kV | 120 kV |
| Tube current | Smart mA (auto mA) mA range: minimum 50–maximum 100 | Smart mA (auto mA) mA range: minimum 50–maximum 100 | Smart mA (auto mA) mA range: minimum 30–maximum 100 | Smart mA (auto mA) mA range: minimum 120–maximum 650 |
| Noise index | 12.35 | 12.35 | 12.35 | 12.35 |

*Table 2. Parameters for ct aquisitions*







response may be underestimated on CT. If a decrease in tumour size is short-lived and followed by rapid tumour regrowth, CT may overestimate the beneficial effects of treatment. Many tumours, such as lymphomas, sarcomas, mesotheliomas and gastrointestinal stromal tumours (GISTs), do not shrink even in response to effective therapy. On radiological follow-up, changes in CT attenuation, contrast enhancement patterns and changes may better indicate response in such situations [1,4,8].

## POTENTIAL CONTRAINDICATIONS AND PITFALLS OF DIAGNOSTIC CT

Adverse reactions to iodine-based contrast media comprise non-renal reactions, renal adverse reactions and miscellaneous reactions. Depending on the time of referral, these may be defined as: acute – within 1 hour of contrast medium injection, late – 1 hour to 1 week after contrast medium injection, and very late – more than 1 week after contrast medium injection [9].

Depending on their severity, adverse reactions may be classified as mild, moderate or severe, as shown in **Table 3**.

Risk factors for acute, non-renal adverse reactions to iodine-based contrast media and related recommendations are shown in **Table 4**.

Risk factors for late and very late non-renal adverse reactions to iodine-based contrast media and related recommendations are shown in **Table 5**.

Renal adverse reactions to iodine-based contrast media and related recommendations are shown in **Table 6**.

Contrast medium extravasation (CME) is another well-known event related to diagnostic contrast-enhanced CT imaging. It refers to the leakage of intravenously

| SEVERITY | REACTION |
|---|---|
| MILD | Nausea, mild vomiting<br>Urticaria<br>Itching |
| MODERATE | Vomiting<br>Marked urticaria<br>Bronchospasm<br>Facial/laryngeal oedema<br>Vasovagal attack |
| SEVERE | Hypotensive shock<br>Respiratory arrest<br>Cardiac arrest<br>Convulsion |

*Table 3. Adverse reactions to iodine-based contrast media – according to severity*

| **Risk factors for acute reactions** | |
|---|---|
| PATIENT-RELATED | Patient with a history of:<br>Previous moderate or severe acute reaction (see classification above) to an iodine-based contrast agent.<br>Asthma.<br>Allergy requiring medical treatment. |
| CONTRAST MEDIUM-RELATED | High-osmolality ionic contrast media. |
| **To reduce the risk of an acute reaction** | |
| For all patients | • Use a non-ionic contrast medium.<br>• Keep the patient in the Department for 30 min after contrast medium injection.<br>• Have the drugs and equipment for resuscitation readily available * |
| For patients at increased risk of reaction (see risk factors above) | • Consider an alternative test not requiring an iodine-based contrast agent.<br>• Use a different iodine-based agent for previous reactors to contrast medium.<br>• Consider the use of premedication. Clinical evidence of the effectiveness of premedication is limited. If used, a suitable premedication regime is prednisolone 30 mg (or methylprednisolone 32 mg) given orally 12 and 2 hours before contrast medium. |
| Extravascular administration of iodine-based contrast media | When absorption or leakage into the circulation is possible, take the same precautions as for intravascular administration. |
| ***First-line emergency drugs and instruments which should be in the examination room** | Oxygen<br>Adrenaline 1:1,000<br>Atropine<br>β2-agonist metered dose inhaler<br>I.V. fluids – normal saline or Ringer's solution<br>Anti-convulsive drugs (diazepam)<br>Sphygmomanometer<br>One-way mouth "breather" apparatus |

*Table 4: Acute adverse reactions to iodine-based contrast media*







| LATE REACTIONS: | Skin reactions similar in type to other drug-induced eruptions. Maculopapular rashes, erythema, swelling and pruritus are most common. Most skin reactions are mild to moderate and self-limiting.<br><br>A variety of late symptoms (e.g., nausea, vomiting, headache, musculoskeletal pains, fever) have been described following contrast medium, but many are not related to contrast medium. |
|---|---|
| RISK FACTORS FOR SKIN REACTIONS: | Previous late contrast medium reaction.<br>Interleukin-2 treatment.<br>Use of non-ionic dimers. |
| MANAGEMENT | Symptomatic and similar to the management of other drug-induced skin reactions e.g. antihistamines, topical steroids and emollients. |
| RECOMMENDATIONS: | Patients who have had a previous contrast medium reaction, or who are on interleukin-2 treatment should be advised that a late skin reaction is possible and that they should contact a doctor if they have a problem.<br><br>Patch and delayed reading intradermal tests may be useful to confirm a late skin reaction to contrast medium and to study cross-reactivity patterns with other agents.<br><br>To reduce the risk of repeat reaction, use another contrast agent than the agent precipitating the first reaction. Avoid agents which have shown cross-reactivity in skin testing.<br><br>Drug prophylaxis is generally not recommended. |
| VERY LATE REACTION | Thyrotoxycosis |
| AT RISK | - Patients with untreated Graves' disease<br>- Patients with multinodular goitre and thyroid autonomy, especially if they are elderly and/or live in area of dietary iodine deficiency |
| NOT AT RISK | Patients with normal thyroid function |
| RECOMMENDATIONS | Iodinated contrast media should not be given to patients with manifest hyperthyroidism.<br>Patients at risk should be closely monitored by endocrinologists after iodine- based contrast medium injection.<br>Patients undergoing therapy with radioactive iodine should not have received iodine-based contrast media for at least two months before treatment.<br>Isotope imaging of the thyroid should be avoided for two months after iodine-based contrast medium injection. |

*Table 5. Late and very late adverse reactions to iodine-based contrast media*

| RISK FACTORS FOR CONTRAST MEDIUM-INDUCED NEPHROPATHY | |
|---|---|
| PATIENT-RELATED | eGFR less than 60 ml/min/1.73 m2 before intra-arterial administration<br>eGFR less than 45 ml/min/1.73 m2 before intravenous administration<br>In particular in combination with:<br>Diabetic nephropathy<br>Dehydration<br>Congestive heart failure and low LVEF<br>Recent myocardial infarction (< 24 h)<br>Intra-aortic balloon pump<br>Peri-procedural hypotension<br>Low haematocrit level<br>Age over 70<br>Concurrent administration of nephrotoxic drugs<br>•Known or suspected acute renal failure |
| PROCEDURE-RELATED | •Intra-arterial administration of contrast medium<br>•High-osmolality agents<br>•Large doses of contrast medium<br>•Multiple contrast medium administrations within a few days |
| **RECOMMENDATIONS** | |
| Before examination | Identify patients who require measurement of renal function and determine eGFR (or SCr) within 7 days of contrast medium administration |
| At-risk patients | •Consider an alternative imaging method not using iodine-based contrast media.<br>•Discuss the need to stop nephrotoxic drugs with the referring physician.<br>•Start volume expansion. A suitable protocol is intravenous normal saline, 1.0–1.5 ml/kg/h, for at least 6 h before and after contrast medium. |
| At time of examination | •Use of low or iso-osmolar contrast media.<br>•Use of the lowest dose of contrast medium consistent with a diagnostic result. |
| After the examination<br>At-risk patients | •Continue volume expansion<br>•Determine eGFR 48–72 h after contrast medium |
| Patients taking metformin<br>1. With eGFR equal to or > 60 ml/min/1.73m2 can continue to take metformin normally.<br>2. With eGFR => 45 ml/min/1.73 m2 and receiving intravenous contrast medium can continue to take metformin normally.<br>3. With eGFR between ***30 and 44 ml/min/1.73 m2***, should ***stop metformin 48 h before contrast medium*** and should only restart metformin 48 h after contrast medium if renal function has not deteriorated.<br>4. In patients with eGFR ***less than 30 ml/min/1.73 m2***, or with an intercurrent illness causing reduced liver function or hypoxia, ***metformin is contraindicated*** and iodine-based contrast media should be avoided | |

*Table 6. Renal adverse reactions to iodine-based contrast media*







administered contrast media from the normal intravascular compartment into surrounding soft tissues. It occurs relatively infrequently, in approximately 0.5% of cases. CME is usually recognised at the time it happens. Subclinical CME occurs when no soft tissue injury is discernible, usually when the extravasated volume is less than 20 mL. Patients are asymptomatic or may complain of local symptoms such as pain and tenderness, swelling, itching, redness and/or tightness of the skin at the injection site. With larger extravasated volumes, the affected area appears erythematous, oedematous and tender. Although the majority of cases resolve spontaneously in 2–4 days, in rare cases complications may be serious; they may progress to skin blistering, ulceration and tissue necrosis and can include compartment syndrome. Often, the severity of CME injury cannot be ascertained at the initial examination; scarring around nerves, tendons or joints may occur even if the skin is initially intact. Compartment syndrome, one of the most feared of all the CME complications, presents with a dense, dusky and oedematous extremity with reduced or absent arterial pulses. Most CME occurs as a result of incorrectly positioned intravenous access or venous rupture. Various confounding factors may increase the likelihood of CME. Risk factors, recommendations and basic treatment in case of contrast medium extravasation are shown in **Table 7** [7,9,10,11].

If CT imaging is intended for diagnostic assessment (with or without contrast media enhancement) it implies a higher radiation dose compared to a standard procedure. This is an important issue, especially in patients in whom repeated PET/CT examination has to be performed during the course of the disease and follow-up. The definition of the CT purpose and choice of the associated acquisition protocol is the first step towards patient dose optimisation. To reduce the radiation burden on patients referred for PET/CT imaging, imaging departments are focusing on the development of institution-specific guidelines for the CT part of combined PET/CT protocols, tailored to a specific clinical question [5].

When a diagnostic CT study is needed in addition to a standard whole-body PET/CT exam, the diagnostic CT region of interest may differ from the conventional PET "skull base-to-mid-thigh" tumour imaging. Often the diagnostic CT study requires a limited field of view (for example chest only), which is a subset of the PET study. Some state-of-the-art PET/CT scanners offer the option of performing the diagnostic CT study (with or without contrast enhancement) over the diagnostic region of interest only, and then a low-dose study over the remaining body regions to provide attenuation correction throughout the PET study. With the flexibility for axially varied »low-high-low CT« acquisitions, radiation exposure is limited to the appropriate regions. If a

PET/CT scanner does not support different CT acquisition modes axially, it is wise to acquire the diagnostic CT over the body region of interest only and a separate CT for attenuation correction over the entire PET scan region, especially in the case of patient motion, or the potential for patient motion, between the diagnostic CT and PET scan [12].

| | |
|---|---|
| Type of injuries | Most are minor – swelling, erythema.<br>Severe – include skin ulceration, soft tissue necrosis, and compartment syndrome. |
| Risk factors – technique-related | • Use of a power-automated injector.<br>• Less optimal injection sites including lower limb and small distal veins.<br>• Large volume of contrast medium.<br>• High-osmolality contrast media. |
| Risk factors – patient-related | • Inability to communicate (children, elderly, unconscious patients)<br>• Fragile or damaged veins, peripheral veins with multiple punctures.<br>Use of metal needles<br>Use of indwelling i.v. catheters inserted over 20 h before use (due to thrombophlebitis that may have developed in the cannulated veins).<br>• Patients with arterial or venous insufficiency, as well as those with lymphatic obstruction, e.g. diabetics; venous thrombosis and compromised lymphatic and/or venous drainage following radiation or regional lymph node dissection<br>• Obesity |
| To reduce the risk | • Intravenous technique should always be meticulous using appropriate-sized plastic cannula placed in a suitable vein to handle the flow rate used during the injection.<br>Replacement of cannula if it has been inserted for over 20 h<br>• Test injection with normal saline to ensure patency.<br>• Use non-ionic iodine-based contrast medium.<br>Monitoring the patient/injection site while the contrast is being administered |
| Treatment | • Conservative management – adequate in most cases:<br>limb elevation<br>apply ice packs<br>careful monitoring<br>• If a serious injury is suspected, seek the advice of a surgeon. |

*Table 7. Risk factors, recommendations and basic treatment in case of contrast medium extravasation*







## REFERENCES:


1. Boellaard R, Delgado-Bolton R, Oyen WJG et al: FDG PET/CT: EANM procedure guidelines for tumour imaging: version 2.0. Eur J Nucl Med Mol Imaging (2015); 42:328–354.
2. Morbelli S, Conzi R, Campus C et al: Contrast-enhanced 18F-fluorodeoxyglucose-positron emission tomography/computed tomography in clinical oncology: tumor-, site-, and question-based comparison with standard positron emission tomography/computed tomography. Cancer Imaging 2014; 14:10.
3. Antoch G, Freudenberg LS, Beyer T et al: To Enhance or Not to Enhance? 18-F-FDG and CT Contrast Agents in Dual-Modality 18-F-FDG PET/CT. J Nucl Med 2004; 45: 56S-65S.
4. STANDARD OPERATING PROCEDURES FOR PET/CT: A PRACTICAL APPROACH FOR USE IN ADULT ONCOLOGY, IAEA Human Health Series, No.26, International atomic energy agency, Vienna, 2013.
5. Pfannenberg AC, Aschoff P, Brecjhtel K, et al: Value of contrast enhanced multiphase CT in combined PET/CT protocols for oncological imaging. The British Journal of Radiology 2007; 80:437-445.
6. ICRP. Radiation dose to patients from radiopharmaceuticals. Addendum 3 to ICRP Publication 53. ICRP Publication 106. Approved by the Commission in October 2007. Ann ICRP 2008; 38(1-2):1–197.
7. ACR Committee on Drugs and Contrast Media. ACR manual on contrast media. ACR, American College of Radiology 2021; ISBN: 978-1-55903-012-0.
8. Eisenhauer EA, Therasseb P, Bogaertsc J et al: New response evaluation criteria in solid tumours: Revised RECIST guideline (version 1.1). European Journal of Cancer 2009; 45: 228–247.
9. European Society of Urogenital Radiology. ESUR guidelines on contrast media. http://www.esur.org/guidelines).
10. Sum W, Ridley LJ: Recognition and management of contrast media extravasation. Australasian Radiology 2006; 50: 549–552.
11. Behzadi AH, Farooq Z, Newhouse JH: MRI and CT contrast media extravasation - A systematic review. Medicine 2018; 97: 9 (e0055): 1-8.
12. Akin EA, Torigian DA, Colleti PM, Yoo DC: Optimizing Oncologic FDG-PET/CT Scans To Decrease Radiation Exposure. https://www.imagewisely.org, American College of Radiology, 2017.

# 4

# PET/CT ARTEFACTS AND PITFALLS

*by Tyler Middlebrooks*

The purpose of this chapter is to introduce artefacts and pitfalls that are observed in positron emission tomography/computed tomography (PET/CT) imaging and discuss how to identify and prevent them in future. The use of PET/CT has changed the landscape of nuclear medicine and is currently pushing the forefront of theragnostics in medicine. PET/CT has shown to be an asset in the detection of cancers, as well as neurological and cardiac diseases.

Artefacts are routinely seen in all radiology modalities. Artefacts that are encountered daily in computed tomography (CT) include noise, motion, beam hardening, ring, and helical artefacts. The computer software and hardware image quality has continued to improve, and this looks likely to remain the case for years to come. With the increased use of computers, software, and digital applications the likelihood of encountering artefacts increases.

## COMPUTED TOMOGRAPHY

One of the most widely used modalities in radiology is CT for its high resolution, short exam time, and three-dimensional imaging capability. Like most modalities in radiology, CT has a degree of noise that must be overcome to ensure the signal-to-noise ratio is at acceptable levels. Noise can be calculated by obtaining a region of interest (ROI) on a CT image and then calculating the standard deviation, see Figure 1. In this section we will discuss and illustrate artefacts that can be seen during the CT portion of the PET/CT exam.

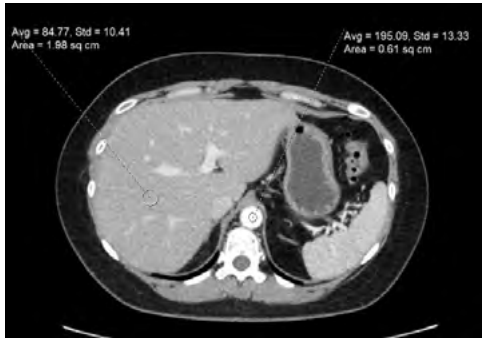


*Figure 1. Region of interest (ROI) displaying measurements of the descending aorta and liver. (Image courtesy of CARTI Cancer Center, Little Rock, Arkansas, USA)*







### Helical Artefacts

Helical artefacts are caused by rapid movement during the scan acquisition. This occurs when the scanned anatomy changes position during acquisition, which causes the reconstruction algorithm to interpolate the data. This is mostly seen in the lungs and liver due to the patient breathing during the scan. It typically appears as a spiral shape causing lower Hounsfield Units (HU) on CT images. This is routinely seen in the lung base due to breathing during the CT exam.

| ARTEFACT TYPE: | HELICAL ARTEFACT |
|---|---|
| Diagnosis: | Caused by movement along the axis during helical acquisition. |
| Prevention: | The technologist should instruct the patient to take small shallow breaths throughout the exam. |
| Techniques to Utilise: | The use of an abdominal strap to prevent deep inspiration can assist in reducing a helical artefact. |

### Metal Artefacts

Metal artefacts are the most frequent artefacts seen on CT scans. When a patient has an internal metallic artefact, many different artefacts can occur as seen in Figure 2. The bright white streaks appearing around the metallic implant are metal artefacts, beam hardening, scatter effect and quantum mottle. The dark area displayed is beam hardening and a scatter effect. It is particularly important to remove all metal in the scan field of view (SFOV) to reduce metal artefacts and improve image quality. In newer CT and PET/CT scanners an automated exposure technique is used to help reduce the radiation burden to the patient while also ensuring a prescribed noise index that has been agreed upon by the interpreting physician(s). Internal metallic implants are not a direct contraindication, but an implant should be taken into consideration if it could possibly yield a non-diagnostic exam or prevent the interpreting physician from evaluating the area of disease.

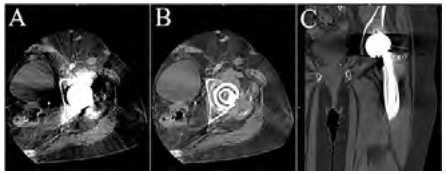


*Figure 2. MDT reduces many different types of metal artefacts and can reveal new findings. (A) Bright streak near hip replacement is mostly due to beam hardening and scatter without artefact reduction. (B) The MDT image clearly shows a swelling and inflammation adjacent to the left hip replacement. (C) A coronal image of left hip replacement. (Image courtesy of CARTI Cancer Center, Little Rock, Arkansas, USA)*

| ARTEFACT TYPE: | METAL ARTEFACT |
|---|---|
| Diagnosis: | Caused by a dense/metallic object inside the SFOV. |
| Prevention: | If possible, the technologist must remove all metal from the patient that is located inside the SFOV. |
| Techniques to Utilise: | The use of metal subtraction software has been shown to dramatically reduce image artefacts and improve overall image quality. |

## Motion Artefacts

Motion artefacts are typically caused by movement of the heart, bowels, lungs, or by voluntary or involuntary movements. The images appear to have a double exposure or a blurred look, with long streaks along high contrast edges on the anatomy. The most effective way to reduce motion artefact is for the technologist to explain to the patient how critical it is to ensure good quality images. One method of reducing image motion, if the patient is unable to remain still, is to scan faster, giving the patient less time to move during the exam. This can be achieved by increasing the tube rotation, increasing table speed, or increasing rows of detectors to allow for volume scanning. CT imaging of the heart has typically utilised a fast rotation speed, volume acquisition and cardiac gating to image the heart in the same position. See Figure 3 demonstrating motion during a CT exam.

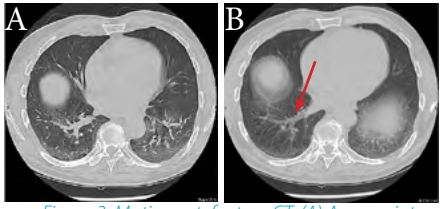


*Figure 3. Motion artefact on CT. (A) Appropriate breath hold during CT acquisition. (B) Breathing during breath hold causing doubled image, blurring and image quality loss. (Images courtesy of CARTI Cancer Center, Little Rock, Arkansas, USA)*

| ARTEFACT TYPE: | METAL ARTEFACT |
|---|---|
| Diagnosis: | Caused by movement during scan (double image, blurring and streaks) |
| Prevention: | 1. The technologist must explain the importance of remaining still during the exam.<br>2. Increase rotation time, table speed, and/or acquire volume data sets in patients who are unable to remain still during the exam. |
| Techniques to Utilise: | The use of straps and stabilisation techniques to help the patient remain still during the exam. Also, the use of cardiac and pulmonary gating has shown to be extremely helpful in improving the temporal resolution. |

## Image Noise / Quantum Mottle

Noise or quantum mottle is a statistical error due to low photon counts in an image. This can appear as random dark or bright areas. When there is increased noise in an image, higher contrast objects like bones still have good image quality, but lower contrast objects start to lose resolution and the edges start to become more obscured. [1]







| ARTEFACT TYPE: | NOISE OR QUANTUM MOTTLE |
|---|---|
| Diagnosis: | Caused by low number of photons imaged (bright and dark areas in image) |
| Prevention: | 1. Improve the technique; increase electrical current or mA of the exam.<br>2. Decrease the rotation time. |
| Techniques to Utilise: | Iterative reconstruction, filtered back-projection, and other noise reduction software can assist in noise reduction without increasing the patient's dose. |

## Out of Field of View Artefact

Out of field of view (OFOV) artefacts are typically caused by a suboptimal reconstruction algorithm resulting from an object being outside the scanned field of view. A small field of view is a great way to reduce the radiation burden to your patient. If the sinogram edges are set to stretch to the end values, the out of field artefact will be greatly eliminated. If this is not an option, include all of the anatomy in the scanned field of view and reconstruct the display field of view to display the desired anatomy only, as seen in Figure 4.

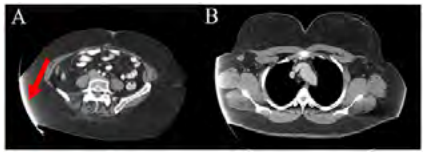


*Figure 4. Out of field of view artefact on CT. (A) artefact near right iliac crest. (B) artefact on the same patient near the right shoulder. (Image courtesy of CARTI Cancer Center, Little Rock, Arkansas, USA)*

| ARTEFACT TYPE: | OUT OF FIELD OF VIEW ARTEFACT |
|---|---|
| Diagnosis: | Caused by the patient being outside the field of view (seen as bright streaks in image). |
| Prevention: | 1. Align the patient so that all anatomy is inside the SFOV.<br>2. Adjust/optimise the reconstruction algorithm. |
| Techniques to Utilise: | The use of straps to narrow the patient can help the patient remain inside the scan field of view. The addition of a software reconstruction algorithm can reduce the OFOV artefact in large and small FOVs. |

## RING ARTEFACTS

Ring artefact is caused by a miscalibrated or defective detector element, which results in rings or a water ripple effect on the image. This can often be remedied by recalibrating the detector. A miscalibrated or defective detector element creates a bright or dark ring that is centred on the centre of rotation. This can sometimes simulate pathology. Usually, recalibrating the detector is sufficient to fix this artefact although occasionally the detector itself needs to be replaced. Ring artefacts typically show a small ring in the exam FOV. This can range in severity from a single circle to multiple rings. In some cases it resembles a water ripple through the image, centred around the centre of the FOV. Subtle ring artefacts in the head can simulate lesions. Pons pseudolesions can be seen in some ring artefacts at the centre of the reconstruction FOV in a head

CT. [1] Faint ring artefact seen in Figure 5, showing a chest CT without contrast with water ripple ring artefact.

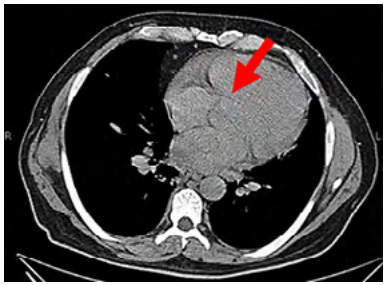

*Figure 5. Faint ring artefact seen on a chest CT without contrast. (Image courtesy of CARTI Cancer Center, Little Rock, Arkansas, USA)*

| ARTEFACT TYPE: | RING ARTEFACT |
|---|---|
| Diagnosis: | Caused by a miscalibrated or defective detector |
| Prevention: | 1. Daily phantom and QA checks.<br>2. Routine preventative maintenance. |
| Techniques to Utilise: | N/A |

## POSITRON EMISSION TOMOGRAPHY (PET)

In this section we will discuss and illustrate artefacts that can be seen during the PET portion of the PET/CT exam and review ways to reduce or eliminate these artefacts. In recent years the use of combination PET and CT imaging has grown exponentially, and this will be a major component of radiology in the future.

### Contrast Media and Metallic Artefacts

Intravenous or oral contrast media can negatively affect the image quality. Administration of contrast media can alter the quantitative and qualitative accuracy of the PET images, just as metallic implants in CT imaging. These areas of high density caused by contrast media will artificially increase the standard uptake value (SUV) in these areas, causing a false positive result. The severity or degree of the misinterpretation is dependent on the concentration of contrast in the area. Figure 6 shows a contrast medium artefact due to barium. [1] This can also occur with high-density objects inside the body, such as pacemakers and metallic implants.

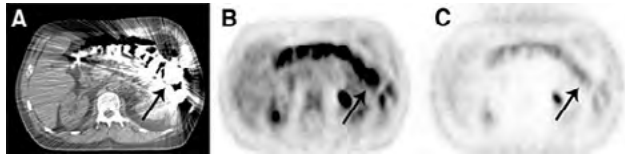


*Figure 6. (A) A patient ingested barium for an oesophagogram 1 d before PET/CT scan. Concentration of contrast medium in colon. (B) High CT numbers of residual barium overcorrect PET data. (C) No increased 18F-FDG uptake is seen on image without attenuation correction. (Reprinted, with permission, from reference 1*







| ARTEFACT TYPE: | CONTRAST MEDIUM ARTEFACT |
|---|---|
| Diagnosis: | Caused by area of dense contrast media (may resemble a metal artefact) |
| Prevention: | 1. Avoid the use of contrast during exam or after a contrasted exam.<br>2. Perform a CT with/without contrast media. Increased radiation exposure should be considered if the benefit outweighs the risk. |
| Techniques to Utilise: | The use of metal subtraction software has been shown to reduce image artefacts caused by high-density contrast media in PET/CT imaging. |

### Noise / Quantum Mottle

Image noise relating to PET imaging is remarkably similar to the noise sometimes found in CT. Noise is a statistical error due to low photon counts in an image, which can appear as random dark or bright areas. Typically, noise in nuclear medicine exams is due to a low count rate. However, noise in the PET image is not related to the CT quality, but can be present for different reasons including low tracer activity, reduced acquisition time per bed, or inherent noise caused by the image resolution limits on the equipment. As acquired counts increase, the signal-to-noise ratio rises while image quality improves and image noise decreases, as seen in Figure 7.

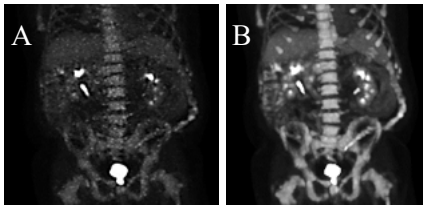


| ARTEFACT TYPE: | NOISE / QUANTUM MOTTLE (SIGNAL-TO-NOISE RATIO) |
|---|---|
| Diagnosis: | Caused by low acquired counts |
| Prevention: | Ensure exam acquisition time per bed is appropriate for the given activity |
| Techniques to Utilise: | Noise reduction or image enhancement software can be used to decrease noise and increase edge enhancement without increasing the patient's dose. |

### Respiratory Motion Artefact

Respiratory motion is one of the most frequent artefacts seen in PET/CT imaging. Due to the long acquisition time, the acquired images are a representation of several breathing cycles. In addition, some patients (without being instructed) will hold their breath or suspend breathing during the CT portion of the exam, thus causing an increased misalignment near the diaphragm. Several studies have tried to determine whether a breath hold at mid-inspiration or shallow breathing is better. The breath hold at mid-inspiration technique showed an improvement of the CT images during the exam but caused PET alignment artefacts. In contrast, shallow breathing failed to accurately

*Figure 7. (A) Increased image noise or quantum mottle due to suboptimal scan time with low signal-to-noise ratio. Retrospectively reconstructed with 66% decreased scan time per PET bed. (B) Noise reduced with adequate exam time giving the scanner time to acquire the appropriate number of counts to avoid noise. (Image courtesy of CARTI Cancer Center, Little Rock, Arkansas, USA)*

match the CT and PET portions while producing a moderate breathing artefact on the CT images through the lungs. The most commonly seen respiratory motion artefact is the curvilinear cold region, where the dome of the liver and the diaphragm have moved between the CT and PET acquisitions. Figure 8 shows a respiratory motion artefact. Neither shallow breathing nor mid-breath hold has a clear advantage, since both cause an artefact in both the CT and PET portions of the exam.

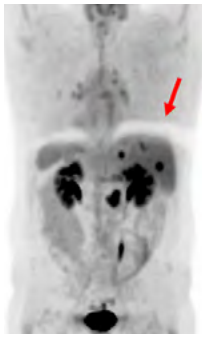

*Figure 8. Respiratory motion artefact seen at the level of the diaphragm due to breathing during PET acquisition. (Image courtesy of CARTI Cancer Center, Little Rock, Arkansas, USA)*

| ARTEFACT TYPE: | RESPIRATORY MOTION |
|---|---|
| Diagnosis: | Breathing during the exam |
| Prevention: | The technologist must instruct the patient to take shallow breaths during the entire exam. |
| Techniques to Utilise: | The use of respiratory gating and shallow breathing has shown to dramatically increase the exam quality throughout the lungs while increasing sensitivity at the same time. |

## Injection Site Artefact

Vascular access is a particularly important step to secure prior to injection. In some cases, proper vascular access is not obtained, and a portion of the injection is infiltrated. In most cases this is not severe enough to repeat the exam, but it can range in severity and in some cases produce a non-diagnostic scan. Verify vascular access prior to administration, and if access is questionable start a new IV and confirm patency. Figure 9 shows an infiltration or injection site artefact.

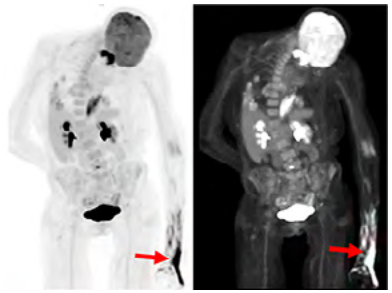

*Figure 9. (A) Inverse MIP image showing injection site artefact in the left hand. (B) Linear MIP showing the same artefact. (Image courtesy of CARTI Cancer Center, Little Rock, Arkansas, USA)*

| ARTEFACT TYPE: | INJECTION SITE / INFILTRATION ARTEFACT |
|---|---|
| Diagnosis: | Caused by poor vascular access resulting in infiltration of the radiotracer. |
| Prevention: | Ensure free-flowing vascular access prior to administration. |
| Techniques to Utilise: | If infiltration is suspected, increase the counts collected or, if applicable, use a scanner that has the highest crystal efficiency. |







## Truncation

In PET/CT imaging truncation is possible when the CT FOV and the PET FOV are different. If anatomy is outside the CT FOV then truncations can occur, producing incorrect (AC) data. Previously, PET/CT scanners would routinely have a 50cm CT FOV and a 70cm PET FOV, which is where the size differences originate. Most current PET/CT scanners now have a large-bore CT FOV that allows an equal CT and PET FOV. It is best practice for the technologist to position the patient at the isocentre of the scanner with their arms above their head to reduce the likelihood of a truncation artefact. It is now possible to completely eliminate this type of artefact by ensuring the same FOV for both PET and CT. Figure 10 shows truncation of the top of the skull with PET activity seen beyond the CT FOV. Arm motion during the exam can cause truncation inside the scanned FOV, ranging in severity from minimal effects to completely missing information. Reviewing the non-attenuated corrected images can help to clarify missing information, but in some severe cases the patient may possibly need to be rescanned to guarantee a complete and accurate exam.

| ARTEFACT TYPE: | TRUNCATION ARTEFACT |
|---|---|
| Diagnosis: | Caused by patient's anatomy being outside the CT FOV and inside the PET FOV. |
| Prevention: | Ensure all of patient's anatomy is inside both FOV where possible. |
| Techniques to Utilise: | Optimising reconstruction FOVs to different sizes can better display anatomy for both CT and PET. Where possible use the smallest FOV for both CT and PET, matching diameter and including all anatomy. |

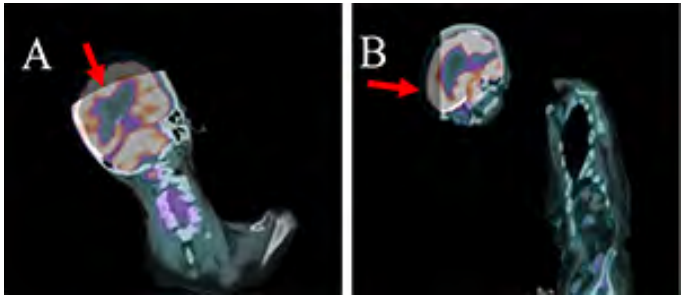


*Figure 10. (A) Axial fused image showing truncation. The patient is outside the CT FOV, with attenuated corrected image expanding outside the CT image. This area is not represented in the CT reconstructions and has no attenuation correction values for the corresponding region. (B) Sagittal fused image showing truncation. (Images courtesy of CARTI Cancer Center, Little Rock, Arkansas, USA)*

## INTERPRETATION PITFALLS

PET/CT imaging is a combination of diagnostic procedures, making it difficult to interpret and with artefacts and pitfalls often seen. An extensive knowledge of physiological variation and normal distributions is a must for technologists and radiologists, who must also be mindful of a host of false positives, false negatives, and pitfalls during interpretation. It is essential for the technologist to be aware of the importance of patient preparation, administration, and acquisition to ensure the highest quality exam. With suboptimal technologist practice, interpreting these scans becomes difficult and may lead to misdiagnosis.

Movement during acquisition can be detrimental to the exam quality. The arms are routinely positioned above the patient's head, so a common location for motion artefact is around the arms and head. In whole body imaging patients, the arms are down by the patient's side, but they periodically move during acquisition. This artefact manifests due to an underestimation of radiotracer concentration, which becomes more significant with increasing misalignment and can cause streaking cold artefacts on PET images. Reconstruction artefacts due to patient arm motion can be substantial, and it is important that they are identified because they can affect both qualitative and quantitative assessment of PET. [1]

## CONCLUSION

PET/CT imaging is a complex modality using complicated systems, which all need to work together in order to produce clear diagnostic results. Technologists are responsible for ensuring exam accuracy and validity. PET/CT exams are routinely used to diagnose, stage and restage oncological, neurological and cardiological diseases. Knowledgeable and diligent technologists can minimise artefacts and other potential problems with image acquisition, and are thus instrumental in producing better-quality PET/CT images. [2]

## REFERENCES

1. Sureshbabu, W., CNMT, PET, & Mawlawi, O., PhD. (2005). PET/CT Imaging Artifacts*. Journal of Nuclear Medicine Technology, 33(3), 156-161.

2. Lodge MA, Mhlanga JC, Cho SY, Wahl RL. Effect of patient arm motion in whole-body PET/CT. J Nucl Med. 2011 Dec;52(12):1891-7. doi: 10.2967/jnumed.111.093583. Epub 2011 Nov 11. PMID: 22080444; PMCID: PMC4337880.



CHAPTER 4

PET/CT ARTEFACTS AND PITFALLS

# 5

# ADVANCED RADIOPHARMACEUTICALS

*by Guy Bormans*
*Frederik Cleeren*

## INTRODUCTION

The general structure of a radiopharmaceutical consists of a radionuclide which is chemically connected to a vector molecule (Figure 1A). The vector molecule is responsible for the specific interaction with the target cells or tissues. This results in a higher concentration of the radionuclide in the target tissue compared to the background tissue and generates the PET image contrast, enabling tissue that interacts with the vector (target tissue, Figure 1A) to be distinguished from tissue that does not (non-target tissue, Figure 1B).

For some radiopharmaceuticals, the radionuclide also functions as its vector: [$^{18}$F]fluoride consists solely of the anion form of fluorine, which will avidly bind to bone tissue and can be used for PET bone scans. Usually, however, the vector consists of a small molecule (e.g. glucose for [$^{18}$F]FDG) or larger peptides or proteins (e.g. octreotide derivatives, antibodies to which the radionuclide is bound). The radionuclide can be bound by covalent binding or by complexation (chelation), which is the general binding mode for radiometals. Radiopharmaceuticals that need to cross biomembranes, e.g. the blood-brain barrier (for brain-targeted radiopharmaceuticals) or the cell membrane (for intracellular targets) usually employ small molecules derived from biochemicals or xenobiotics. In this case, the presence of a radiometal/chelator may hamper the biomembrane penetration; therefore, small molecules with intracellular or brain targets are generally labelled with carbon-11, fluorine-18 or iodine-124.

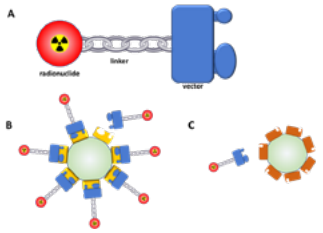


*Figure 1* ***A.*** *General structure of a radiopharmaceutical* ***B.*** *Tissue interacting with the radiopharmaceutical, resulting in high local concentration of the radionuclide.* ***C.*** *Tissue not interacting with the radiopharmaceutical, resulting in low local concentration of the radionuclide.*

For positron emission tomography (PET), the radionuclide is unstable as its nucleus has an excess of protons. In order to get rid of this excess, a proton is converted to a neutron, a positron and a neutrino. After travelling for a short distance, the positron will combine with an electron and the mass of both particles will be converted into two annihilation gamma rays of 511 keV each, emitted at an angle of 180°. The coincident detection of both gamma rays by the PET camera allows the reconstruction of an image reflecting the concentration of the radionuclide in the body.







## PET RADIONUCLIDES

Important characteristics (half-life, production route, decay mode, positron energy and chemical characteristics) of the most frequently used PET radionuclides are summarised in Table 1.

| Radio-nuclide | $T_{1/2}$ | Production | Decay mode | $\beta^+$ Emax (Mev) | Chemistry |
|---|---|---|---|---|---|
| $^{82}$Rb | 1.3 min | $^{82}$Sr/$^{82}$Rb generator | $\beta^+$ (100%) | 3.4 | only used as $Rb^+$ |
| $^{15}$O | 2.0 min | Cyclotron $^{14}$N(d,n) $^{15}$N(p,n) | $\beta^+$ (100%) | 1.7 | Limited by short half-life to rapid on-line conversion (e.g. [$^{15}$O]$H_2O$) |
| $^{13}$N | 10.0 min | Cyclotron $^{16}$O(p,α) | $\beta^+$ (100%) | 1.2 | Limited by short half-life to in- target production or rapid conversion (e.g. [$^{13}$N]$NH_3$) |
| $^{11}$C | 20.4 min | Cyclotron $^{14}$N(p,α) | $\beta^+$ (100%) | 1.0 | carbon organic chemistry (synthesis module) |
| $^{68}$Ga | 67.6 min | $^{68}$Ge/$^{68}$Ga generator or cyclotron $^{68}$Zn(p,n) | $\beta^+$ (89%) | 1.9 | radiometal (chelation), kit based/synthesis module |
| $^{18}$F | 109.8 | Cyclotron $^{18}$O(p,n) | $\beta^+$ (97%) | 0.6 | halogen organic chemistry (synthesis module) – Al$^{18}$F chelation |
| $^{64}$Cu | 12.7h | Cyclotron $^{64}$Ni(p,n) | $\beta^+$ + EC (61%); $\beta^-$ (39%) | 0.7 | radiometal (chelation) |
| $^{89}$Zr | 3.3 days | Cyclotron $^{89}$Y(p,n) | $\beta^+$ (23%) | 0.9 | radiometal (chelation) |
| $^{124}$I | 4.2 days | Cyclotron $^{124}$Te(p,n) | $\beta^+$ (26%) | 2.1 | halogen organic chemistry (synthesis module) |

*Table 1 Characteristics of commonly used PET radionuclides*

### Radionuclide half-life

From the **radiation protection point of view**, the half-life ($T_{1/2}$) of the radionuclide should be as short as possible in order to limit the time period during which the patient is exposed to ionising radiation. Administration of PET radiopharmaceuticals labelled with radionuclides with longer $T_{1/2}$ will indeed result in a higher radiation dose to the patient. The low radiation dose associated with short-lived radionuclides (e.g. $^{15}O$, $^{11}C$, $^{82}Rb$) allows repeated injections and PET scans to be performed in the same subject within reasonable radiation dose limits.

From the **radiopharmaceutical production point of view**, the half-life of the radionuclide should be sufficiently long to at least allow chemical coupling (radiosynthesis) of the radionuclide to its vector and to perform quality control of the resulting radiopharmaceutical. Very short-lived radionuclides can only be used in the chemical form in which they are obtained from the cyclotron or generator (e.g. [$^{15}O$]$O_2$, [$^{13}N$]$NH_3$ and $^{82}RbCl$) or after fast online chemical conversion (e.g. [$^{15}O$] H2O, [$^{15}O$]CO).

A longer half-life allows multiple patients to be injected from a single production batch and the radiopharmaceutical to be transported to remote PET centres. For an identical production cost per batch, the cost per patient dose will thus be lower and the radiopharmaceutical will be more cost-efficient.

From an **imaging point of view**, the physical half-life of the radionuclide should be long enough in relation to the kinetics of the radiopharmaceutical, which are dictated by the characteristics of the vector. As radiopharmaceuticals are injected intravenously, high-contrast images can only be obtained after sufficient accumulation of the radiopharmaceutical in the target tissue and sufficient clearance of the radiopharmaceutical from non-target tissue, including the vascular compartment. Plasma can be cleared by the kidneys (polar vector molecules <60 kDa) with urinary excretion from the body, or by the liver with excretion to the bile (lipophilic and large vector molecules).

Antibodies have a relatively long plasma half-life (days to weeks), so when using these proteins as vector, the half-life of the radionuclide should be long enough to allow for a waiting period of several days between injection and imaging. In this case $^{64}Cu$ (half-life 13h), $^{89}Zr$ (half-life 3.3 days) or $^{124}I$ (half-life 4.2 days) can be used as radionuclide.

### Radionuclide production route

PET radionuclides can be obtained from a cyclotron or a radionuclide generator.

In a cyclotron for production of medical radionuclides, protons or deuterons (usually as negatively charged hydride or deuteride ions) are accelerated in consecutive cycles by application of an oscillating electric field and are forced to follow a spiral-like trajectory during which they gain kinetic energy. Finally, the accelerated particles will collide with nuclei of the target, resulting in a nuclear reaction during which the accelerated particle is absorbed, followed by the ejection of (an) other particle(s). Table 1 lists the most common nuclear reactions for cyclotron-produced, positron-emitting radionuclides. The production of fluorine-18 applies the $^{18}O(p,n)^{18}F$ nuclear reaction, during which a proton (p) that has been accelerated in the cyclotron will collide with oxygen-18 (one of the stable isotopes of oxygen with a natural abundance of 0.2%) and a neutron (n) will be ejected, resulting in the formation of fluorine-18. The target material that is irradiated in the cyclotron can be a gas (production of $^{15}O$ and $^{11}C$) or a liquid (production of $^{13}N$ and $^{18}F$), which can be easily and efficiently transferred from the cyclotron to the radiochemistry lab through small-diameter tubing. Cyclotron production of $^{68}Ga$, $^{64}Cu$, $^{89}Zr$, and $^{124}I$ involves the irradiation of a solid metal coin that afterwards needs to be processed by dissolution or high-temperature heating followed by purification of the radionuclide before the latter can be used for radiolabelling. $^{68}Ga$ can also be produced by irradiation of aqueous $^{68}Zn$ solutions. The production yields of the latter will be lower compared to irradiation of a solid target, but transfer and post-target processing is easier.

Cyclotron production obviously requires a large investment to install and maintain the cyclotron, but also for a heavy concrete vault and auxiliary equipment (e.g. HVAC and radioactivity monitoring). In addition, operation and maintenance also requires specialised staff (e.g. cyclotron engineer), leading to a total cost of several million euros. Cyclotron production usually provides much higher amounts of radionuclide activity compared to radionuclide generators.

A radionuclide generator is far simpler and cheaper to install and operate, but its application is limited to goldilocks combinations of a parent and daughter isotope that are both radioactive, as is the case with the $^{99}Mo/^{99m}Tc$ generator. Decay of the parent radionuclide generates the daughter radionuclide, and the generator column will retain the parent radionuclide, whereas the daughter radionuclide can be harvested by elution of the generator with an appropriate solution. The parent radionuclide half-life thereby defines the operating period of the generator, while the daughter radionuclide half-life defines the interval between subsequent elutions.

Although other PET radionuclide generators have been described in the literature, commercial generators for clinical use are only available for $^{68}Ga$ and $^{82}Rb$. The $^{82}Sr/^{82}Rb$ rubidium generator is marketed by Draximage (Ruby-fill) and Bracco Imaging (CardioGen-82) in the US, although a European Medicines Agency

application has also been filed[7]. The parent radionuclide $^{82}$Sr has a half-life of 25 days, implying that the generator can be used for up to about 60 days, and the short half-life of $^{82}$Rb allows for short elution intervals (<10 min). $^{82}$Sr is strongly retained on the generator column, whereas the short-lived daughter radionuclide $^{82}$Rb (half-life 76 s) is eluted from the generator with a saline solution and directly infused into the patient. $Rb^+$ is a substrate for the $Na^+/K^+$ ATPase pump and is retained in myocardium depending on the myocardial blood flow, although its application for tumour detection has also been evaluated recently[8].

Several $^{68}$Ge/$^{68}$Ga generators (e.g. Galli Ad (Rotop), Elit (IRE), GalliaPharm (Eckert and Ziegler)) have been registered by EMA and can be obtained commercially. The long half-life of the parent radionuclide ($^{68}$Ge, 271 days) allows the generator to be used for more than a year. The short half-life of $^{68}$Ga (68 min) implies that good yields of $^{68}$Ga can be obtained with elution intervals of a couple of hours. $^{68}$Ge/$^{68}$Ga generators are eluted with acidic HCl solutions (0.05M–1M depending on the type of generator). This has to be considered when generator eluate $^{68}$Ga is used for downstream labelling, as the chelation reaction will critically depend on the pH of the reaction mixture.

## Beta energy and prompt gamma emission

The positron emitted upon decay from the nucleus of a PET radionuclide will travel for a distance that depends on the positron energy. The energy of the positron can vary across the typical energy spectrum characterised by a mean and a maximum energy that are specific to a given radionuclide. The range of the positron may lead to loss of spatial resolution in the resulting PET images, and although this effect will be limited in current commercially available clinical PET scanners, which have a spatial resolution of 4 mm, the effect will be noticeable in small-animal PET scanners and next-generation clinical PET scanners.

$^{11}$C, $^{18}$F, $^{64}$Cu, and $^{89}$Zr are typical short-range positron emitters, whereas $^{13}$N, $^{15}$O, $^{68}$Ga, $^{82}$Rb, and $^{124}$I can be considered as long-range positron emitters (>1 mm range in tissue). $^{11}$C, $^{13}$N, $^{15}$O, and $^{18}$F are almost "pure" positron-emitting radionuclides with high (>97%) $\beta^+$ decay branching ratios and absence of coincident gamma ray emission. $^{89}$Zr has a low $\beta^+$ decay branching ratio (23%) and its decay is accompanied by emission of a 909-keV gamma ray (generated by decay of short-lived daughter $^{89m}$Y), which is, however, emitted with a short delay after emission of the positron and does not behave as a "prompt" (coincident) gamma. $^{64}$Cu decays to either $^{64}$Zn via $\beta^-$ decay (38%) or to $^{64}$Ni via EC (45%) or $\beta^+$ decay (18%) without emission of prompt gammas.







Prompt gamma radiation may produce false coincidences in the PET camera, leading to image blurring and quantification errors. This is only slightly the case for $^{68}$Ga (3%, 1077 keV gamma) but more so for $^{82}$Rb (15%, 777 keV gamma) and $^{124}$I (62% 602 keV gamma; 11% 1.691 keV gamma)[9].

## Radiochemistry: metals and non-metals

In a limited number of cases, the required chemical form of PET radionuclides is obtained from cyclotron production (e.g. $[^{18}F]F^-$, $[^{13}N]NH_3$) or the radionuclide generator (e.g. $^{82}Rb^+$), so that no further chemical conversion is required and sterile filtration of the radionuclide solution provides the corresponding radiopharmaceutical.

Usually, however, the radionuclide will need to be chemically coupled to 'radiolabel' its vector molecule using radionuclide-specific radiochemical methodology. The presence of the radionuclide should not interfere with the binding of the vector to its target, nor with the vector's access to its target. The latter is especially important for intracellular and CNS targets. Ideally, the radiolabelling reaction should proceed quickly (to avoid loss of activity due to radionuclide decay and to simplify the radiolabelling process) and efficiently (a high fraction of the radionuclide chemically bonded to the vector). A fast and efficient reaction may provide the radiopharmaceutical immediately in a form that can be injected intravenously as such. This is achieved in the "kit" preparation method largely applied for preparation of $^{99m}$Tc-radiopharmaceuticals used for SPECT. An important aspect of this approach is that the radiochemical reaction should be carried out in aqueous conditions with high yield (>90%), and that reagents and precursors required for labelling should be compatible with IV injection and should not compete with binding of the radiopharmaceutical to its target. If these conditions are met, no downstream purification is required and the kit preparation procedure will be limited to adding the radionuclide solution (from a generator or cyclotron) to the radiolabelling kit.

Radiometal chelation (complexation or coordination) involves binding of the radiometal via multiple bonds (up to 6 or more) with multiple atoms of the chelator (complexating agent, ligand). The complexation is a reversible equilibrium reaction consisting of association and dissociation of the metal with the chelator. The charge, oxidation state and radius of the radiometal are important parameters that define the interaction of the radiometal with the chelator. The structures of frequently used chelators for radiometal-based PET radiopharmaceuticals are shown in Figure 2.

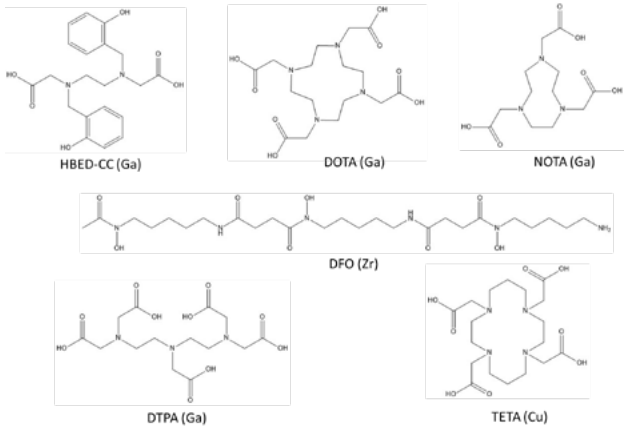


*Figure 2 Frequently used chelators for positron-emitting radiometal-based radiopharmaceuticals*

Vector molecules such as peptides, and especially larger proteins, including antibodies, can be coupled with the relatively bulky chelator/radiometal combinations without compromising their affinity for the target. Radiometal-based labelling thus provides an excellent match with vectors consisting of peptides and proteins. Complexation of radiometals by chelator peptides or chelator- protein conjugates can be performed at room temperature and in aqueous conditions in the absence of organic solvents. This can be performed using either "kit" labelling or more complicated radiochemical procedures in automated synthesis modules.

Small molecule-based radiopharmaceuticals are usually derived from xenobiotics (including drugs) or small biochemicals (e.g. [$^{18}$F]FDG). They generally do not tolerate derivatisation with bulky chelator/radiometal constructs, as this will lead to loss of affinity for the envisaged target and/or compromised access to the target (e.g. brain or intracellular targets). In this case radiolabelling by covalent binding with non-metals ($^{11}$C, $^{18}$F) is applied. For carbon-11, "isotopic" labelling can be applied in which a stable carbon atom is substituted for carbon-11 so that the resulting $^{11}$C-labelled radiopharmaceutical will have identical pharmacological characteristics to its stable counterpart (e.g. [$^{11}$C]methionine will behave identically to the natural amino acid methionine). As incorporation of fluorine-18 and carbon-11 in the vector molecule has minimum or no impact on the target affinity, both are excellent radionuclides for radiolabelling of small molecules.

Covalent binding is achieved by organic chemistry methodology. This involves the use of specific precursor molecules, organic solvents (e.g. acetonitrile, dimethylformamide, dimethylsulfoxide, etc.), specific reagents (e.g. kryptofix for radiofluorination) and heating to high temperatures. This may involve different consecutive reactions and often requires purification of the radiopharmaceutical by means of high-performance liquid chromatography (HPLC). Radiosynthesis of carbon-11 and fluorine-18 radiopharmaceuticals is performed in automated synthesis modules placed in lead-shielded (5–10 cm) hot cells. Quality control of fluorine-18 and carbon-11-labelled radiopharmaceuticals generally requires analysis using HPLC (identity confirmation) and gas chromatography (GC, assay for residual organic solvents). Overall, the preparation of carbon-11 and fluorine-18 radiopharmaceuticals is therefore more complex than preparation of radiometal complexes.

## PET RADIOPHARMACEUTICALS

A limited number of PET radiopharmaceuticals (Figure 3) are discussed in more detail in the following to illustrate the principles discussed above.

### [$^{18}$F]FDG

2-[$^{18}$F]Fluoro-2-deoxy-D-glucose ([$^{18}$F]FDG) is the most widely used PET radiopharmaceutical and is applied in oncology, cardiology and neurology. [$^{18}$F]FDG is a glucose analogue and is a substrate for the "GLUT" glucose transporters that allow passage of glucose (and [$^{18}$F]FDG)

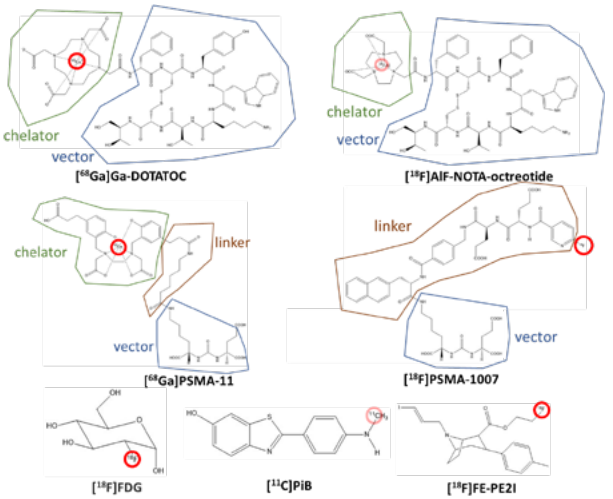


*Figure 3 Chemical structure of some examples of PET radiopharmaceuticals*

across the cell membrane. In the cell, [$^{18}$F]FDG is enzymatically converted to [$^{18}$F]FDG-6-phosphate by hexokinase in a similar way to the conversion of glucose to glucose-6-phosphate. Due to the substitution of the carbon-2 hydroxyl group in glucose by a fluorine atom, [$^{18}$F]FDG-phosphate is not a substrate for the next metabolic step and remains trapped in the cell. The cellular concentration of [$^{18}$F]FDG-6-phosphate will thus reflect cellular glucose metabolism.

Glucose metabolism is up-regulated in almost all tumour cells (due to the Warburg effect), and therefore [$^{18}$F]FDG /PET is applied in oncology for staging and treatment monitoring of a variety of tumours.

Brain uses glucose as its main energy source and therefore [$^{18}$F]FDG/PET can be used to image characteristic patterns of glucose hypometabolism, allowing diagnosis of neurodegenerative diseases. As activated inflammatory cells show increased glucose metabolism, [$^{18}$F]FDG/PET can also be used to visualise infections and inflammation. Furthermore, [$^{18}$F]FDG/PET can also be used in cardiology to identify ischaemic but viable myocardium which may thus benefit from revascularisation therapy[16].

Glucose can be considered as a biochemical-based small molecule vector which is difficult if not impossible to radiolabel with a chelator/radiometal without jeopardising its affinity for GLUT and hexokinase.

### [$^{11}$C]PiB, [$^{18}$F]Florbetapir, [$^{18}$F] Florbetaben and [$^{18}$F]Flutemetamol

[$^{11}$C]PiB (Pittsburg compound -B, 2-(4-N-[$^{11}$C]methylaminophenyl)-6-hydroxybenzothiazole) is a small molecule derived from Thioflavin-T, a reagent which has been used for decades by neuropathologists to stain amyloid plaques in brain slices. [$^{11}$C]PiB binds with high affinity to amyloid-beta plaques in the brain of Alzheimer's disease patients, aiding the diagnosis of this neurodegenerative disease.

Due to its short half-life (20.4 min), labelling with carbon-11 restricts the use of [$^{11}$C]PiB to PET centres that have a cyclotron in their immediate vicinity. Several fluorine-18 derivatives ([$^{18}$F] Florbetapir, [$^{18}$F]Florbetaben and [$^{18}$F] Flutemetamol) were therefore developed to allow production of large batches of the radiopharmaceutical that can be shipped over long distances to remote PET centres.

### [$^{18}$F]FE-PE2I

[$^{18}$F]FE-PE2I is a small-molecule cocaine derivative that binds with high affinity to the dopamine transporter (DAT) in brain. Parkinson's patients suffer from progressive degeneration of nigrostriatal dopaminergic neurons that selectively express the DAT. [$^{18}$F]FE-PE2I/PET imaging allows diagnostic work-up of patients with Parkinsonism and [$^{18}$F]FE-PE2I/PET produces better resolution compared to $^{123}$I-FP-CIT-SPECT, which has been used clinically for several decades.







### [$^{68}$Ga]PSMA-11 and [$^{18}$F]PSMA-1007

Prostate-specific membrane antigen (PSMA) is a proteolytic transmembrane glycoprotein which is strongly overexpressed on prostate cancer cells. The pseudopeptide glutamate urea-lysine has high affinity for PSMA and has been used as a vector molecule for different radiolabelled derivatives that have been pursued for prostate cancer imaging with PET. [$^{68}$Ga]PSMA-11 is a derivative in which HBED-CC, a specific chelator for gallium, is conjugated via a linker to glutamate-urea-lysine. [$^{68}$Ga]PSMA-11 can be easily prepared using a "kit" approach or alternatively using a synthesis module.

In the case of [$^{18}$F]PSMA-1007, 2-[$^{18}$F] fluoro nicotinic acid is conjugated via a tetrapeptide linker to the glutamate-urea-lysine vector. In contrast to[$^{68}$Ga] PSMA-11, [$^{18}$F]PSMA-1007 is not excreted via the urine, facilitating detection of local relapse of prostate cancer as interfering activity in the bladder and urethra is absent. Furthermore, [$^{18}$F]PSMA-1007 can be produced in large batches and shipped over longer distances, making it a more economically efficient alternative to [$^{68}$Ga] PSMA-11.

### SSTR-targeting PET radiopharmaceuticals

Somatostatin receptors (SSTR) are highly expressed on tumour cells of gastroenterohepatic neuroendocrine tumours. Somatostatin is the endogenous peptide which has affinity for the somatostatin receptors, but it is quickly degraded ***in vivo*** and therefore not suitable as a vector molecule. The synthetic somatostatin derivative octreotide is an eight-amino-acid cyclic peptide with high affinity and stability and is used as a vector for several SSTR-targeting radiopharmaceuticals.

[$^{68}$Ga]Ga-DOTATOC, [$^{68}$Ga]Ga-DOTATATE and [$^{68}$Ga]Ga-DOTANOC are conjugates of the DOTA chelator with structurally related derivatives of octreotide that are used clinically for SSTR-PET.

Various fluorine-18-labelled octreotide derivatives have been proposed, and the initial clinical application of [$^{18}$F]AlF-NOTA-octreotide has recently been reported. This radiopharmaceutical combines aluminium metal chelation chemistry with the favourable physical properties of fluorine-18. The vector is derivatised with the NOTA chelator, which forms a complex with aluminium [$^{18}$F]fluoride.

### [$^{18}$F]fluoride

[$^{18}$F]Fluoride is one of the smallest radiopharmaceuticals and combines the vector function with the radionuclide. [$^{18}$F] fluoride is obtained as such from cyclotron irradiation of [$^{18}$O]$H_2O$ and is purified on an anion exchange cartridge to remove radiometal contaminants associated with cyclotron irradiation. The resulting [$^{18}$F] fluoride solution is sterile filtered to provide [$^{18}$F]fluoride as a radiopharmaceutical. Although the earliest reports of the use of [$^{18}$F]fluoride for bone scanning date from the 1960s, it underwent a revival after the introduction of clinical PET cameras as an alternative to $^{99m}$Tc-diphosphonate/SPECT for bone scanning. Both tracers share chemisorption to bone as their binding mechanism, where fluoride is chemically incorporated in bone as [$^{18}$F]fluoro-apatite. [$^{18}$F]fluoride/PET has a better accuracy for detection of bone metastases compared to $^{99m}$Tc-diphosphonate/SPECT. Whereas a waiting time of 3h is required for $^{99m}$Tc-disphophonate, patients can be scanned 60 min after [$^{18}$F]fluoride injection due to the faster blood clearance of [$^{18}$F]fluoride.

## GA-68-LABELLED VS. F-18-LABELLED RADIOPHARMACEUTICALS

PET imaging of neuroendocrine tumours with $^{68}$Ga-labelled somatostatin analogues (e.g. [$^{68}$Ga]Ga-DOTATATE) is a well-established and validated technique. The advantage of gallium-68 is that it can be made available from a $^{68}$Ge/$^{68}$Ga generator in nuclear medicine departments, thus not requiring a cyclotron. In the beginning, these generators were only available in larger nuclear medicine departments with dedicated radiopharmacy staff. However, the fast clinical roll-out of [$^{68}$Ga]PSMA-11 for imaging of prostate cancer patients has made $^{68}$Ge/$^{68}$Ga generators more widely available over the last couple of years. Although $^{68}$Ga-PET has been a success story, the use of gallium-68 as a radionuclide also has several disadvantages, mainly of a logistical nature.

Because 1) the overall activity yield per production batch of $^{68}$Ga-labelled compound is low (capacity of two to four patients per production), 2) the half-life of gallium-68 is relatively short (68 min), and 3) there is a high demand for $^{68}$Ga-PET scans in the clinics (e.g. [$^{68}$Ga]PSMA-11, [$^{68}$Ga]Ga-DOTATATE, etc.), no centralised production and distribution is possible and waiting lists for $^{68}$Ga-PET scans are long. Furthermore, nuclear medicine departments that have no $^{68}$Ge/$^{68}$Ga generator on site cannot offer $^{68}$Ga-PET scans to their patients. In future, advances in the cyclotron production of gallium-68 may open up further possibilities in this field. Apart from the logistical disadvantages, gallium-68 also has drawbacks based on its physical characteristics. It has a relatively high positron energy and thus a relatively long positron range (>1 mm range in tissue) which may result in suboptimal spatial resolution, especially in low-density tissue such as the lungs. However, this effect will be minimal and only of clinical relevance in the next generation of clinical PET scanners.

Among positron-emitting radionuclides, fluorine-18 is the most commonly used for clinical PET imaging and offers several logistical advantages over gallium-68: fluorine-18 can be produced by cyclotrons in large amounts (>100 patient doses) and its longer half-life of 109.8 min allows fluorine-18-labelled tracers to be transported over long distances. Therefore, production and quality control of $^{18}$F-labelled radiopharmaceuticals can be centralised and they can be shipped to remote hospitals that do not have a cyclotron on site, so that these remote PET centres do not need to invest in dedicated radiopharmacy staff and expensive production and quality control infrastructure. Fluorine-18 also has a low positron energy and hence a shorter positron range (<1 mm range in tissue), offering higher intrinsic spatial resolution compared to $^{68}$Ga.

For PET imaging of PSMA in prostate cancer, $^{18}$F-labelled compounds such as [$^{18}$F]PSMA-1007 have been developed to accommodate the high tracer demand in this field. Development of $^{18}$F-labelled compounds has likewise been successful in PET imaging of SSTR, an excellent example being [$^{18}$F]AlF-NOTA-octreotide. In this case the Al$^{18}$F-labelling method combines the advantages of a chelator-based radiolabelling method with the unique properties of fluorine-18. The same approach has been used in the field of fibroblast-activating protein inhibitor (FAPI) tracers (see 5). Al$^{18}$F-FAPI tracers (e.g. [$^{18}$F]AlF-FAPI-74) have been developed in parallel with $^{68}$Ga-FAPI tracers (e.g. $^{68}$Ga-FAPI-46) to accommodate the expected high demand for this new class of tracers[27].

## FAPI TRACERS

[$^{18}$F]FDG is by far the most often-used PET tracer in nuclear medicine. However, [$^{18}$F]FDG has some disadvantages such as 1) variable uptake in normal organs such as muscle, heart, brown fat, bowel, etc. and 2) low uptake in a range of tumour types that exhibit a low glycolytic phenotype (low GLUT, low hexokinase, high glucose-6-phosphatase). Most alternatives to [$^{18}$F]FDG are radiotracers that target the overexpression of one specific target, mostly present on the surface of the cancer cells, making these radiotracers very specific to a single tumour type that overexpresses this key molecule. They are therefore of little use in most tumoural entities, where [$^{18}$F]FDG performs poorly.

Since 2018, a novel class of "FAPI" PET tracers has emerged with a strong potential to replace or complement [$^{18}$F]FDG as a general tumour tracer. FAPI tracers do not target the cancer cells themselves, but

target cancer-associated fibroblasts (CAFs) in the tumour micro-environment (also called tumour stroma). Indeed, malignant tumours consist of cancer cells and a variety of non-malignant cells that form the tumour micro-environment. CAFs are the most abundant type of cells in the tumour stroma and can make up as much as 90% of the total tumoural volume. These CAFs overexpress fibroblast activation protein α (FAP), a type II membrane-bound glycoprotein that plays an important role in tumour development and progression. Furthermore, FAP is also overexpressed in lung and heart myofibroblasts and can thus be used as a biomarker for fibroblast activity in heart and lung disease. In contrast, no or only insignificant levels of the protein are present in normal fibroblast and in healthy adult tissue.

This novel class of PET tracers is based on FAP inhibitors (FAPI) and consists of a quinoline-based vector molecule connected to a suitable chelator allowing chelation of radiometals such as gallium-68. These FAPIs specifically bind to the enzymatic domain of FAP and are then internalised[25]. A whole series of FAPI ligands has been developed, with $^{68}$Ga-FAPI-04 and $^{68}$Ga-FAPI-74 being the most promising to have been evaluated in clinical studies so far (Figure 4).

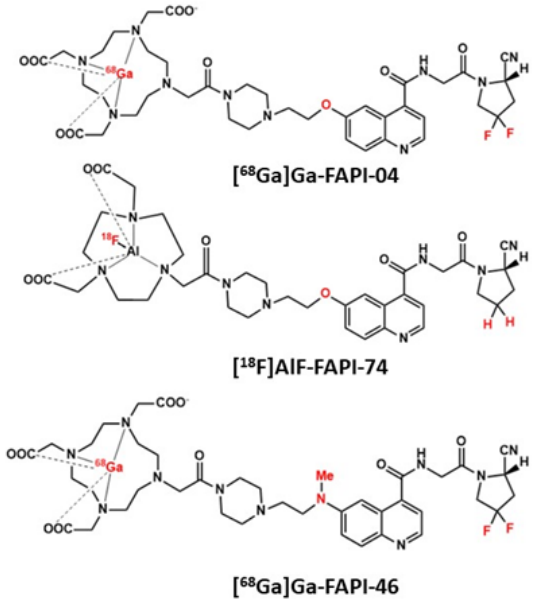


*Figure 4. Chemical structures of a selection of the most promising fibroblast-activating protein inhibitor (FAPI) PET tracers*







FAPI PET images are characterised by rapid kinetics, very low background activity (no uptake in brain, muscle, brown fat, bowel, etc.) and high target (tumour)-to-background contrast as fast as 10 min after tracer administration. Interestingly, in contrast to [$^{18}$F]FDG PET, no diet or fasting is required in preparation for the $^{68}$Ga-FAPI PET examination. Initial publications with $^{68}$Ga-FAPI tracers in patients show high tumour uptake and good detection of metastases in a variety of human cancer types. Furthermore, radioactivity was seen only in the renal pelvis and the bladder with no accumulation in the kidneys, which is favourable for therapeutic applications. Indeed, since the FAPI ligands are chelator-based (DOTA), these molecules may also be used for therapeutic applications labelled with β- or α-emitters. $^{68}$Ga-FAPIs have the potential to become a routine clinical tracer for low [$^{18}$F]FDG-avid tumours and a biomarker for fibroblast activity in heart and lung disease, which may have a significant impact on diagnosis and determination of prognosis, as well as on the clinical management of these patients.

Recently, $^{18}$F-labelled FAPIs have also been developed (e.g. [$^{18}$F]AlF-FAPI-74 (see Figure 4) and [$^{18}$F]AlF-FAPI-04)[7]. These consist of a quinoline-based vector molecule connected to a suitable chelator allowing chelation of [$^{18}$F]AlF. $^{18}$F-labelled tracers have many logistical advantages over $^{68}$Ga-labelled PET tracers (see chapter 4), therefore this development can be considered as a major upgrade. FAPI tracers are expected to become part of clinical routine, and there will be a high clinical demand for FAPI-PET in the near future.

## REFERENCES


1. Vermeulen K, Vandamme M, Bormans G, Cleeren F. Design and Challenges of Radiopharmaceuticals. Semin Nucl Med. 2019 Sep;49(5):339-356. doi: 10.1053/j.semnuclmed.2019.07.001. Epub 2019 Jul 20.
2. Natarajan A.Copper-64-immunoPET imaging: bench to bedside. Q J Nucl Med Mol Imaging. 2020 Dec;64(4):356-363. doi: 10.23736/S1824-4785.20.03310-5. Epub 2020 Oct 12.
3. ImmunoPET: Concept, Design, and Applications.Wei W, Rosenkrans ZT, Liu J, Huang G, Luo QY, Cai W. Chem Rev. 2020 Apr 22;120(8):3787-3851. doi: 10.1021/acs.chemrev.9b00738. Epub 2020 Mar 23.
4. Kumar K, Ghosh A. Radiochemistry, Production Processes, Labeling Methods, and ImmunoPET Imaging Pharmaceuticals of Iodine-124. Molecules. 2021 Jan 14;26(2):414. doi: 10.3390/molecules26020414.
5. Thisgaard H, Kumlin J, Langkjær N, Chua J, Hook B, Jensen M, Kassaian A, Zeisler S, Borjian S, Cross M, Schaffer P, Dam JH. Multi-curie production of gallium-68 on a biomedical cyclotron and automated radiolabelling of PSMA-11 and DOTATATE. EJNMMI Radiopharm Chem. 2021 Jan 7;6(1):1. doi: 10.1186/s41181-020-00114-9.
6. Rodnick ME, Sollert C, Stark D, Clark M, Katsifis A, Hockley BG, Parr DC, Frigell J, Henderson BD, Abghari-Gerst M, Piert MR, Fulham MJ, Eberl S, Gagnon K, Scott PJH.Cyclotron-based production of (68)Ga, [(68)Ga]GaCl(3), and [(68)Ga]Ga-PSMA-11 from a liquid target. EJNMMI Radiopharm Chem. 2020 Nov 12;5(1):25. doi: 10.1186/s41181-020-00106-9.
7. Am J Nucl Med Mol Imaging 2019;9(1):30-66 www.ajnmmi.us /ISSN:2160-8407/ajnmmi0086228
8. Ahmadi A, Klein R, Lewin HC, Beanlands RSB, deKemp RA. Rubidium-82 generator yield and efficiency for PET perfusion imaging: Comparison of two clinical systems. J Nucl Cardiol. 2020 Oct;27(5):1728-1738. doi: 10.1007/s12350-020-02200-6. Epub 2020 May 20.
9. https://www.ema.europa.eu/en/medicines/human/paediatric-investigation-plans/emea-000882-pip03-11-m04
10 . Ghotbi AA, Kjaer A, Hasbak P.Review: comparison of PET rubidium-82 with conventional SPECT myocardial perfusion imaging. Clin Physiol Funct Imaging. 2014 May;34(3):163-70
11. Kostenikov NA, Zhuikov BL, Chudakov VM, Iliuschenko YR, Shatik SV, Zaitsev VV, Sysoev DS, Stanzhevskiy AA.Application of 82 Sr/82 Rb generator in neurooncology. Brain Behav. 2019 Mar;9(3):e01212. doi: 10.1002/brb3.1212
12. Jochumsen MR, Bouchelouche K, Nielsen KB, Frøkiær J, Borre M, Sörensen J, Tolbod LP. Repeatability of tumor blood flow quantification with (82)Rubidium PET/CT in prostate cancer- a test-retest study. EJNMMI Res. 2019 Jul 4;9(1):58. doi: 10.1186/s13550-019-0529-2.
13. Conti M, Eriksson L. Physics of pure and non-pure positron emitters for PET: a review and a discussion. EJNMMI Phys. 2016 Dec;3(1):8. doi: 10.1186/s40658-016-0144-5. Epub 2016 May 23.
14. Mohan AM, Beindorff N, Brenner W. Nuclear Medicine Imaging Procedures in Oncology. Methods Mol Biol. 2021;2294:297-323. doi: 10.1007/978-1-0716-1350-4_21
15. Cecchin D, Garibotto V, Law I, Goffin K. PET Imaging in Neurodegeneration and Neuro-oncology: Variants and Pitfalls.Semin Nucl Med. 2021 Apr 3:S0001-2998(21)00016-7. doi: 10.1053/j.semnuclmed.2021.03.003
16. Zhuang H, Codreanu I. Growing applications of FDG PET-CT imaging in non-oncologic conditions. J Biomed Res. 2015 May;29(3):189-202. doi: 10.7555/JBR.29.20140081
17. Suppiah S, Didier MA, Vinjamuri S. The Who, When, Why, and How of PET Amyloid Imaging in Management of Alzheimer's Disease-Review of Literature and Interesting Images.Diagnostics (Basel). 2019 Jun 25;9(2):65. doi: 10.3390/diagnostics9020065.
18. Delva A, Van Weehaeghe D, van Aalst J, Ceccarini J, Koole M, Baete K, Nuyts J, Vandenberghe W, Van Laere K. Quantification and discriminative power of 18F-FE-PE2I PET in patients with Parkinson's disease. Eur J Nucl Med Mol Imaging. 2020 Jul;47(8):1913-1926. doi: 10.1007/s00259-019-04587-y
19. Pastorino S, Riondato M, Uccelli L, Giovacchini G, Giovannini E, Duce V, Ciarmiello A. Toward the Discovery and Development of PSMA Targeted Inhibitors for Nuclear Medicine Applications. Curr Radiopharm. 2020;13(1):63-79. doi: 10.2174/1874471012666190729151540
20. Ebenhan T, Vorster M, Marjanovic-Painter B, Wagener J, Suthiram J, Modiselle M, Mokaleng B, Zeevaart JR, Sathekge M. Development of a Single Vial Kit Solution for Radiolabeling of 68Ga-DKFZ-PSMA-11 and Its Performance in Prostate Cancer Patients. Molecules. 2015 Aug 14;20(8):14860-78. doi: 10.3390/molecules200814860
21. Pauwels E, Cleeren F, Bormans G, Deroose CM.Somatostatin receptor PET ligands - the next generation for clinical practice. Am J Nucl Med Mol Imaging. 2018 Oct 20;8(5):311-331.
22. Pauwels E, Cleeren F, Tshibangu T, Koole M, Serdons K, Dekervel J, Van Cutsem E, Verslype C, Van Laere K, Bormans G, Deroose CM. [18F]AlF-NOTA-octreotide PET imaging: biodistribution, dosimetry and first comparison with [68Ga]Ga-DOTATATE in neuroendocrine tumour patients. Eur J Nucl Med Mol Imaging. 2020 Dec;47(13):3033-3046. doi: 10.1007/s00259-020-04918-4
23. Ahuja K, Sotoudeh H, Galgano SJ, Singh R, Gupta N, Gaddamanugu S, Choudhary G. 18F-Sodium Fluoride PET: History, Technical Feasibility, Mechanism of Action, Normal Biodistribution, and Diagnostic Performance in Bone Metastasis Detection Compared with Other Imaging Modalities.J Nucl Med Technol. 2020 Mar;48(1):9-16. doi: 10.2967/jnmt.119.234336.
24. Tshibangu T, Cawthorne C, Serdons K, Pauwels E, Gsell W, Bormans G, Deroose CM, Cleeren F. Automated GMP compliant production of [18F]AlF-NOTA-octreotide.EJNMMI Radiopharm Chem. 2020 Jan 29;5(1):4.
25. Hicks RJ, Roselt PJ, Kallur KG, Tothill RW, Mileshkin L. FAPI PET/CT: Will It End the Hegemony of 18F-FDG in Oncology? J Nucl Med. 2021 Mar;62(3):296-302.
26. Kalluri R. The biology and function of fibroblasts in cancer. Nat Rev Cancer. 2016 Aug 23;16(9):582-98
27. Altmann A, Haberkorn U, Siveke J. The Latest Developments in Imaging of Fibroblast Activation Protein. J Nucl Med. 2021 Feb;62(2):160-167.
28. Giesel FL, Kratochwil C, Lindner T, Marschalek MM, Loktev A, Lehnert W, Debus J, Jäger D, Flechsig P, Altmann A, Mier W, Haberkorn U. 68Ga-FAPI PET/CT: Biodistribution and Preliminary Dosimetry Estimate of 2 DOTA-Containing FAP-Targeting Agents in Patients with Various Cancers. J Nucl Med. 2019 Mar;60(3):386-392.
29. Giesel FL, Adeberg S, Syed M, Lindner T, Jiménez-Franco LD, Mavriopoulou E, Staudinger F, Tonndorf-Martini E, Regnery S, Rieken S, El Shafie R, Röhrich M, Flechsig P, Kluge A, Altmann A, Debus J, Haberkorn U, Kratochwil C. FAPI-74 PET/CT Using Either (18)F-AlF or Cold-Kit (68)Ga Labeling: Biodistribution, Radiation Dosimetry, and Tumor Delineation in Lung Cancer Patients. J Nucl Med. 2021 Feb;62(2):201-207.
30. Jiang X, Wang X, Shen T, Yao Y, Chen M, Li Z, Li X, Shen J, Kou Y, Chen S, Zhou X, Luo Z, Cheng Z. FAPI-04 PET/CT Using [18F]AlF Labeling Strategy: Automatic Synthesis, Quality Control, and In Vivo Assessment in Patient. Front Oncol. 2021 Mar 19;11:649148.

# 6

# ADVANCES IN NEUROIMAGING

*by Donatienne Van Weehaeghe*

PET/CT scans are an established clinical tool in neurodegenerative dementias and epilepsy. The most clinically used PET tracer is [$^{18}$F]FDG. [$^{18}$F]FDG allows visualisation of brain metabolism ***in vivo*** and is a proxy for neuronal activity.

The EANM Tech Guide of 2016 provides a general overview of the different brain tracers. In this chapter we will focus on the clinical applications of [$^{18}$F]FDG PET/CT imaging in epilepsy and neurodegenerative disorders such as amyotrophic lateral sclerosis (ALS), Alzheimer's disease (AD) and several parkinsonian syndromes. Depending on the clinical question, the CT scan can be performed using a regular tube current (diagnostic CT if anatomical information is needed) or a low tube current (low-dose CT for attenuation correction only). The main advantage of PET/CT scans is the faster acquisition time compared to the stand-alone PET scans, where attenuation correction is performed using a transmission scan. Especially in non-compliant patients, fast acquisition times are essential to increase patient comfort and clinical applicability.

Ideally, patients should fast for at least 4 hours and blood glucose levels should be < 160 mg/dl. Typically, 150 MBq is administered and a 15-minute static scan is started at least 30 minutes post injection. More information regarding acquisition can be found in the EANM procedure guidelines of 2009 (***1***).

## [$^{18}$F]FDG PET/CT IN EPILEPSY

Fifty out of every 100 000 people per year develop epilepsy. In a third of these patients, seizures cannot be controlled by anti-epileptic drugs. If a focal epileptogenic focus can be identified and patients are fit for surgery, epileptic surgery can be performed (2).

Localisation of the epileptogenic focus is crucial prior to epileptic surgery. Functional imaging using [$^{18}$F]FDG PET and SPECT tracers is recommended in the guidelines published by the neuroimaging subcommission of the International League Against Epilepsy (3). SPECT tracers, such as HMPAO and ECD, are used to evaluate regional blood flow as a proxy for neuronal activity (4). Sensitivity and specificity are ameliorated by subtracting ictal from interictal scans and co-registration with a structural MRI scan (5). [$^{18}$F]FDG PET scans are performed in an interictal state to detect focal regions of hypometabolism. Seizure activity during the [$^{18}$F]FDG uptake period (from time of injection to scan) can lead to false positive and negative results (6). Therefore, EEG recording prior to and after [$^{18}$F]FDG injection is needed to confirm the absence of seizure activity. Although the observed hypometabolism is sensitive, it is not specific. Brain metabolism should therefore be interpreted on the basis of clinical and other neuroimaging findings (6).

The exact reason for the hypometabolism remains unclear, although it is suggested to reflect disturbances in neuronal activity caused by epileptogenic tissue. The hypometabolic area is called the functional deficit zone. The functional deficit zone can be larger than the seizure focus as it represents both the focus and the projections / additional neuronal disturbances of the seizure activity (7). Figure 1 demonstrates the functional deficit zone in a patient with temporal lobe epilepsy.

### Prognostic impact

Patients with temporal lobe epilepsy in which more of the functional deficit zone was resected had a better postoperative outcome (8). However, patients with hypometabolism distant from the seizure focus had a worse prognosis (9, 10). Moreover, a similar outcome was observed in patients with unilateral temporal lobe epilepsy and a clear functional deficit zone concordant with EEG findings and in patients with an abnormal MRI (6, 11). Currently, most studies focus on patients with temporal lobe epilepsy, while evidence in still scarce in extratemporal lobe epilepsy. Nevertheless, in extratemporal lobe epilepsy results are promising when PET scans function as a guide to localise the epileptogenic focus (11). [$^{18}$F]FDG is thus valuable in localising the functional deficit zone prior to epileptic surgery.

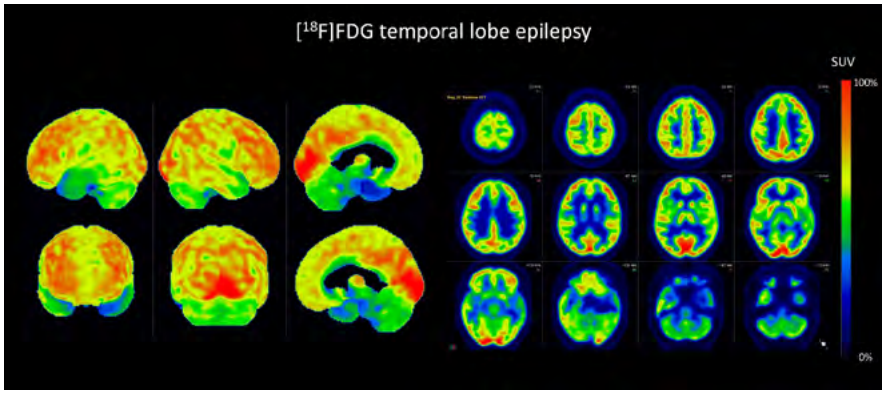


*Figure 1: Functional deficit zone in the left temporal cortex in a patient with temporal lobe epilepsy.*

## PET/CT IN NEURODEGENERATIVE DISEASES

### Amyotrophic lateral sclerosis

ALS is a neurodegenerative motor neuron disease. Patients present with a variety of motor symptoms such as dysphagia, dysarthria, muscle weakness and drop foot (*12*). There exists a continuum between ALS and frontotemporal dementia (FTD). Fifty per cent of patients have some minor cognitive and behavioural complaints, while 5–15% have overt FTD (*13*). Clinical diagnosis is based on clinical and electrophysiological tests. However, differential diagnosis with other (neuro)muscular diseases (ALS mimics) is challenging, as demonstrated by the average diagnostic delay of about one year (*12*). ALS mimics are a heterogeneous group consisting of patients with symptoms mimicking the symptoms of ALS, such as Kennedy's diseases, cervical stenosis, and polyneuropathy. After final diagnosis is reached, the disease trajectory is difficult to predict. ALS is considered as a heterogeneous syndrome rather than a single disease entity, with a broad range of clinical symptoms and survival durations. Some patients only live several months, while others survive for decades. Currently no effective treatment is available, although Edaravone and Riluzole – the only clinically available drugs – prolong life by several months in a subgroup of the disease (*13*).

### Metabolic pattern

Patients with ALS display hypometabolism in the primary, pre- and supplementary motor cortices, extending to the frontoparietal cortex, and hypermetabolism in the medial temporal cortex, cerebellum and brain stem. This brain metabolic pattern provides prognostic information, as patients with extensive frontotemporal hypometabolism have a worse prognosis (*14*). An example of the metabolic pattern in a patient with ALS with and without FTD can be found in Figures 2 and 3, respectively.

Moreover, it has been demonstrated that this brain metabolic pattern is able to discriminate between ALS and controls with an accuracy higher than 90% (*14–16*). In a real-life clinical setting, the diagnostic dilemma is not between ALS and controls but between ALS and ALS mimics. Recently, our group showed that spinal cord metabolism differs significantly between ALS and ALS mimics, with a diagnostic accuracy of 80%. By contrast, brain metabolism had no discriminatory value as it was comparable in both groups. However, adding brain metabolic information to spinal cord metabolism resulted in a slightly higher predictive power (82%) to differentiate between ALS and ALS mimics (*17*).

In conclusion, brain [$^{18}$F]FDG scans have some prognostic power on an individual patient level, while diagnostic power is limited. [$^{18}$F]FDG spinal cord scans are a novel technique which can help in differential diagnosis between ALS and ALS mimics.







## ALZHEIMER'S DISEASE

AD is a neurodegenerative disease with cognitive and functional decline associated with age and finally resulting

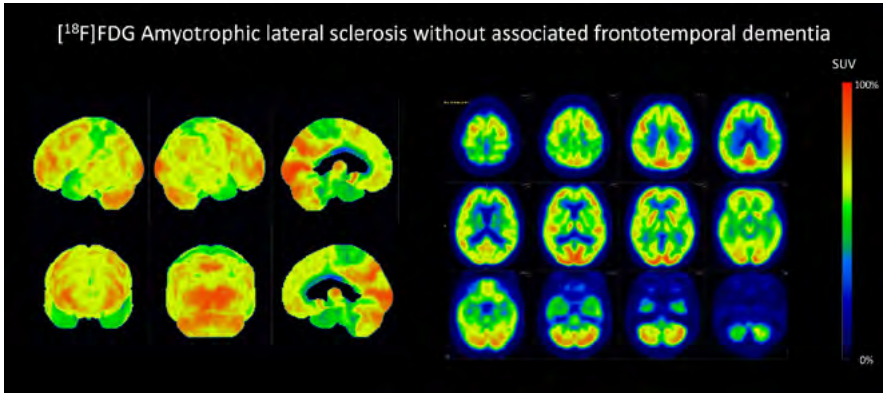


*Figure 2: Brain metabolic pattern in amyotrophic lateral sclerosis.*

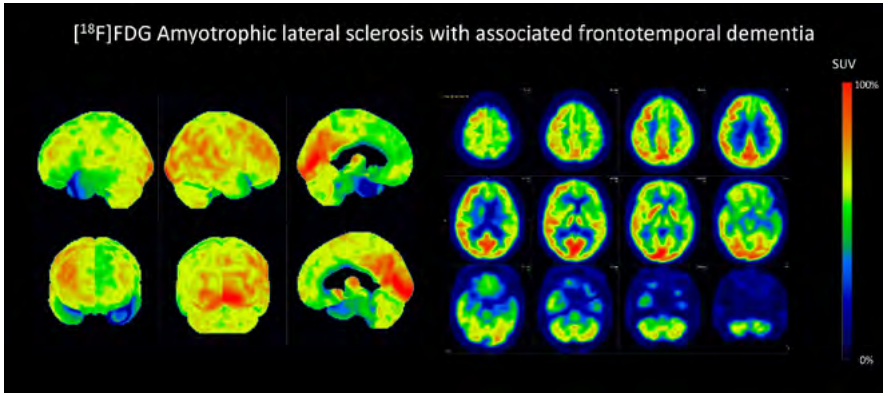


*Figure 3: Brain metabolic pattern in amyotrophic lateral sclerosis with concomitant frontotemporal dementia.*

in death. In patients with AD, amyloid deposits and neurofibrillary tangles of hyperphosphorylated tau are accumulated (***18***).

In 2018, the National Institute on Aging / Alzheimer's Association refined the clinical diagnostic criteria to take account of the added value of biomarkers in the diagnosis and identification of preclinical stages of the disease (***19***).

## Metabolic pattern

The disease-specific metabolic pattern consists of hypometabolism in the temporoparietal lobe, the precuneus and the posterior cingulate and is illustrated on Figure 4 (***20, 21***). [$^{18}$F]FDG PET is able to discriminate AD from other causes of dementia such as Lewy body dementia (LBD) and FTD. In LBD there is a partial overlap of the hypometabolic pattern, however the relative preservation of the posterior cingulate cortex (cingulate island sign) and hypometabolism in the visual cortex allows differentiation. Accuracy in discriminating between AD and LBD is 72–96% (***22***). In FTD the disease-specific pattern consists of hypometabolism in the frontal, anterior temporal and anterior cingulate cortices (***21***). Diagnostic accuracy in discriminating between FTD and AD is 87–89% (***22***).

Besides having a diagnostic value, the brain metabolic pattern also has a prognostic one as patients with hypometabolism on [$^{18}$F]FDG PET scans have a faster cognitive decline and brain atrophy as compared to patients without (***23***).

## Amyloid imaging

The deposition of amyloid deposits is suggested to precede the cognitive symptoms of AD (***21***). Several groups

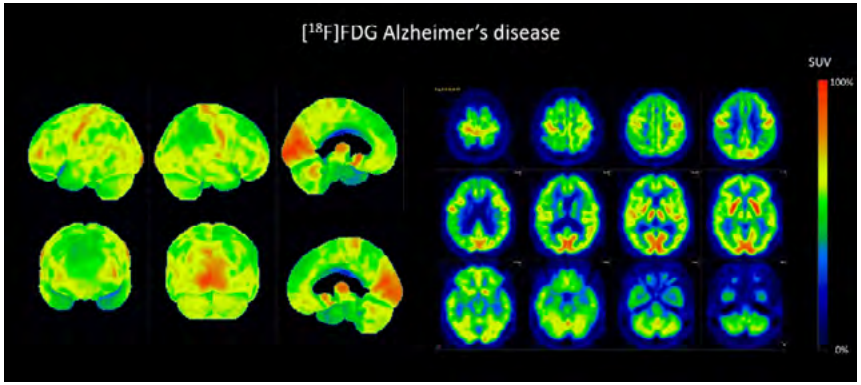


*Figure 4: Brain metabolic pattern in Alzheimer's disease.*







demonstrated a correlation between amyloid PET scans using [$^{11}$C]PIB and the amyloid deposition observed on pathological brain specimens. Thus, amyloid imaging may function as a preclinical marker (***24, 25***). In contrast to [$^{18}$F]FDG PET, amyloid scans have no prognostic value as the amount of cortical binding of amyloid PET tracers (such as [$^{11}$C]PIB, [$^{18}$F]flutemetamol, [$^{18}$F]florbetapir, [$^{18}$F]florbetaben) does not correspond to the cognitive impairment. Moreover, the amyloid PET uptake remains fairly stable across the disease. Additionally, amyloid positivity is not specific to AD, as LBD and cerebral amyloid angiopathy can also cause a positive amyloid scan (***21***). Nonetheless, amyloid scans can discriminate between FTD and AD with an accuracy of 97% (***26***). An illustrative example of a [$^{11}$C]PIB scan in an AD patient is given in Figure 5.

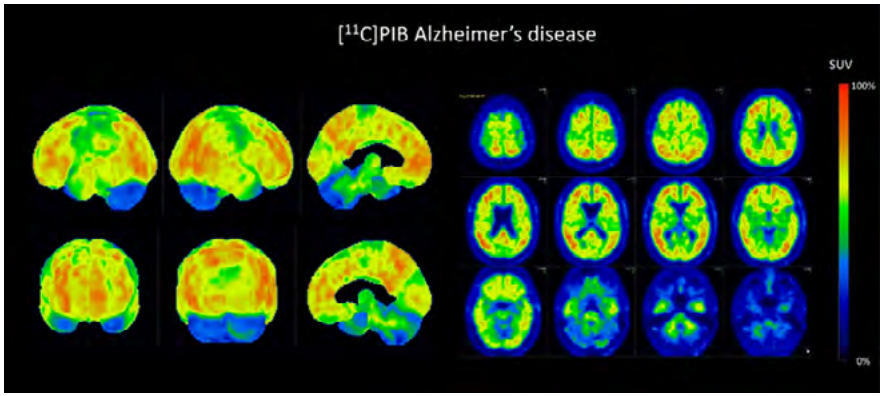


*Figure 5: [$^{11}$C]PIB positive scan in Alzheimer's disease ( high cortical [$^{11}$C]PIB uptake).*

## PARKINSONIAN SYNDROMES

Parkinson's disease is a chronic neurodegenerative disease characterised by bradykinesia and rigidity with or without resting tremor. Besides these cardinal motor symptoms, non-motor symptoms such as anosmia, constipation, depression and sleep disorders might be associated (***27***). The clinical presentation is heterogeneous, and differential diagnosis between PD and other types of parkinsonism can be difficult. Progressive supranuclear palsy (PSP), the parkinsonian variant of multiple system atrophy (MSA-P), corticobasal dementia (CBD) and non-neurodegenerative forms of parkinsonism (essential tremor, vascular, drug-induced) may mimic PD in the early stages of the disease (***28***).

Dopamine transport imaging (DAT scan) can differentiate between PD and the non-neurodegenerative forms of parkinsonism with a sensitivity of 87–98% and a specificity of 80–100% (***28***). In most centres dopamine transporter imaging is currently performed using [$^{123}$I]FP-CIT, a SPECT radioligand. However, several PET radioligands have been developed with promising results, such as [$^{18}$F]PE2I (***29***).

### Parkinson's disease

In PD striatal hypermetabolism is observed, in contrast to the striatal hypometabolism seen in MSA, CBD and PSP. Therefore, [$^{18}$F]FDG PET enables differential diagnosis between PD and MSA/CBD/PSP.

[$^{18}$F]FDG PET is also useful in predicting the risk of developing parkinsonian dementia. PD patients with associated cognitive impairment (mild cognitive impairment of dementia) have a characteristic pattern of hypometabolism in the posterior and temporal regions (***30***). Recently it has been demonstrated that [$^{18}$F]FDG PET has a sensitivity of 85% and a specificity of 88% in predicting which patients will progress to dementia in the following 4 years (***31***).

### Progressive supranuclear palsy

PSP patients may present with a variety of clinical symptoms. The most frequent phenotypes are PSP-Richardson's syndrome, i.e. patients with early postural instability and vertical ocular motor dysfunction, and PSP-parkinsonism, i.e. patients with symptoms similar to PD (***32***). The disease- specific pattern consists of hypometabolism in the medial frontal and anterior cingulate cortex, striatal and mid-brain regions (Figure 6) (***33***).

### Corticobasal dementia

CBD is another atypical parkinsonian syndrome. The main symptoms are dystonia, rigidity, akinesia, myoclonus, and tremor. Moreover, in most cases there is a marked asymmetry of the clinical symptoms, together with a marked asymmetry of the hypometabolic pattern (Figure 7) (***33***).

### Multiple system atrophy

MSA is characterised by parkinsonism, autonomic dysfunction and cerebellar ataxia. There are two subtypes of MSA: MSA-C, in which the cerebellar dysfunction is dominant, and MSA-P in which parkinsonism predominates. The hypometabolic pattern of MSA-P is mainly located in the bilateral putamen, while bilateral cerebellar hypometabolism is the hallmark of MSA-C (Figure 8) (***34***).

Overall, the specificity is > 90% in differentiating PD from atypical parkinsonism, while sensitivity is 83–86% (***33***).

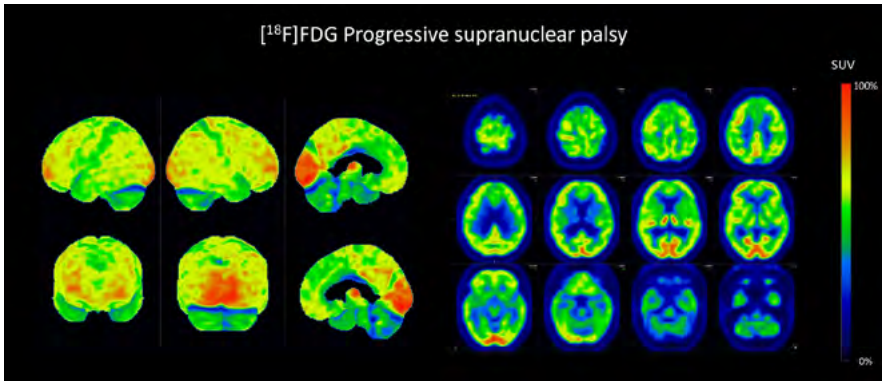


*Figure 6: Brain metabolic pattern in progressive supranuclear palsy.*

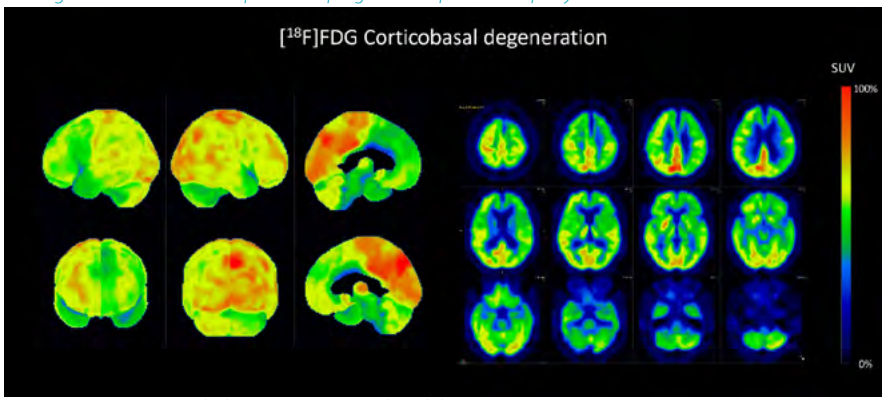


*Figure 7: Brain metabolic pattern in corticobasal dementia.*

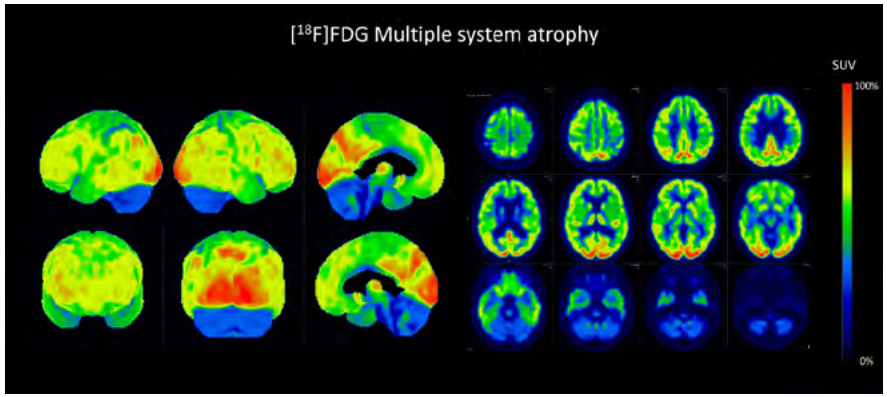


*Figure 8: Brain metabolic pattern in multiple system atrophy.*

## REFERENCES


1. Varrone A, Asenbaum S, Vander Borght T, et al. EANM procedure guidelines for PET brain imaging using [18F]FDG, version 2. Eur J Nucl Med Mol Imaging. 2009;36(12):2103-2110.
2. . The Epilepsies: The Diagnosis and Management of the Epilepsies in Adults and Children in Primary and Secondary Care: Pharmacological Update of Clinical Guideline 20. London; 2012.
3. Neuroimaging Subcommision of the International League Against E. Commission on Diagnostic Strategies: recommendations for functional neuroimaging of persons with epilepsy. Epilepsia. 2000;41(10):1350-1356.
4. Biersack HJ, Reichmann K, Winkler C, et al. 99mTc-labelled hexamethylpropyleneamine oxime photon emission scans in epilepsy. Lancet. 1985;2(8469-70):1436-1437.
5. O'Brien TJ, So EL, Mullan BP, et al. Subtraction ictal SPECT co-registered to MRI improves clinical usefulness of SPECT in localizing the surgical seizure focus. Neurology. 1998;50(2):445-454.
6. Cendes F, Theodore WH, Brinkmann BH, Sulc V, Cascino GD. Neuroimaging of epilepsy. Handb Clin Neurol. 2016;136:985-1014.
7. Knowlton RC. The role of FDG-PET, ictal SPECT, and MEG in the epilepsy surgery evaluation. Epilepsy Behav. 2006;8(1):91-101.
8. Vinton AB, Carne R, Hicks RJ, et al. The extent of resection of FDG-PET hypometabolism relates to outcome of temporal lobectomy. Brain. 2007;130(Pt 2):548-560.
9. Wong CH, Bleasel A, Wen L, et al. The topography and significance of extratemporal hypometabolism in refractory mesial temporal lobe epilepsy examined by FDG-PET. Epilepsia. 2010;51(8):1365-1373.
10. Wong CH, Bleasel A, Wen L, et al. Relationship between preoperative hypometabolism and surgical outcome in neocortical epilepsy surgery. Epilepsia. 2012;53(8):1333-1340.
11. Pittau F, Grouiller F, Spinelli L, et al. The role of functional neuroimaging in pre-surgical epilepsy evaluation. Front Neurol. 2014;5:31.
12. Salameh JS, Brown RH, Jr., Berry JD. Amyotrophic Lateral Sclerosis: Review. Semin Neurol. 2015;35(4):469-476.
13. van Es MA, Hardiman O, Chio A, et al. Amyotrophic lateral sclerosis. Lancet. 2017;390(10107):2084-2098.
14. Van Weehaeghe D, Ceccarini J, Delva A, et al. Prospective Validation of 18F-FDG Brain PET Discriminant Analysis Methods in the Diagnosis of Amyotrophic Lateral Sclerosis. J Nucl Med. 2016;57(8):1238-1243.
15. Pagani M, Oberg J, De Carli F, et al. Metabolic spatial connectivity in amyotrophic lateral sclerosis as revealed by independent component analysis. Hum Brain Mapp. 2016;37(3):942-953.
16. Van Laere K, Vanhee A, Verschueren J, et al. Value of 18fluorodeoxyglucose-positron-emission tomography in amyotrophic lateral sclerosis: a prospective study. JAMA Neurol. 2014;71(5):553-561.
17. Van Weehaeghe D, Devrome M, Schramm G, et al. Combined brain and spinal FDG PET allows differentiation between ALS and ALS mimics. Eur J Nucl Med Mol Imaging. 2020;47(11):2681-2690.
18. Sery O, Povova J, Misek I, Pesak L, Janout V. Molecular mechanisms of neuropathological changes in Alzheimer's disease: a review. Folia Neuropathol. 2013;51(1):1-9.
19. Soria Lopez JA, Gonzalez HM, Leger GC. Alzheimer's disease. Handb Clin Neurol. 2019;167:231-255.
20. Arbizu J, Festari C, Altomare D, et al. Clinical utility of FDG-PET for the clinical diagnosis in MCI. Eur J Nucl Med Mol Imaging. 2018;45(9):1497-1508.
21. Marcus C, Mena E, Subramaniam RM. Brain PET in the diagnosis of Alzheimer's disease. Clin Nucl Med. 2014;39(10):e413-422; quiz e423-416.
22. Nestor PJ, Altomare D, Festari C, et al. Clinical utility of FDG-PET for the differential diagnosis among the main forms of dementia. Eur J Nucl Med Mol Imaging. 2018;45(9):1509-1525.
23. Ou YN, Xu W, Li JQ, et al. FDG-PET as an independent biomarker for Alzheimer's biological diagnosis: a longitudinal study. Alzheimers Res Ther. 2019;11(1):57.
24. Ikonomovic MD, Klunk WE, Abrahamson EE, et al. Post-mortem correlates of in vivo PiB-PET amyloid imaging in a typical case of Alzheimer's disease. Brain. 2008;131(Pt 6):1630-1645.
25. Leinonen V, Alafuzoff I, Aalto S, et al. Assessment of beta-amyloid in a frontal cortical brain biopsy specimen and by positron emission tomography with carbon 11-labeled Pittsburgh Compound B. Arch Neurol. 2008;65(10):1304-1309.
26. Rabinovici GD, Rosen HJ, Alkalay A, et al. Amyloid vs FDG-PET in the differential diagnosis of AD and FTLD. Neurology. 2011;77(23):2034-2042.
27. Politis M, Wu K, Molloy S, et al. Parkinson's disease symptoms: the patient's perspective. Mov Disord. 2010;25(11):1646-1651.
28. Pagano G, Niccolini F, Politis M. Imaging in Parkinson's disease. Clin Med (Lond). 2016;16(4):371-375.
29. Delva A, Van Weehaeghe D, van Aalst J, et al. Quantification and discriminative power of (18)F-FE-PE2I PET in patients with Parkinson's disease. Eur J Nucl Med Mol Imaging. 2020;47(8):1913-1926.
30. Huang C, Mattis P, Perrine K, et al. Metabolic abnormalities associated with mild cognitive impairment in Parkinson disease. Neurology. 2008;70(16 Pt 2):1470-1477.
31. Pilotto A, Premi E, Paola Caminiti S, et al. Single-subject SPM FDG-PET patterns predict risk of dementia progression in Parkinson disease. Neurology. 2018;90(12):e1029-e1037.
32. Hoglinger GU, Respondek G, Stamelou M, et al. Clinical diagnosis of progressive supranuclear palsy: The movement disorder society criteria. Mov Disord. 2017;32(6):853-864.
33. Walker Z, Gandolfo F, Orini S, et al. Clinical utility of FDG PET in Parkinson's disease and atypical parkinsonism associated with dementia. Eur J Nucl Med Mol Imaging. 2018;45(9):1534-1545.
34. Zhao P, Zhang B, Gao S, Li X. Clinical features, MRI, and 18F-FDG-PET in differential diagnosis of Parkinson disease from multiple system atrophy. Brain Behav. 2020;10(11):e01827.

# 7

# NOVELTIES IN CARDIAC IMAGING

*by Elisabetta Cerudelli*

While single photon emission computed tomography (SPECT) remains the workhorse of nuclear myocardial imaging, many hospital imaging departments are looking at installing positron emission tomography (PET) to add additional capabilities to their nuclear imaging programmes. The growing interest in cardiac PET is strongly linked to its inherently superior image quality and to new tracer development, which is resulting in better performance. The role of PET in characterising several cardiac functional processes is widely recognised, and in particular PET shows a good diagnostic capability in perfusion imaging (MPI), metabolic and vitality assessment, detection of infective foci and evaluation of receptor activity.

## PERFUSION IMAGING

Dynamic cardiac PET protocol for perfusion assessment is probably the most demanding of the cardiac PET protocols. Because it has a higher spatial and temporal resolution than SPECT, as well as inherently accurate depth-independent attenuation correction, PET MPI allows quantification of basal and hyperaemic regional and basal myocardial blood flow (MBF). However, due to the high cost of imaging systems and the technological development of SPECT, PET MPI is not performed in all patients. PET is particularly preferable in obese patients with high soft-tissue attenuation, or in patients with higher pre-test likelihood of multivessel or balanced CAD, i.e. patients in which SPECT may fail to detect true perfusion changes. The most widely used tracers in MPI PET are $^{13}$N-NH$_3$ and $^{82}$Rubidium.

### $^{13}$N-Ammonia

This radiotracer is produced by a cyclotron by means of the $^{16}$O(p,a)$^{13}$N reaction. The physical half-life of $^{13}$N-NH$_3$ is 9.96 min. It has a low positron energy (1.19 MeV) and a positron range of 2.53 mm, resulting in high-quality images (1). In blood, $^{13}$N-NH$_3$ mainly circulates as ammonium ion ($NH^{4+}$), which is actively transported through the cell membrane by the sodium-potassium pump, getting trapped. The remaining circulating $^{13}$N-NH$_3$ diffuses passively across cell membranes and gets trapped inside the cell by conversion through glutamine synthase to $^{13}$N-glutamine (2). The myocardial extraction fraction of $^{13}$N-NH$_3$ is about 80%: rapid clearance from the blood pool is characteristic of this tracer. $^{13}$N-NH$_3$ extraction is inversely and non-linearly correlated to myocardial blood flow (MBF). This means that while the tracer correctly quantifies the blood flow at baseline, in hyperaemic condition, the higher the flow, the higher the underestimation. Nevertheless, $^{13}$N-NH$_3$ has been validated and is widely used for the absolute quantification of MBF and coronary flow reserve (CFR) (3). Standardised protocols consist of two injections of 370–400 MBq each. The effective dose per administered activity is 3.4 mSv/MBq (4).

### $^{82}$Rubidium

This radionuclide can be obtained on demand after elution of a $^{82}$Sr/$^{82}$Rb generator. Currently this kind of generator is commercially available in the USA and Canada only. The physical half-life is 75s. While 4.5% of $^{82}$Rb decays by gamma emission, 95.5% decays through emission of high-energy positrons (3.15 MeV), resulting in a lower spatial resolution and image quality than $^{13}$N-NH$_3$. $^{82}$Rb passes through the myocardial cell membranes via the Na-K pump. The first-pass myocardial extraction fraction is lower than $^{13}$N-NH$_3$ in basal condition (65%), and is even lower with increasing blood flow (5–6). Nevertheless, the tracer extraction performance is better than the most common $^{99m}$Tc-labelled radiopharmaceuticals. The increasingly widespread use of $^{82}$Rb as an MBF tracer is mainly due to its short half-life, which enables the acquisition of a stress-rest test in 30 minutes (vs. more than 2 hours for $^{13}$N-NH$_3$), and to the fact that its production does not require a cyclotron on site, but only a small generator. The suggested activity to administer for adults is 740–1110 MBq, and the effective dose per administered activity is 1.26 mSv/MBq (7-8).

## VIABILITY ASSESSMENT

The assessment of myocardial metabolism and viability in patients with ischaemic left ventricular dysfunction is important to identify patients who would benefit from coronary artery revascularisation. Under fasting and aerobic conditions, fatty acids are the preferred energy source; however, in ischaemic conditions the myocardium is able to switch to glucose metabolism, which is not oxygen dependent. By using $^{18}$F-Fluorodeoxyglucose (FDG) it is possible to identify the stunned and hibernating myocardial tissue, which corresponds to cells that are using glycolysis for survival and could hence benefit from myocardial revascularisation. Recognised by glucose transporter (GLUT), FDG gets into the cell and is phosphorylated by enzyme hexokinase and trapped (9). To ensure that myocardial tissue metabolism is switched to glycolysis, several preparation methods are possible. To circumvent the problem of insulin resistance, it is possible to apply the euglycemic hyperinsulinemic clamp (EHC) technique. Other options are oral glucose loading, usually followed by intravenous insulin, or the intake of Acipimox, a

nicotine acid derivate that lowers free-circulating fatty acid levels. The suggested activity to administer for adults ranges from 185 to 400 MBq. The assessment of myocardial viability needs to be integrated with the MPI, which may even be done the same day using $^{99m}$Tc-labelled radiopharmaceuticals, $^{13}$N-NH$^{3}$ or $^{82}$Rb, or other perfusion tracers. The hibernating myocardium is characterised by reduced perfusion and preserved or increased metabolism. Tissue with reduced perfusion and metabolism is classified as scar (10). FDG is not the only metabolic tracer: we can also cite $^{11}$C-glucose for glucose metabolism; $^{11}$C-palmitate, $^{18}$F-fluoro-6-thia-heptadecanoic acid and $^{18}$F-16-fluoro-4-thia-palmitate (FTP) for fatty acid metabolism; or $^{11}$C-acetate and $^{15}$O2 for oxidative and oxygen metabolism. However, with the exception of $^{18}$FDG, these tracers are primarily experimental (11).

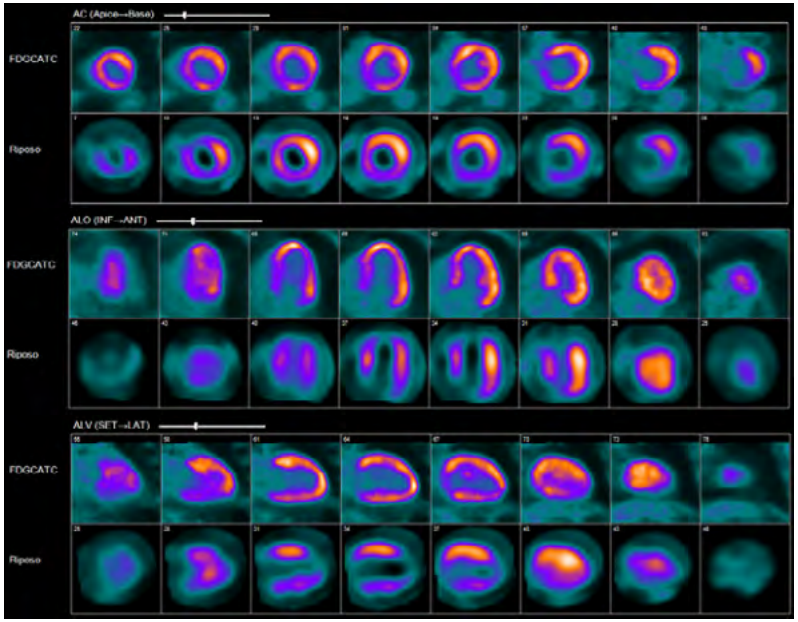


*Fig.1 $^{18}$F-FDG PET myocardial viability scan showing mismatch pattern. The resting perfusion images performed with $^{99m}$Tc-labelled tracer on CZT SPECT show a reduction in uptake in the anterior wall and apex (lower rows). The $^{18}$F-FDG metabolism images (upper rows) show significant $^{18}$F-FDG uptake in the anterior wall and apex, indicating that there is significant perfusion-metabolism mismatch, or hibernating myocardium in these regions.*







### Detection of infective foci

Early diagnosis of infective endocarditis (IE) and cardiac implantable electronic device infection (CIED) is key to improve outcomes. Echocardiography, along with blood culture and clinical presentation, are the cornerstones in the diagnosis of IE. They have limitations, however, and often have to be supplemented by additional imaging modalities to improve diagnostic accuracy. FDG PET-CT, according to the latest update from the European Society of Cardiology (ESC), is now included in the diagnostic flowchart for IE and CIED. FDG is accumulated in cells with increased metabolic activity, such as those involved in infection and inflammation, especially neutrophiles and macrophages that are able to express high levels of GLUT. The strength of FDG PET-CT is its ability to localise and evaluate the extent of cardiovascular infection with excellent spatial resolution. It can also add information about the presence of associated cardiac complications such as abscess, pseudoaneurysm or aneurysm, and in addition it has the ability to detect extra-cardiac foci of infection (often located in spleen or musculoskeletal areas) (12). In order to improve the diagnostic accuracy, it is essential to ensure an adequate suppression of the physiological myocardial FDG uptake, which is achieved through 12 to 18 h of pre-test fasting, or pre-test administration of unfractionated heparin, or a high-fat, low-carbohydrate diet for 12–24 hours prior to testing (13). The imaging protocol is the same as that used in oncology. The European Association of Nuclear Medicine guidelines recommend 2.5–5.0 MBq/kg FDG for imaging of infection. The usefulness of delayed imaging in cardiac infection is still under debate (14).

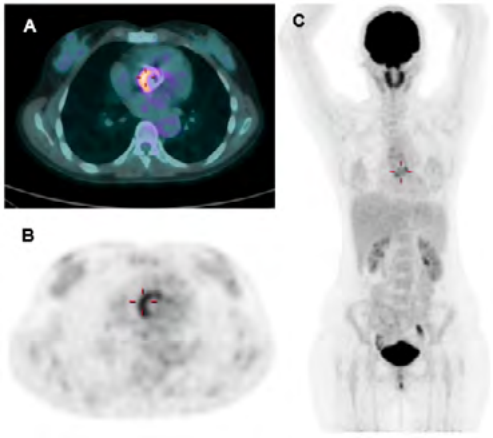


*Fig.2 $^{18}$F-FDG PET/CT performed in a 33-year-old female with biological prosthetic aortic valve. The PET/CT fusion transaxial image (A) shows a linear increased uptake in the right region of the valve. This pathological uptake is suspicious for IE. PET image (B) and maximum intensity projection (C) of the same patient.*

### Receptor activity

A less conventional use of cardiac PET is in the evaluation of the sympathetic innervation of the heart. The most routinely used tracers here are $^{11}$C-meta-hydroxyephedrine (HED), an analogue of norepinephrine, and $^{18}$F-fluorodihydroxyphenylalanine (FDOPA), an analogue of L-DOPA. The sympathetic nervous system plays a primary role in normal cardiovascular function and disease. PET imaging has proven helpful in understanding the pathophysiology and prognosis of many cardiovascular diseases, especially in heart failure and cardiac transplantation (15). More recent studies have also shown a role in the differential diagnosis of idiopathic Parkinson's disease (IPD) or Lewy body disease (LBD) from parkinsonism. With the two named tracers it is possible to identify the cardiac denervation that is characteristic of IPD and LBD but not of parkinsonism (16).

## WHAT'S NEW IN CARDIAC PET

### New tracers and new uses

Innovations in cardiac PET concern both novel use of well-known tracers and the development of new radiopharmaceuticals, as well as new technologies.

### FDG PET in sarcoidosis

Sarcoidosis is an inflammatory disease characterised by the growth of tiny collections of inflammatory cells (granulomas) in any part of the body. Cardiac involvement is rare; however, it is strongly linked to an increase in morbidity and mortality. FDG PET/CT has emerged as a leading modality by which to detect cardiac sarcoidosis non-invasively. Despite the lack of evidence-based guidelines for the assessment of cardiac sarcoidosis, contemporary guidelines have included FDG PET/CT in the diagnostic algorithm, thus recognising its clinical power (17-18). Diagnosis is based on the comparison of two resting images: one to assess the myocardial inflammation, and one to assess the myocardial perfusion and motion. The first study involves the use of FDG as radiotracer and requires adequate suppression of physiological myocardial uptake of FDG for a correct interpretation (preparation is as described under Detection of infective foci). Ten- to 30-minute non-gated images are acquired from 60 minutes to 90 minutes after the administration of FDG. The field of view is extended to include the base of the skull to the upper thigh in order to evaluate cardiac and extra-cardiac localisations of the disease. Gated perfusion imaging is typically performed using either $^{13}$N-NH$^3$ or $^{82}$Rb, but a SPECT study with $^{99m}$Tc-labelled radiopharmaceuticals is also permissible. Using PET tracers it is possible to complete a perfusion exam within one day, taking advantage of their short physical half-life, whereas two days are needed in the case of SPECT perfusion assessment (19). If focal FDG uptake matches to a perfusion defect, the finding is likely to be indicative of inflammation and the presence of active sarcoidosis. If FDG uptake is lacking in the region corresponding to a perfusion defect, perhaps also with regional alteration of motion, scar tissue is likely to be present. Furthermore, abnormal right ventricular FDG uptake has proved to be a negative predictive factor. Nevertheless, although FDG PET has been shown to have the highest diagnostic accuracy among both invasive and non-invasive techniques, quantitative assessment of myocardial inflammation is not yet well clarified, and neither is its role in the evaluation of therapeutic response (20).

### $^{18}$F-flurpiridaz in MPI

In the last few years several $^{18}$F-labelled PET MPI tracers have been developed to overcome the limits of the well-known $^{82}$Rb or $^{13}$N-NH$^3$, such as their short half-life and the necessity of having a monthly generator or on-site cyclotron. The most successful of these radiopharmaceuticals in phase 3 multicentre clinical trials is $^{18}$F-flurpiridaz. This tracer is characterised by a very rapid uptake in cardiomyocytes (time to 1/2-maximum uptake: 35s) and subsequent prolonged retention, with a slow washout (more than 120 min) due to the bind to mitochondrial complex. Biodistribution studies showed a specific accumulation in the heart, with favourable heart-liver and heart-lung ratios. The half-life is linked to $^{18}$F (110 minutes), so the problem of needing an on-site cyclotron or generator – typical of the other MPI PET tracers – is overcome. Furthermore, the combination of long half-time and prolonged retention allow a treadmill exercise stress protocol: the patient injected at peak has time to move over to the camera and still be effectively imaged (21-22). In phase 2 and 3 clinical trials two different protocols were developed, taking account of the relationship between rest-stress contamination and dosing: for the one-day rest-stress protocol a minimum dose ratio of 3.0 is needed, with 60 minutes waiting time between the two injections for the exercise protocol and 30 minutes waiting for the pharmacological protocol. Another advantage of $^{18}$F-flurpiridaz is the low positron range (1.03 mm), which produces higher image resolution and better image quality than both classical PET and SPECT MPI radiotracers. The registered extraction fraction is elevated

(94%), better than $^{82}$Rb (42%) or $^{13}$N-NH$_3$ (82%), and compared to the latter does not change significantly at stress flow. Consequently, assuming a linear relationship between uptake and MBF, a clearer difference between normal and under-perfused regions is expected (23). Phase 3 studies showed $^{18}$F-flurpiridaz PET to have superior sensitivity to SPECT in the detection of coronary artery disease (78.8% vs. 61.5%, p=0.02), with no significant difference in specificity (76.5% vs. 73.5%). In addition, thanks to the high and flow-independent extraction fraction, preliminary data have also confirmed the potential value of $^{18}$F-flurpiridaz in quantitative assessment: in particular, it could be used for accurate absolute MBF quantification (24). Considering these multiple qualities, this new tracer has the capability to revolutionise cardiac perfusion imaging and it is hoped that it will soon be granted final approval for clinical use.

### $^{18}$F-fluoride in atherosclerosis

In the last few years, a new application has been found for PET/CT with $^{18}$F-fluoride ($^{18}$F-NaF), particularly in the cardiovascular field. Developed as a bone tracer, $^{18}$F-NaF seems to be able to mark vascular microcalcifications which occur early in the atherosclerotic disease process (25). Atherosclerosis is the leading cause of death and disability in the developed world because of its close correlation with myocardial infarction and ischaemic stroke, and the microcalcification process is presumed to increase the potential for plaque rupture. However, diagnostic techniques to detect atherosclerosis are still limited, especially prior to symptomatic manifestation. In contrast to anatomical imaging modalities that visualise macroscopic structural changes only, $^{18}$F-NaF binds the surface of macrocalcific deposits in the active phase of mineralisation, especially in the presence of increased microcalcifications. It is thus the only existing in vivo modality that can detect and non-invasively quantify vulnerable and high-risk plaques in the coronary arteries, as well as in the carotid arteries, aorta and distal arteries (26). Clinical trials are underway, but $^{18}$F-NaF PET-CT seems to be a promising assessment tool for accurate cardiovascular risk stratification, potentially providing useful prediction of disease progression and clinical events (27).

## RECENT TECHNICAL ADVANCES IN CARDIAC PET

### New PET detectors

One of the innovations in PET instrumentation is the release of new scintillating detector material. We know that denser materials have a higher photoelectric fraction, so they have a better ability to stop incoming 511-keV radiation completely on the first interaction and inter-detector scatter is therefore lower. A high luminosity is also useful with regard to the signal-to-noise ratio, and, lastly, a high light emission speed and a short decay time are essential for 3D and dynamic acquisition in MPI studies. In fact, these features can translate into reduced image noise during the first-pass transit through the heart, which is a fundamental prerequisite for higher accuracy in MBF quantification (28). Among the new materials, cerium-doped lutetium oxyorthosilicate (Lu2SiO5(Ce) or LSO) is widely used for its combination of high density, low decay time, and a light output that comes closest to the NaI(Tl) standard. The most recent commercially available PET/CT scanners incorporate lutetium yttrium orthosilicate (LYSO:Ce), a variant of LSO in which lutetium is partly replaced by yttrium while maintaining the useful characteristics of the former (29).

| | DENSITY (G/CM3) | ATTENUATION LENGTH (MM) | LIGHT OUTPUT (PHOTONS/MEV) | LIGHT DECAY TIME (NS) |
|---|---|---|---|---|
| BGO | 7.1 | 10.4 | 9,000 | 300 |
| GSO | 6.7 | 14.1 | 8,000 | 60 |
| LSO | 7.4 | 11.4 | 30,000 | 40 |
| LYSO | 7.4 | 11.8 | 30,000 | 40 |

*BGO: bismuth germanate; GSO: gadolinium oxyorthosilicate; LSO: lutetium oxyorthosilicate; LYSO: lutetium yttrium oxyorthosilicate*

*Tab. 1 Characteristics of inorganic scintillating materials commonly used in PET.*

### Time Of Flight (TOF)

The introduction of new fast scintillation crystals such as LSO and LYSO has led to the implementation of time-of-flight (TOF) technology in modern PET scanners. TOF is based on the evaluation of the difference in arrival times of two coincident gamma rays, which is translated into a distance from the centre of the line-of-response (LOR). Thanks to the good timing resolution of lutetium-based scintillators,

the location of the annihilation event can be determined with an uncertainty of only 7.5 cm, resulting in a reduction in the propagation of noising along each LOR and in an improved signal-to-noise ratio (30). The ensuing increase in image quality and lesion detection capability in PET oncology studies is well established (31-32). On the other hand, however, there is very little data evaluating the advantages in cardiac application. The most significant benefits of TOF are documented in oncological studies covering a large field of view (FOV), searching for hotspots on a warm background (31, 33). In contrast, the region of interest in cardiac imaging is small, concentrated in the heart, and perfusion imaging is a search for cold spots on a hot background, while viability imaging is an evaluation of hot uptake in the myocardial wall on a cool background. Consequently, the most significant improvements in image quality in cardiac imaging with TOF scans are expected in overweight subjects (obesity is often found in cardiovascular patients). In this kind of patients, the cross-sectional area in the FOV is large, resulting in strong attenuation and scatter phenomena in the emission data and non-uniform artefactual distribution of the tracer. TOF has demonstrated the ability to register a higher number of true iterations with a consequent improvement in contrast, leading to a reduction in false positive or false negative interpretations in obese patients (34). Furthermore, TOF has also been shown to have a positive impact on qualitative and quantitative myocardial perfusion analysis. In particular, it is known that in non-TOF scans the myocardial retention of 13N-ammonia is heterogeneous because of a lower count in the apical and lateral wall due to both cardiac motion and breathing artefacts in addition to small myocardial thickness (35). TOF technology, being more able to precisely detect signals, reduces the deterioration of apex and lateral wall counts, thus improving image quality and the reproducibility of the visual interpretation. In addition, this better detection of count, the better signal-to-noise performance and the lower partial volume effects mitigate the flow quantification, resulting in increased MBF and reduction of CFR by a maximum of 10%, especially in the apical segments and under relatively low perfusion conditions, as reported by Tomiyama et al (36). In conclusion, the benefits of TOF technology in cardiac PET have been demonstrated, but further studies are needed to evaluate the improvement achieved in clinical settings. It is also likely that new different thresholds will be released for MBF and CMR in cardiac perfusion PET.

### Smaller digital silicon photomultipliers (SiPM)

There is also a second technical advance in PET that will undoubtedly influence the image quality and the information derived from cardiac scans. Some recent digital PET designs feature smaller digital silicon photomultipliers (SiPM) to achieve outright 1-to-1 correspondence between photomultipliers and detectors. This results in a very good intrinsic timing resolution (44 ps) and increased dynamic range, meaning that SiPMs improve both the sensitivity and the maximum count rate (37).

This improved image resolution could have a positive impact on myocardial perfusion PET imaging, and in particular on the quantification of MBF. At present, however, the literature on the application of this equipment in cardiac imaging is limited.

### CT-based attenuation correction

Nowadays, the use of CT to manage the attenuation of the photons is mandatory in cardiac PET. CT-based attenuation correction relies on the creation of a map of the attenuation coefficients of the CT scan using Hounsfield units (HU) (38). In this context, each manufacturer has developed a protocol for AC. The advantages of this approach to attenuation correction are the low-noise attenuation maps and fast data acquisition, but the downside is that the patient is exposed to an additional dose of radiation. Thus, every patient must be studied before the exam, trying to find an adequate compromise between the increase in radiation exposure and the improvement in image quality (39). CT scans for attenuation correction only should be performed at the lowest possible settings, for example, with adjustment of the tube voltage depending on the patient's size (i.e. body mass). At the same time, however, the rotation speed must be slow (at least 1/s or less), thus increasing the effective dose but obtaining a blur of the cardiac motion to prevent misalignments and artefact errors (40).

### Combination of attenuation correction and coronary artery calcium score

Patients with suspected ischaemic cardiac disease usually undergo non-contrast CT to assess the coronary artery calcium score (CCS). The CCS plays an important role in cardiovascular risk stratification as a strong predictor factor for coronary events, providing information about the amount of calcium deposits in the coronary arteries (41). To optimise the radiation exposure, the use of AC CT has been proposed to evaluate the CCS, or the use of CCS CT to create a CT attenuation map for PET imaging. The challenge of this approach is inherent in the different acquisition methods: the AC CT is performed without gating and with free breathing, while the CCS CT is performed with electrocardiogram (ECG) gating at the end of expiration (42). In the last few

years several studies have explored this possibility with good results, highlighting the possible bias factors and artefacts. When the AC image is used for the CCS, the different tube current influences the image noise as well as the HU and consequently the CCS (43). In addition, the larger slice thickness and the blurring caused by non-gated images result in underestimation of the CCS. In CCS CT used for AC, on the other hand, mistakes could derive from the manual alignment or the lack of blurring of ECG-gated images, which could cause an alteration in quantification of the flow in PET scans (44-45). Both protocols still require deeper studies to find an adequate compromise between the two methods, but we hope for fast optimisation of the technical parameters in response to society's increasing concern about radiation exposure.







## REFERENCES


1. Sanchez-Crespo A, Andreo P, Larsson SA; Positron flight in human tissues and influence on PET image spatial resolution. Eur J Nucl Med Mol Imaging, 2004;31:44-51
2. Schelbert HR, Hack S, Tewson T et al, Cardiac PET imaging for the detection and monitoring of coronary artery disease and microvascular health. JACC Cardiovasc Imaging, 2010; 3:623-640
3. DeGrado TR, Hanson MW, Turkington TG et al, Estimation of myocardial blood flow for longitudinal studies with 13N-labeled ammonia and positron emission tomography. J Nucl Cardiol, 1996;3:494-507
4. Case JA, deKemp RA, Slomka PJ et al, Status of cardiovascular PET radiation exposure and strategies for reduction: an information statement from the Cardiovascular PET Task Force. J Nucl Cardiol, 2017;24:1427-39.
5. Go RT, Marwick TH, MacIntyre WJ et al, A prospective comparison of 82-Rubidium PET and 201-Thallium SPECT myocardial perfusion imaging utilizing a single dipyridamole stress in the diagnosis of coronary artery disease. J Nucl Med, 1990; 31:1899-905
6. Patridge M, Spinelli A, Ryder W et al., The effect of beta+ energy on performance of a small animal PET camera, Nucl Instrum Methods Phys Res Sect A, 2006;568:933-6
7. Garcia EV, Galt JR, Faber TL et al, Principles of nuclear cardiology imaging. IN: Dilsizian, Vasken; Narula, Jagat, editors, Atlas of Nuclear Cardiology, 4th edition, Springer Science; 2013 p1-53, Chapter 1
8. Sciagrà R, Lubberink M, Hyafil F et al, EANM procedural guidelines for PET/CT quantitative myocardial perfusion imaging, Eur J Nucl Med Mol Imaging, 2020;2:1-30
9. Gosh N, Rimoldi O, Beanlands R, Camici C, Assessment of myocardial ischemia and viability: Role of positron emission tomography, Eur Hear Journ, 2010, 31:2984-95
10. Dilsizian V, Bacharach SL, Beanlands RS et al, PET myocardial perfusion and metabolism clinical imaging. J Nucl Cardiol 2009;16:651.
11. Sun KT, Yeatman L, Buxton Det al, Simultaneous measurement of myocardial oxygen consumption and blood flow using [1-Carbon-11] acetate. J Nucl Med 1998;39:272–280.
12. Habib G, Lancellotti P, Antunes MJ, et al: 2015 ESC Guidelines for the management of infective endocarditis: The Task Force for the Management of Infective Endocarditis of the European Society of Cardiology (ESC) Endorsed by: European Association for Cardio-Thoracic Surgery (EACTS), the European Association of Nuclear Medicine (EANM). Eur. Heart J. 36:3075-3128, 2015
13. Osborne MT, Hulten EA, Murthy VL, et al: Patient preparation for cardiac fluorine-18 fluorodeoxyglucose positron emission tomography imaging of inflammation. J. Nucl. Cardiol. Off. Publ. Am. Soc. Nucl. Cardiol. 24:86-99, 2017
14. Boellaard R, Delgado-Bolton R, Oyen WJ, et al: FDG PET/CT: EANM procedure guidelines for tumor imaging: version 2.0. Eur. J. Nucl. Med. Mol. Imaging 42:328-354, 2015.
15. Boutagy N, Sinusas A, Recent Advances and Clinical Applications of PET Cardiac Autonomic Nervous System Imaging, Curr Cardiol Rep. 2017; 19(4): 33
16. Eshuis SA, Maguire RP, Leenders, KL et al, Comparison of FP-CIT SPECT with F-DOPA PET in patients with de novo and advanced Parkinson's Disease. Eur Jour of Nucl Med and Mol Imag, 2006, 33: 200-209
17. Bois JP, Muser D, Chareonthaitawee P, PET/CT evaluation of Cardiac Sarcoidosis, PET Clin, 2019; 14:223-232
18. Chareonthaitawee P, Beanlands RS, Chen W, et al, Joint SNMMI-ASNC expert consensus document on the role of (18)F-FDG PET/CT in cardiac sarcoid detection and therapy monitoring, J Nucl Med, 2017;58(8):1341–53.
19. Dilsizian V, Bacharach SL, Beanlands RS, et al, ASNC imaging guidelines/SNMMI procedure standard for positron emission tomography (PET) nuclear cardiology procedures, J Nucl Cardiol, 2016;23(5):1187–226.
20. Bois JP, Chareonthaitawee P, Optimizing radionuclide imaging in the assessment of cardiac sarcoidosis, J Nucl Cardiol 2016;23(2):253–5.
21. Yalamanchili P, Wexler E, Hayes M et al., Mechanism of uptake and retention of F-18 BMS-

747158-02 in cardiomyocytes: A novel PET myocardial imaging agent, J Nucl Cardiol, 2007;14:782-788

22. Maddahi J, Czernin J, Lazewatsky J et al, Phase I, first-in-human study of BMS747158, a novel 18F-labeled tracer for myocardial perfusion PET: Dosimetry, biodistribution, safety, and imaging characteristics after a single injection at rest, J Nucl Med, 2011;52:1490-1498

23. Berman DS, Maddahi J, Tamarappoo BK et al, Phase II safety and clinical comparison with single-photon emission computed tomography myocardial perfusion imaging for detection of coronary artery disease: Flurpiridaz F 18 positron emission tomography, J Am Coll Cardiol, 2013;61:469-477

24. Moody JB, Poitrasson-Riviere A, Hagio T et al., Added value of myocardial blood flow using 18F flurpiridaz PET to diagnose coronary artery disease: the Flurpiridaz 301 Trial, J Nucl Cardiol, 2020, https://doi.org./10.1007/s12350-020-02034-2.

25. Dweck MR, Chow MWL, Joshi NV et al., Coronary arterial $^{18}$F-sodium fluoride uptake: a novel marker of plaque biology, J Am Coll Cardiol, 2012;59:1539-1548.

26. Irkle A, Vesey AT, Lewis DY et al., Identifying active vascular microcalcification by (18)F-sodium fluoride positron emission tomography, Nat Commun, 2015;6:7495.

27. Fiz F, Morbelli S, Bauckneht M et al., Correlation between thoracic aorta 18F-natrium fluoride uptake and cardiovascular risk, World J Radiol, 2016;8:82-89.

28. Lewellen TK, Recent developments in PET detector technology, Phys Med Biol, 2008;53:R287-R317

29. Pichler B, Boning C, Lorenz E et al., Studies with a prototype high resolution pet scanner based on LSO-APD modules, IEEE Trans Nucl Sci 1998;45:1298-1302.

30. Wells RG, deKemp RA, Does time-of-flight improve image quality in the heart?, J Nucl Cardiol, 2019;26:413-6

31. Karp JS, Surti S, Daube-Witherspoon ME et al., Benefit of time-of-flight in PET: experimental and clinical results, J Nucl Med, 2008;49:462-470.

32. Lois C, Jakoby BW, Long MJ, et al., An assessment of the impact of incorporating time-of-flight information into clinical PET/CT imaging, J Nucl Med, 2010;51:237–45.

33. Conti M, Focus on time-of-flight PET: the benefits of improved time resolution, Eur J Nucl Med Mol Imaging, 2011; 38:1147-1157.

34. DiFilippo FP, Brunken RC, Impact of time-of-flight reconstruction on Cardiac PET images of obese patients, Clin Nucl Med 2017;42:103-108.

35. Klein R, Beanlands R, Dekemp R., Quantification of myocardial blood flow and flow reserve: Technical aspects, J Nucl Cardiol 2010;17:555-70.

36. Tomiyama T, Ishihara K, Suda M, et al., Impact of time-of-flight on qualitative and quantitative analyses of myocardial perfusion PET studies using 13N-ammonia, J Nucl Cardiol, 2014;1–10.

37. van Dam HT, Seifert S, Schaart DR, The statistical distribution of the number of counted scintillation photons in digital silicon photomultipliers: Model and validation, Phys Med Biol, 2012;57:4885-4903

38. Verberne HJ, Acampa W, Anagnostopoulos C, et al, EANM procedural guidelines for radionuclide myocardial perfusion imaging with SPECT and SPECT/CT: 2015 revision., Eur J Nucl Med Mol Imaging, 2015;42(12): 1929–1940.

39. Yu L, Li H, Fletcher JG, McCollough CH, Automatic selection of tube potential for radiation dose reduction in CT: a general strategy, Med Phys , 2010;37(1):234–243.

40. Chan C, Dey J, Grobshtein Y, et al, The impact of system matrix dimension on small FOV SPECT reconstruction with truncated projections, Med Phys,2016;43(1):213–224.

41. Greenland P, Bonow RO, Brundage BH, et al, ACCF/AHA 2007 clinical expert consensus document on coronary artery calcium scoring by computed tomography in global cardiovascular risk assessment and in evaluation of patients with chest pain: a report of the American College of Cardiology Foundation Clinical Expert Consensus Task Force (ACCF/AHA Writing Committee to Update the 2000 Expert Consensus Document on Electron Beam Computed Tomography) developed in collaboration with the Society of Atherosclerosis Imaging and Prevention and the Society of Cardiovascular Computed Tomography, J Am Coll Cardiol,2007;49(3):378–402.

42. Camoni L, Santos A, Attard M, et al., Best practice for nuclear medicine technologist in CT-based attenuation correction and calcium score for nuclear cardiology, Eur J Hybr Imaging, 2020;4:11.

43. Einstein AJ, Johnson LL, Bokhari S, et al, Agreement of visual estimation of coronary artery calcium from low-dose CT attenuation correction scans in hybrid PET/CT and SPECT/CT with standard Agatston score, J Am Coll Cardiol, 2010;56(23):1914–1921.

44. Schepis T, Gaemperli O, Koepfli P, et al, Use of coronary calcium score scans from standalone multislice computed tomography for attenuation correction of myocardial perfusion SPECT, Eur J Nucl Med Mol Imaging,2007;34(1):11–19.

45. Hecht HS, Cronin P, Blaha MJ, et al, 2016 SCCT/STR guidelines for coronary artery calcium scoring of non-contrast noncardiac chest CT scans: a report of the Society of Cardiovascular Computed Tomography and Society of Thoracic Radiology, J Cardiovasc Comput Tomogr,2017;11(1):74–84.

# 8

# NEW SOLUTIONS IN THE ONCOLOGY

*by Andrej Doma*

PET technology is technically superior to SPECT by virtue of its enhanced sensitivity and detection accuracy, as well as its capabilities of whole-body imaging, dynamic acquisition and better quantification. The higher sensitivity of PET in detecting radioactive decay is achieved through the design of the PET scanner, where the ring of PET detectors surrounds the body, whereas in a SPECT camera, a planar detector with integrated collimator rotates around the body: hence approximately 1% of the emitted photons are detected with PET, in comparison to only 0.1% with SPECT. The use of collimators in SPECT limits the ability to separate small nearby activity sources, whereas in PET the detector crystals are of small size and thus also capable of detecting small-scale time differences in a photon impact, resulting in very accurate localisation of the annihilation event (time-of-flight technology). The acquisition of data in PET is faster as a result of the rapid scintillation of PET crystals, which enables dynamic tomographic imaging of activity changes within a short time-frame [1].

Another advantage is the short duration of a PET scan: a standard whole-body PET lasts around 20 minutes, a fact welcomed by patients. In SPECT, a planar whole body scan takes up to 30 minutes, with an additional 20–40 minutes for one or several tomographic acquisitions. An accurate single whole-body PET investigation combining high-sensitivity FDG PET and high-specificity CT also reduces the need for additional investigations, limiting both patient anxiety and cost. Further progress is anticipated with a new PET/CT system with a longer axial length of 106 cm, which has recently been approved by the FDA for human use [2]. This system boasts increased sensitivity and enables a very short acquisition time of one minute for a total-body PET/CT. This will potentially reduce the amount of administered radioactivity and consequently reduce patient radiation exposure, thereby potentially enabling the use of PET imaging as a screening tool. Simultaneous dynamic imaging of multiple organs will also open up opportunities for bio-distribution, blood flow, or receptor density studies [3].

The inherent ability of PET to perform non-invasive quantification enables the identification of targets suitable for targeted therapy. Advanced attenuation correction and image reconstruction algorithms have recently also enabled quantitative SPECT [4], but quantification in SPECT remains challenging. PET offers a much wider variety of biologically relevant radiotracers than SPECT, though there has been a recent revival of interest in SPECT imaging with the surge in radionuclide therapies and image-dosed dosimetry [5].







Looking at the number of nuclear medicine (NM) investigations performed in the last 20 years, a steady shift can be observed from conventional planar and SPECT studies towards PET studies. In 2017, the number of single-photon tracer examinations performed was reported to have decreased by 6% in the last 5 years, 24% in the last 10 years, and 42% in the last 20 years. Conversely, the number of PET scanners installed and PET examinations performed had both increased exponentially by 25% in the last 5 years. In 2017, PET investigations outnumbered single-photon tracer examinations by approximately 2:1 in oncology applications, a ratio likely to have shifted even further in favour of PET since then. Bone scan scintigraphy remains by far the most common conventional NM procedure in oncology, followed by sentinel node scintigraphy [6].

18F-fluorodeoxyglucose PET/CT (FDG PET/CT) is highly versatile and presents unique qualities of accuracy in numerous oncology conditions [7], as well as in infection and inflammation [8]. Typical indications for oncological PET/CT are diagnosis, staging patients before therapy to determine the presence of metastatic disease, and evaluation of treatment response early after initiation of treatment and after the end of therapy protocol to appropriately modify treatment regimens. Despite being non-tumour-specific, FDG remains the most commonly used PET tracer due to its great sensitivity in a vast array of malignancies, as well as its wide availability and low cost. It enables assessment of the quantitative metrics metabolic tumour volume (MTV), total lesion glycolysis (TLG) and metabolic burden of disease [9]. FDG PET studies account for 98.2% of all PET studies [6].

In radiotherapy treatment, imaging has a key role both for treatment planning and assessment of response. Anatomical imaging such as CT or MRI relies on morphological parameters to distinguish between neoplasms and normal tissue. This limits its use in the delineation of vital tumours in previously treated areas, and in the differentiation of early relapse from inflammation or radiation-induced changes. Functional imaging such as PET/CT overcomes the limitations of morphological imaging by evaluating changes in metabolism and receptor expression at a molecular level. PET is increasingly being used for accurate delineation of target volumes in treatment planning, for planning of the spatial distribution of radiation dose in target volume according to quantitative parameter maps (dose painting), and for monitoring of response [10].

In oncology, the scope of PET/CT has broadened in the last decade. From diagnosis, staging and restaging, the reach of FDG PET/CT has expanded to radiotherapy planning, determination of the duration of progression-free survival

and overall survival, and early therapy response prediction. On the other hand, however, FDG PET is of limited value in certain common cancers, and several non-FDG PET radiotracers have become widely available, targeting specific processes or characteristics of cancer cells. The next generation of oncology radiotracers targets other metabolic pathways or receptors that are specific to cancers not well characterised by FDG. Novel PET tracers demonstrate greater target specificity, which improves staging and allows for determination of the expression of specific therapeutic targets in cancer cells. Non-invasive quantification on PET omits the limitations of relying on histopathology obtained from a single site and can identify tumour heterogeneity with well-differentiated and poorly differentiated disease occurring concurrently at different sites. The supreme PET–CT capabilities of non-invasive quantification of regional radiotracer uptake are changing the paradigm of imaging from anatomical lesion identification and measurement to whole-body identification and quantification of targets suitable for radionuclide therapy (theranostics, covered in the next chapter) or other specific therapies and early assessment of therapy response. In other words, precision PET diagnostics is paving the way for true personalised medicine. In this chapter, the topic of advanced PET/CT imaging in breast, prostate and brain cancers will be discussed.

## PET/CT IN BREAST CANCER IMAGING

Breast cancer (BC) is both the most common cancer and the leading cause of cancer-related death among women worldwide, with incidence and mortality of 48% and 14%, respectively [11]. Staging of BC is based on seven criteria: extent of the tumour (T), spread to nearby lymph nodes (N), metastases to distant sites (M), grade of the cancer (G), and oestrogen- (ER), progesterone- (PR) and HER2- (HER2) receptor statuses [12]. The success of breast cancer treatment depends on the ability to precisely define the extent of the disease and on characterisation of histological subtypes, grade and receptor expression.

Breast cancer grades 1, 2 and 3 describe levels of similarity of tumour cells compared to the appearance of normal breast cells. Well-differentiated, low-grade (1) cancer bears a similar appearance to normal breast cells, while the look of poorly differentiated, high-grade (3) cancer cells is significantly changed. Histologically, the most common type of breast cancer is infiltrating ductal carcinoma (IDC), followed by infiltrating lobular carcinoma (ILC), which respectively account for 80% and 15% of all primary breast malignancies. While high-grade cancers and the IDC subtype of breast cancer are typically FDG avid, the uptake of FDG in low-grade cancers and in both ILC primary tumours and metastases is lower [13].







The use of 18F-FDG PET/CT in breast cancer patients is clinically important for systemic staging of locally advanced disease, monitoring of treatment response in metastatic disease, and disease recurrence assessment. Whole-body FDG PET/CT displays low specificity to distinguish between carcinoma and FDG-avid benign tumours or physiological FDG-avid breast tissue, and poor sensitivity to detect primary breast cancers smaller than 1 cm in diameter. The former has been challenged by the introduction of positron emission mammography (PEM) and more recent dedicated breast PET systems. In PEM, a pair of detectors is placed above and below the breast, applying mild compression of the breast, while in dedicated breast PET systems the breast is placed within a ring of detectors that rotate around the breast without applying any compression. Both techniques are far more sensitive than whole-body FDG PET/CT for detection of primary breast cancer, displaying a higher spatial resolution of up to 2.4 mm [14,15]. However, the wider use of PEM is hampered by the problem of high whole-body radiation exposure in dedicated breast positron imaging, and by the lower cost and wider availability of breast MRI of equal sensitivity.

In assessing the status of locoregional axillary lymph nodes, a sentinel lymph node biopsy (SLN) with blue dye or radioactive tracer or both remains the method of choice to evaluate lymph node metastases. However, in extra-axillary lymph nodes, including supra- and infra-clavicular, internal mammary and mediastinal nodes, FDG PET/CT can detect unsuspected metastatic lymph node spread that cannot be identified by SNB, resulting in changes in disease staging and modification of local surgery or radiotherapy plans [16].

The standard approach in systemic staging of breast cancer in advanced stages includes bone scan and a CT scan of the chest, abdomen, and pelvis. FDG PET/CT was shown to be able to identify distant metastases not identified by conventional imaging in all stages of the disease. The rate of PET detection of unsuspected metastases increased according to the pre-PET/CT stage, from 2% in stage II patients up to 47% in stage III patients [16]. FDG PET/CT is able to detect early bone metastases before both bone scan and diagnostic CT [17,18].

FDG PET/CT was found to have similar efficacy in determining response to neoadjuvant chemotherapy (NAC) in breast cancer to breast MRI, ultrasound and physical examination [19]. However, due to the possible persistence of low-volume residual disease, pathological examination was found to be superior in differentiating partial and complete response [20].

In early assessment of response, a decrease in metabolic activity on PET after one to three cycles of chemotherapy in metastatic breast cancer was associated

with clinical response at the end of treatment and with overall survival [21,22].

FDG PET/CT was superior in predicting both progression-free survival and disease-specific survival in the evaluation of treatment in patients with metastatic breast cancer in comparison to RECIST criteria evaluated on contrast-enhanced CT [23]. FDG PET/CT was also found to be better in assessment of suspected disease recurrence than the combination of CE-CT and bone scan [24].

The three main receptors in breast cancer for which targeted drug therapies are available are oestrogen receptors (ER), androgen receptor (AR), and human epidermal growth factor receptor 2 (HER2). Novel PET tracers target receptor expression in breast cancer cells. Accurate whole-patient PET assessment of breast cancer receptor expression offers several advantages over biopsy with immunohistochemistry analysis of primary tumour and a single metastasis, which is currently the gold standard. Advantages include improved staging of the disease and accurate identification of the presence of therapeutic targets for precision endocrine therapy for both therapeutic and prognostic purposes. PET can also identify whole-body changes in receptor expression in primary tumour and metastases throughout the duration of the disease, with both over-expression and disappearance of receptors possible.

ER is over-expressed in 70% of breast cancer patients. Three endocrine therapy options targeting ER are available: selective modulators that competitively bind to the ER (tamoxifen), aromatase inhibitors that inhibit the conversion of androgens into oestrogens, and selective ER down-regulators that degrade the ER [25].

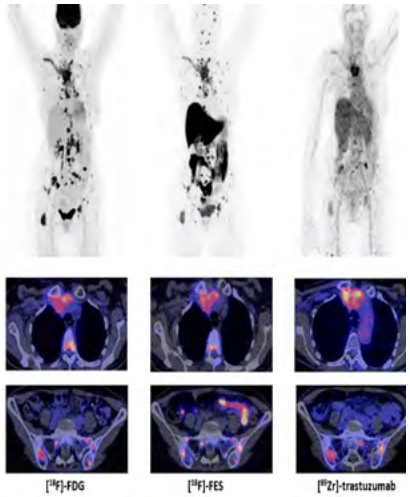


*FIGURE A: Comparison of 18F-FDG, 18F-FES and 89Zr-trastuzumab in the same patient [26, listed but not discussed, published in accordance with the Open Access Licence]*







PET imaging of ER expression is possible with 18F-fluoroestradiol (18F-FES), which is a substrate of oestrogen receptors. Initial FES PET imaging improves staging of non-FDG-avid primary tumours and metastases, enables assessment of ER status of all metastases, including those not available for standard biopsy, and provides information on response to endocrine therapy [27]. The sensitivity and specificity of FES PET in comparison to immunohistochemistry analysis is 84% and 98%, respectively, with a SUVmax above the cut-off value of 1.5 predicting the response to endocrine treatment [28]. By evaluating changes in FES uptake between baseline and early interim scan, it is possible to measure the initial response to endocrine therapy and adjust the therapy accordingly. A reduction in uptake of 75% or more between the baseline and post-treatment FES scan is associated with clinical benefit.

HER2 positivity in breast cancer is in the range of 15% to 20%, and HER2 over-expression is associated with highly aggressive disease and poor prognosis in node-positive and node-negative breast cancer [29]. Targeted therapy against HER2 includes the monoclonal antibodies trastuzumab (Herceptin) and pertuzumab, and the small-molecule tyrosine kinase inhibitor lapatinib. The HER2 status is determined from biopsy samples by immunohistochemistry or fluorescence in situ hybridisation (FISH), however HER2 status may differ between primary tumour and metastases and the expression of HER2 receptors may change over time. Since trastuzumab therapy is expensive and associated with severe side effects, the correct HER2 status in both primary tumour and metastases is of great importance. PET/CT imaging of HER2 status is possible with 64Cu- and 89Zr-labelled trastuzumab. 89Zr-trastuzumab PET is able to detect HER2-positive metastases in a patient with HER2-negative primary BC [30], a demonstration of the receptor heterogeneity between primary tumour and metastases. The use of 64Cu- and 89Zr-labelled trastuzumab is limited to clinical studies.

AR is expressed in 80% of BC [31] and may become a potential therapeutic target among AR-positive breast cancer patients. Several AR-targeted drugs have already been approved for prostate cancer, and their use in clinical trials has yielded promising results in AR-positive breast cancer patients.

The PET tracer 18F-dihydrotestosterone (FDHT) is able to visualise AR expression in primary tumours and metastases in BC. The tracer is extensively used in prostate cancer research, but its use in breast cancer is limited. The sensitivity and specificity of FDHT PET in BC is 91% and 100%, respectively [32]. In future, FDHT PET could be involved in clinical whole-body staging, therapy prediction and evaluation of response to therapy.

## PET IMAGING IN PROSTATE CANCER

Prostate cancer is the most common malignancy and the second most common cause of death from cancer among men in the Western countries [11]. Several treatment options are available for patients at different points throughout the duration of the disease, and imaging plays a key role in detection and staging of the disease. Conventional imaging modalities in prostate cancer consist of multiparametric MRI for detection and characterisation of intraprostatic and locally recurrent disease, and CT and bone scintigraphy for systemic staging. However, the combination of these imaging modalities has limited sensitivity and specificity in identifying metastases and early biochemical recurrence after local treatment [33].

FDG PET/CT has not shown clinical utility in prostate cancer due to low glucose metabolism in the early stage of the disease. However, FDG PET/CT is useful in treatment response assessment in castrate-resistant metastatic disease [34]. Because of the limitations of FDG PET, a number of novel PET tracers have been developed for imaging of prostate cancer.

### Choline-based PET imaging:

Choline is a precursor of phospholipids, a major component of the cellular membrane. Choline is increasingly incorporated into proliferating prostate cancer cell membranes and can therefore function as an agent for PET imaging. Choline can be labelled with either 11C or 18F. 11C-choline is chemically identical to endogenous choline and is primarily excreted through the hepatobiliary system, therefore not obscuring potential pathological findings in the pelvic region. 18F-fluorocholine is not chemically identical to endogenous choline. It is excreted through the urine, making assessment of the prostate bed challenging. While the 20-minute physical half-life of 11C requires on-site cyclotron production of 11C-choline, 18F's longer half-life of 110 minutes makes 18F-fluorocholine easily distributed to NM departments without cyclotron production. The sensitivity of both choline tracers for primary tumour and nodal metastases on primary staging is mediocre, yet higher than that of CT [35]. Meanwhile, both tracers offer superior accuracy over conventional imaging modalities for detection of lymph node metastasis and metastatic bone lesions at biochemical recurrence, altering therapeutic management in up to 66% of patients [36]. The detection efficiency of choline PET increases with prostate-specific antigen serum concentration (PSA) values, with high false rates below the PSA range of 1–2 ng/mL [37].

Prostate-specific membrane antigen (PSMA)-targeted tracers:

PSMA is a transmembrane glycoprotein which is up to 1000-fold over-expressed in prostate cancer. Over-expression can be seen in over 90% of prostate cancer patients. PSMA expression positively correlates with advanced disease and with androgen deprivation therapy resistance [38]. Despite its appellation, PSMA receptors are not prostate specific, PSMA being physiologically expressed in salivary and lacrimal glands, small intestine and renal tubules as well.

Several PSMA-labelled tracers are available for PET imaging, two of the most interesting being the urea-based small-molecule PSMA inhibitors 68Ga-PSMA-11 and 18F-PSMA-1007. The use of fluorine-18 isotope bound tracer is preferable due to its ease of production and transport, longer physical half-life, better image quality and slower urinary secretion. In a direct comparison of PSMA PET/CT and choline PET/CT in patients with biochemically recurrent prostate cancer, PSMA was superior to choline, with a detection rate of 86% vs. 70%, respectively. The main advantage of PSMA over choline tracers is the ability to detect small pathological lymph nodes, thus upstaging the disease in two-thirds of patients. PSMA PET is also superior to choline PET in bone lesions, local recurrences and soft-tissue metastases. As in choline PET, the binding of PSMA PET ligands increases with PSA concentration, but the sensitivity of PSMA PET/CT at low PSA values surpasses choline PET/CT sensitivity, being 69% as compared to 44%, respectively [39]. PSMA PET imaging has greatly improved diagnostic accuracy for the detection of metastatic prostate cancer at low PSA levels [40]. PSMA PET/CT also boasts excellent sensitivity and specificity in the detection of bone and bone marrow metastases, both substantially surpassing detection rates achieved with conventional imaging and choline PET/CT.

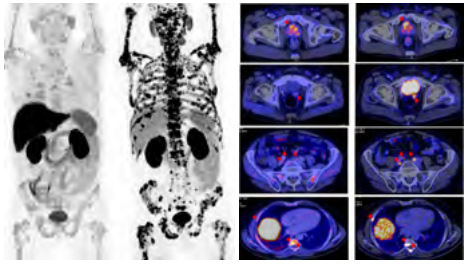

*FIGURE B1: Comparison of MIP whole-body PET 11C-choline (left) and 68Ga-PSMA (right)*

*FIGURE B2: Comparison of transaxial PET/CT 11C-choline (left column) and 68Ga-PSMA (right column); listed from top to bottom: Primary tumours, Local recurrence, Lymph node metastasis, Bone metastasis, Images courtesy of Dr. J. Schwenck, University Hospital Tübingen, Germany, published with permission*

In radiotherapy for prostate cancer, both choline and PSMA PET/CT can identify primary disease and occult nodal or bone metastasis not detected by conventional imaging. This significantly alters radiotherapy planning, both in the initial stages and in recurrent disease.

In primary prostate tumour, the PSMA PET-based contouring of tumour volume allows for escalation of dose to the PSMA-avid lesions [41].

Biochemical recurrence of prostate cancer occurs in 30% of patients within 5 years after surgical removal of the prostate. Locoregionally confined disease is considered curable, with salvage radiotherapy of the prostate bed and pelvic lymph nodes as standard treatment. However, a lot of patients will not benefit permanently from salvage radiotherapy and will develop biochemical progression. In the event of distant metastases, a palliative androgen deprivation therapy is suggested. PSMA PET is able to detect metastases even at very low PSA serum, with detection rates of PSMA and choline PET at PSA level < 1 ng/mL and >2 ng/mL being 52%, 20%, 91% and 76%, respectively [39].

PSMA PET improves the management of biochemical recurrence and the clinical outcome of treatment by adjusting the clinical tumour volume of salvage radiotherapy to areas of PSMA- avid metastatic lymph nodes, allowing for dose escalation to those nodes and abandoning salvage radiotherapy in the event of distant metastasis.

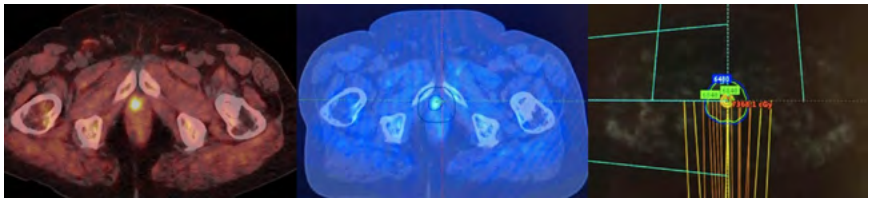

*FIGURE C: Biochemical recurrence after radical prostatectomy, salvage volumetric modulated arc therapy (VMAT) plan of PET hotspot in a prostate bed, courtesy of the author*

In patients with biochemical progression after radical prostatectomy and salvage radiotherapy, the recurrences are often located outside the prostate fossa. Most of the patients have a limited number of metastases, considered oligorecurrent disease, and can benefit from metastasis-directed stereotactic body radiation therapy. PSMA PET is more sensitive than choline PET in detecting oligometastatic disease, with 16% of patients considered oligometastatic on choline PET found to have more than three metastases on PSMA PET [42]. Therefore, PSMA PET can be used with high efficiency to guide radiotherapy in oligorecurrent prostate cancer to selected metastases [43].

## PET/CT IMAGING IN NEURO-ONCOLOGY

18F-FDG PET/CT is extensively used in oncology for the purpose of diagnosis, staging and evaluation of treatment. However, the diagnostic accuracy of FDG PET in brain malignancies is hampered by the intense physiological uptake of FDG in the normal brain and in several inflammatory processes. Amino acid PET tracers have low uptake in grey matter and therefore have greater sensitivity for detecting malignancies, both for primary brain tumours as well as for metastases. Until recently, the most studied amino tracer was 11C-methionine (11C-MET). However, due to 11C's short physical half-life of just 20 minutes, which required a cyclotron on site, 18F-labelled tracers were developed to overcome problems with transportability. The most commonly used tracer in clinical practice nowadays is 18F-fluoroethyl tyrosine (18F-FET). It is incorporated into cells through amino acid transporters, which are over-expressed in gliomas. 18F-FET has good diagnostic performance for the initial characterisation of new brain lesions, with pooled sensitivity and specificity for the diagnosis of malignant vs. non-malignant lesions of 82% and 76%, respectively [44]. However, moderate accumulation of FET can also be observed in inflammatory processes related to multiple sclerosis and in brain abscess and stroke, therefore the gold standard for diagnosis remains a biopsy with histological evaluation.

18F-FET cannot distinguish very accurately between low- and high-grade glioma using static PET acquisition, though the accuracy of glioma grading can be improved by evaluating dynamic PET data. Imaging in dynamic mode starts at the time of intravenous tracer application and lasts for 40 minutes. A steady increase of the time-activity curve can be seen in low-grade glioma, while high-grade lymphoma presents an early activity peak at 10–20 minutes post injection followed by a decline in activity [45].

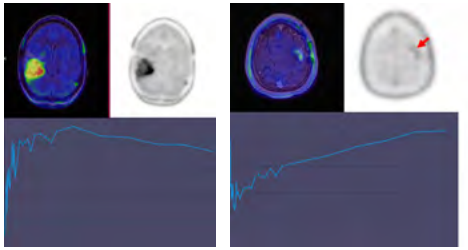

*FIGURE D1: FET-PET transaxial scan and activity curve in high-grade glioma*

*FIGURE D2: FET-PET transaxial scan and activity curve in low-grade glioma, both courtesy of the author*

18F-FET PET/CT can also identify intra-tumour heterogeneity, leading to improved grading through targeted biopsy of the most aggressive portions of the tumour, which determines prognosis and treatment. FET PET/CT can distinguish with great accuracy between tumour, peritumoral oedema and normal brain tissue, and can therefore identify infiltration of tumours beyond the area of MRI tumour contrast enhancement [46]. For this reason, FET PET is used to delineate tumours more accurately prior to surgery or radiotherapy procedures.

FET PET-derived tumour contours are substantially larger than tumour contours provided on CE-MRI [47], and the use of amino acid PET for delineating tumours prior to guided neurosurgical resection is beneficial both in high-grade and low-grade gliomas [48]. A complete removal of the tumour after PET-guided neurosurgical resection results in significantly longer survival of patients with high-grade gliomas [49].

The addition of amino acid PET imaging in determining the most aggressive portions of the tumour and therefore guiding biopsy is beneficial, as illustrated in a comparative study with MRI: of 16 high-grade biopsy specimens, 13 were concurrent with increased baseline uptake on PET, while only 6 were identified on contrast-enhanced MRI (CE-MRI) [50]. FET PET/CT also surpasses MRI in accuracy in identifying post-operative residual tumours [51].

CE-MRI is traditionally used to evaluate tumour relapse. Standard contrast enhancement resulting from increased blood-brain barrier permeability is non-specific, and therefore cannot accurately depict tumour extent and treatment effect. FET PET/CT is frequently used to differentiate treatment-related changes from progression of the disease. Within 12 weeks after chemoradiotherapy, contrast-enhancing lesions due to alterations of blood-brain barrier are often seen on MRI, termed pseudoprogression. These changes are seen in up to 30% of patients and mimic disease progression on CE-MRI. FET PET is able to differentiate pseudoprogression from true tumour progression with an accuracy of up to 90% [44]. Pseudoprogression can occur later than 12 weeks, particularly after radiochemotherapy using temozolomide in combination with lomustine. FET PET has diagnostic accuracy of 85% for differentiating both typical (within 12 weeks) and late (> 12 weeks) pseudoprogression from true tumour progression [52]. 18F-FET has also been proposed for distinguishing between progressive disease and pseudoprogression in brain metastases [53]. Similarly, FET PET is superior to CE-MRI in distinguishing between late radionecrosis and tumour recurrence [54]. The use of amino acid tracers 18F-FET, 18F-DOPA and 11C-MET is recommended by the Response Assessment in Neuro-Oncology (RANO) working group for radiotherapy in neuro-oncology. Indications include target delineation, treatment response assessment, and prognostication for gliomas [55].

Metabolically active tumour volume delineated by FET PET is significantly larger than tumour volume delineated by CE-MRI. Spatial correlation between MRI and FET PET target volumes is low and FET PET target volumes are considerably larger than MRI target volumes, with the areas of FET uptake extended substantially beyond the area of contrast enhancement and also beyond the area of FLAIR hyperintensity [56]. FET PET can also identify the more aggressive hotspots within the tumour, enabling these areas to be included in the radiation boost volume. In patients with glioblastoma (a grade IV glioma), large biological tumour volume (BTV) on FET PET is an independent prognostic factor of poor OS and PFS [57]. Maximal safe tumour resection prior to radiotherapy is of critical importance in these patients. Precise PET-guided preoperative volumetric depiction of the tumour is therefore essential in these patients, because lower BTV before radiotherapy is associated with longer survival [47]. FET PET-guided target volume delineation before radiotherapy therefore significantly affects patient survival.

Following radiotherapy, radiation-induced changes like radiation necrosis occur in up to 25% of patients within 6 months after the therapy. CE-MRI is of limited use in reliably differentiating brain metastasis recurrence or progression from radiation necrosis [58]. FET PET is effective in differentiating recurrence from radiation-induced changes, with both sensitivity and specificity higher than 90% [59].



CHAPTER 8

NEW SOLUTIONS IN THE ONCOLOGY

## REFERENCES:


1 Cal-Gonzalez J, Rausch I, Shiyam Sundar LK, et al. Hybrid Imaging: Instrumentation and Data Processing. Front Phys 2018;6:47.

2 https://www.accessdata.fda.gov/scripts/cdrh/cfdocs/cfpmn/pmn.cfm?ID=K210262. Assessed March, 2021.

3 Cherry SR, Jones T, Karp JS, et al. Total-Body PET: Maximizing Sensitivity to Create New Opportunities for Clinical Research and Patient Care. J Nucl Med 2018;59:3-12.

4 Bailey DL, Willowson KP. An evidence-based review of quantitative SPECT imaging and potential clinical applications. J Nucl Med 2013;54:83-9.

5 Ballinger JR. Theranostic radiopharmaceuticals: established agents in current use. Br J Radiol. 2018;91:20170969.

6 Nishiyama Y, Kinuya S, Kato T, et al. Nuclear medicine practice in Japan: a report of the eighth nationwide survey in 2017. Ann Nucl Med 2019;33:725-732.

7 Krause BJ, Schwarzenböck S, Souvatzoglou M. FDG PET and PET/CT. Recent Results Cancer Res 2013;187:351-69.

8 Vaidyanathan S, Patel CN, Scarsbrook AF, et al. FDG PET/CT in infection and inflammation--current and emerging clinical applications. Clin Radiol 2015;70:787-800.

9 Kung BT, Seraj SM, Zadeh MZ, et al. An update on the role of 18F-FDG-PET/CT in major infectious and inflammatory diseases. Am J Nucl Med Mol Imaging 2019;9:255-273.

10 Fonti R, Conson M, Del Vecchio S. PET/CT in radiation oncology. Semin Oncol 2019;46:202-209.

11 The Global Cancer Observatory. https://gco.iarc.fr/today/data/factsheets/populations/900-world-fact-sheets.pdf. Assessed January, 2021.

12 Hortobagyi GN, Connolly JL, D'Orsi CJ et al. Breast. In: Amin MB, Edge S, Greene F et al, eds; American Joint Committee on Cancer. AJCC cancer staging manual. 8th ed. Springer 2017;589–636

13 Buck A, Schirrmeister H, Kühn T, et al. FDG uptake in breast cancer: correlation with biological and clinical prognostic parameters. Eur J Nucl Med Mol Imaging 2002 29:1317–1323 111.

14 Miyake KK, Nakamoto Y, Togashi K. Current Status of Dedicated Breast PET Imaging. Current Radiology Reports 2016;4:16.

15 Narayanan D, Berg WA. Use of Breast-Specific PET Scanners and Comparison with MR Imaging. Magn Reson Imaging Clin N Am. 2018;26:265-272.

16 Groheux D, Giacchetti S, Espié M, et al. The yield of 18F-FDG PET/CT in patients with clinical stage IIA, IIB, or IIIA breast cancer: a prospective study. J Nucl Med 2011; 52:1526–1534.

17 Champion L, Lerebours F, Cherel P, et al. 18F-FDG PET/CT imaging versus dynamic contrast-enhanced CT for staging and prognosis of inflammatory breast cancer. Eur J Nucl Med Mol Imaging 2013;40:1206–1213.

18 Even-Sapir E. Imaging of malignant bone involvement by morphologic, scintigraphic, and hybrid modalities. J Nucl Med 2005;46:1356–67.

19 Taourel P, Pages E, Millet I, et al. Magnetic resonance imaging in breast cancer management in the context of neo-adjuvant chemotherapy. Crit Rev Oncol Hematol 2018; 132:51–65.

20 Connolly RM, Leal JP, Solnes L, et al. TBCRC026: Phase II Trial Correlating Standardized Uptake Value With Pathologic Complete Response to Pertuzumab and Trastuzumab in Breast Cancer. J Clin Oncol. 2019;37:714-722.

21 Dose Schwarz J, Bader M, Jenicke L, et al. Early prediction of response to chemotherapy in metastatic breast cancer using sequential 18F-FDG PET. J Nucl Med 2005 46:1144–1150.

22 Specht JM, Tam SL, Kurland BF, et al. Serial 2-[18F] fluoro-2-deoxy-D-glucose positron emission tomography (FDG-PET) to monitor treatment of bone-dominant metastatic breast cancer predicts time to progression (TTP). Breast Cancer Res Treat 2007;105:87-94.

23 Riedl CC, Pinker K, Ulaner GA, et al. Comparison of FDG-PET/CT and contrast-enhanced CT for monitoring therapy response in patients with metastatic breast cancer. Eur J Nucl Med Mol Imaging 2017;44:1428–1437.

24 Hildebrandt MG, Gerke O, Baun C, et al. [18F] Fluorodeoxyglucose (FDG)-positron emission tomography (PET)/computed tomography (CT) in suspected recurrent breast cancer: a prospective comparative study of dual-time-point FDG-PET/CT, contrast-enhanced CT, and bone scintigraphy. J Clin Oncol 2016;34:1889–1897.

25 van Kruchten M, de Vries EG, Brown M, et al. PET imaging of oestrogen receptors in patients with breast cancer. Lancet Oncol. 2013;14:e465–e475.

26 Boers J, de Vries EFJ, Glaudemans AWJM, et al. Application of PET Tracers in Molecular Imaging for Breast Cancer. Curr Oncol Rep 2020;22:85.

27 Linden HM, Stekhova SA, Link JM, et al. Quantitative fluoroestradiol positron emission tomography imaging predicts response to endocrine treatment in breast cancer. J Clin Oncol 2006;24:2793–2799.

28 Amir E, Miller N, Geddie W, et al. Prospective study evaluating the impact of tissue confirmation of metastatic disease in patients with breast cancer. J Clin Oncol 2012;30:587–592.

29 Ross JS, Slodkowska EA, Symmans WF, et al.The HER-2 receptor and breast cancer: ten years of targeted anti-HER-2 therapy and personalized medicine. Oncologist 2009;14:320–368.

30 Yang Z, Sun Y, Xue J, et al. Can positron emission tomography/computed tomography with the dual tracers fluorine-18 fluoroestradiol and fluorodeoxyglucose predict neoadjuvant chemotherapy response of breast cancer?--A pilot study. PLoS One 2013;8:e78192.

31 Niemeier L, Dabbs D, Beriwal S, et al. Androgen receptor in breast cancer: expression in estrogen receptor-positive tumors and in estrogen receptor-negative tumors with apocrine differentiation. Mod Pathol 2010;23: 205–212.

32 Venema CM, Mammatas LH, Schroder CP, et al. Androgen and estrogen receptor imaging in metastatic breast cancer patients as a surrogate for tissue biopsies. J Nucl Med 2017;58:1906–1912.

33 Rowe SP, Macura KJ, Mena E, et al. PSMA-Based [(18)F]DCFPyL PET/CT Is Superior to Conventional Imaging for Lesion Detection in Patients with Metastatic Prostate Cancer. Mol Imaging Biol 2016;18:411-9.

34 Jadvar H. Prostate cancer: PET with 18F-FDG, 18F- or 11C-acetate, and 18F- or 11C-choline. J Nucl Med 2011;52:81-9.

35 Evangelista L, Cimitan M, Zattoni F, et al. Comparison between conventional imaging (abdominal-pelvic computed tomography and bone scan) and [(18)F] choline positron emission tomography/computed tomography imaging for the initial staging of patients with intermediate- to high-risk prostate cancer: A retrospective analysis. Scand J Urol 2015;49:345-53.

36 Gómez-de la Fuente FJ, Martínez-Rodríguez I, De Arcocha-Torres M, et al. Effect of positive carbon-11-choline PET/CT results in the therapeutic management of prostate cancer biochemical relapse. Nucl Med Commun 2019;40:79-85.

37 Graziani T, Ceci F, Castellucci P, et al. (11)C-Choline PET/CT for restaging prostate cancer. Results from 4,426 scans in a single-centre patient series. Eur J Nucl Med Mol Imaging 2016;43:1971-9.

38 Ceci F, Castellucci P, Fanti S. Current application and future perspectives of prostate specific membrane antigen PET imaging in prostate cancer. Q J Nucl Med Mol Imaging 2019;63:7-18.

39 Evans JD, Jethwa KR, Ost P, et al. Prostate cancer-specific PET radiotracers: a review on the clinical utility in recurrent disease. Pract Radiat Oncol 2018;8: 28-39.

40 Calais J, Czernin J, Cao M, et al. 68Ga-PSMA-11 PET/CT Mapping of Prostate Cancer Biochemical Recurrence After Radical Prostatectomy in 270 Patients with a PSA Level of Less Than 1.0 ng/mL: Impact on Salvage Radiotherapy Planning. J Nucl Med 2018;59:230-237.

41 Thomas L, Kantz S, Hung A, et al. 68Ga-PSMA-PET/CT imaging of localized primary prostate cancer patients for intensity modulated radiation therapy treatment planning with integrated boost. Eur J Nucl Med Mol Imaging 2018;45:1170-1178.

42 Schwenck J, Rempp H, Reischl G, et al. Comparison of (68)Ga-labelled PSMA-11 and (11)C-choline in the detection of prostate cancer metastases by PET/CT. Eur J Nucl Med Mol Imaging 2017;44:92-101.

43 Oehus AK, Kroeze SGC, Schmidt-Hegemann NS, et al. Efficacy of PSMA ligand PET-based radiotherapy for recurrent prostate cancer after radical prostatectomy and salvage radiotherapy. BMC Cancer 2020;20:362.

44 Dunet V, Rossier C, Buck A, et al. Performance of 18F-fluoro-ethyl-tyrosine (18F-FET) PET for the differential diagnosis of primary brain tumor: a systematic review and Metaanalysis. J Nucl Med 2012;53:207-14.

45 Jansen NL, Graute V, Armbruster L, et al. MRI-suspected low-grade glioma: is there a need to perform dynamic FET PET? Eur J Nucl Med Mol Imaging

2012;39:1021-9.

46 Arbizu J, Tejada S, Marti-Climent JM, et al. Quantitative volumetric analysis of gliomas with sequential MRI and $^{11}$C-methionine PET assessment: patterns of integration in therapy planning. Eur J Nucl Med Mol Imaging 2012;39:771-81.

47 B. Suchorska B, Jansen NL, Linn J, et al. Biological tumor volume in 18FET-PET before radiochemotherapy correlates with survival in GBM. Neurology 2015;84:710-9.

48 Floeth FW, Sabel M, Ewelt C, et al. Comparison of (18)F-FET PET and 5-ALA fluorescence in cerebral gliomas. Eur J Nucl Med Mol Imaging 2011;38:731-41.

49 Pirotte BJ, Levivier M, Goldman S, M, et al. Positron emission tomography-guided volumetric resection of supratentorial high-grade gliomas: a survival analysis in 66 consecutive patients. Neurosurgery 2009;64:471-81.

50 Pafundi DH, Laack NN, Youland RS, et al. Biopsy validation of 18F-DOPA PET and biodistribution in gliomas for neurosurgical planning and radiotherapy target delineation: Results of a prospective pilot study. Neuro-Oncology. 2013;15:1058-67.

51 Buchmann N, Kläsner B, Gempt J,et al. (18) F-Fluoroethyllthyrosine positron emission tomography to delineate tumor residuals after glioblastoma resection: A comparison with standard postoperative magnetic resonance imaging. World Neurosurg 2016;89:420–6.

52 Kebir S, Fimmers R, Galldiks N, et al. Late Pseudoprogression in Glioblastoma: Diagnostic Value of Dynamic O-(2-[18F]fluoroethyl)-L-Tyrosine PET. Clin Cancer Res 2016;22:2190-6.

53 Galldiks N, Langen KJ, Albert NL, Chamberlain M, Soffietti R, Kim MM, Law I, Le Rhun E, Chang S, Schwarting J, Combs SE, Preusser M, Forsyth P, Pope W, Weller M, Tonn JC. PET imaging in patients with brain metastasis-report of the RANO/PET group. Neuro Oncol. 2019 May 6;21(5):585-595. doi: 10.1093/neuonc/noz003. PMID: 30615138; PMCID: PMC6502495.

54 Galldiks N, Stoffels G, Filss C, et al. The use of dynamic O-(2-18F-fluoroethyl)-l-tyrosine PET in the diagnosis of patients with progressive and recurrent glioma. Neuro-Oncology 2015 Sep;17:1293–300.

55 Law I, Albert NL, Arbizu J, et al. Joint EANM/EANO/RANO practice guidelines/SNMMI procedure standards for imaging of gliomas using PET with radiolabelled amino acids and [18F]FDG: version 1.0. Eur J Nucl Med Mol Imaging 2019;46:540-557.

56 Debus C, Waltenberger M, Floca R, et al. Impact of (18)F-FET PET on target volume definition and tumor progression of recurrent high grade glioma treated with carbon-ion radiotherapy. Sci Rep 2018;8:7201.

57 Poulsen SH, Urup T, Grunnet K, et al. The prognostic value of FET PET at radiotherapy planning in newly diagnosed glioblastoma. Eur J Nucl Med Mol Imaging 2017;44:373-381.

58 Shah AH, Snelling B, Bregy A, et al. Discriminating radiation necrosis from tumor progression in gliomas: a systematic review what is the best imaging modality? J Neurooncol 2013;112:141-52.

59 Ceccon G, Lohmann P, Stoffels G, et al. Dynamic O-(2-18F-fluoroethyl)-L-tyrosine positron emission tomography differentiates brain metastasis recurrence from radiation injury after radiotherapy. NeuroOncol 2017;19:281-288.

# 9

# RADIOMICS

*by Florent Tixier*

Radiomics was defined as the extraction of a large number of image features from radiographic images.1 It was named by analogy with other -omics fields such as genomics or proteomics. Today, radiomics refers to the extraction of biomarkers from all types of medical images, not only radiographic ones. It is a very active field of research, with interest in it growing exponentially over several years (Figure 1).

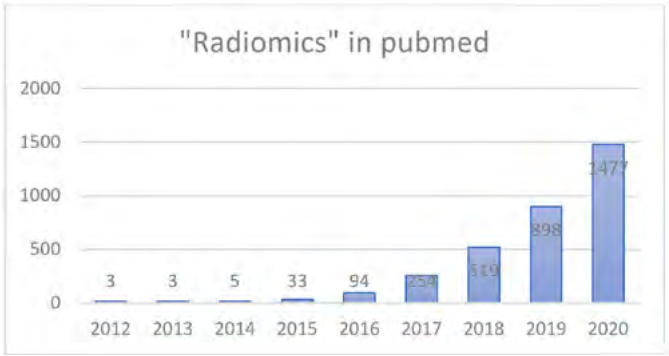


*Figure 1: Number of results per year for the term "radiomics" in PubMed.*

Radiomics has proven useful in oncology for patient management including diagnosis, follow-up, outcome, and therapy response prediction.2 In PET/CT, the first studies showing the possibility of using image features to predict treatment response were carried out before this area of research was even named radiomics.3,4 At that time, the strategy was to identify a limited number of features with a precise idea of the type of information to be characterised from the images (e.g. intra-tumour heterogeneity or tumour shape) and then use them as additional biomarkers after investigating their reproducibility in test-retest studies and their robustness to pre-processing steps (acquisition parameters, reconstruction, tumour segmentation, etc.). The idea behind these new biomarkers was to assess the information in the images that cannot be robustly appreciated by the naked human eye.2,5

These models have the advantage of being clinically understandable, but they only exploit a limited fraction of the information available in the images. For this reason, the large majority of radiomics models nowadays strive to combine the information from multiple radiomics features in order to build models with greater accuracy. This way of investigating radiomics requires robust pipelines to extract and select the features and machine learning algorithms to build the models.

## Radiomics models

The construction of a radiomics model consists of several steps, as described in Figure 2.[6]

The first step consists of acquiring data from PET/CT scans and reconstructing the images. Then, a pre-processing step is performed for the correction of partial volume effects and image denoising. After this step, tumours can be delineated using adapted algorithms for PET/CT images, such as FLAB, to ensure robust segmentation.[7] The obtained tumour volumes are then used to extract radiomics features (see next section for details), which are needed to build models.

The construction of models can be done with several machine learning classification algorithms such as random forests, support vector machines, or decision trees. If there are no clear recommendations regarding the best algorithms to use, it is essential that the study is well designed in order to ensure that the models can be validated and are usable with data coming from multiple institutions.

Because the number of patients in radiomics studies is often low and the number of features is high, with a lot of features highly correlated between them, strategies to reduce the number of features can be considered before starting to build a classification model. The most common algorithms used for this purpose are minimum redundancy maximum relevance (mRMR) and the least absolute shrinkage and selection operator (LASSO).

Models should always be validated on cohorts of external patients, or at least by splitting data into a training and a testing set. Such splitting can be done randomly, but when data are unbalanced it is important to use a strategy that guarantees that there are enough patients with the condition to identify in the testing group. A ratio of 70% for the training set and 30% for the testing set is quite common for radiomics models, which are often built using a limited number of patients.

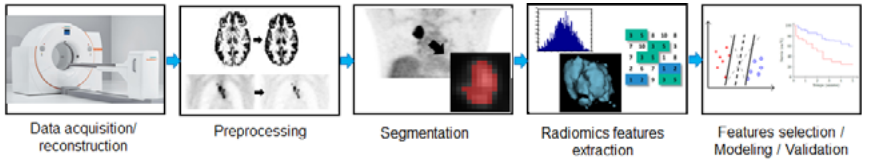


*Figure 2: Usual workflow to build radiomics models*

When cohorts are larger, and with well-balanced data, it is possible to reduce the percentage of patients used for the testing set. To build models on the training set, k-fold cross-validation is often used, with a k between 3 and 10, depending on the size of the dataset. The best model found using the training set can then be used on the testing set to validate the model.

Another important point to take into consideration when models are built from multi-institutional data (with different scanner manufacturers, acquisition parameters, or reconstruction methods) is to make sure that the radiomics features can be compared. Excessively high differences in the data can lead to differences in the radiomics features that can be higher than the differences produced by the effect being classified (for instance, response to therapy treatment). This can result in the elimination of useful features and reduce the predictive power of the models. This multi-centre effect can be corrected by means of two different strategies:

1) Image harmonisation. This strategy aims to harmonise images prior to feature extraction to make the radiomics features comparable. One common method used for this purpose is histogram matching, which allows images to be harmonised to a reference image.8 Working in the image space offers several advantages, including single patient data harmonisation, or the ability to realise other steps beyond radiomics feature extraction, such as e.g. the necessary segmentation step, which could be biased by the variability of image quality.

2) Feature harmonisation. This strategy aims to harmonise the radiomics features after their extraction. This option is particularly useful when images are not available (for instance in multi-institutional studies where the transfer of full images can be restricted due to the protection of personal health information (PHI) data). Feature harmonisation can be done using the ComBat algorithm9, but practitioners are strongly advised to use an improved version such as BM-Combat9, which increases robustness and allows the distribution of the features to be transformed to a chosen reference, which is essential to make a model usable on data coming from additional centres.

Building models coming from multi-institutional data using a harmonisation strategy is often a better choice than building a model from a unique data centre. First, combining data from multiple centres allows more data to be incorporated into the model, and second, these models are more likely to be reusable with data coming from new centres.

R (http://www.r-project.org/), python (http://www.python.org/), and Matlab (http://www.mathworks.com/) are probably the three most common languages used to build such models. They all contain well-maintained packages/ libraries for machine learning modelling and data harmonisation.







## Radiomics features

Radiomics implies the extraction of features to characterise a volume of interest (VOI) in the images. These features allow characterisation of different aspects of the VOIs, which can be classified into distinct categories:

- Histogram-based features are first-order statistics obtained from the voxels included in the VOIs. This category of features includes the minimum, maximum, skewness, kurtosis, median, standard deviation, and interquartile range.
- Texture-based features aim to characterise relationships between voxels in a VOI. Features from this category are extracted in two steps. 1) Computation of matrices describing the relationship between voxels in a VOI (co-occurrence matrix, grey level run length matrix, grey level size zone matrix, or neighbourhood grey tone difference matrix). 2) Extraction of features from these matrices. These features provide measurements of the intra-tumour heterogeneity.
- Edges features. This category of features aims to characterise the edges in a VOI by filtering the original images before computing histogram (or texture-based) features. The most common filters used for this purpose are wavelets, Gabor, and Laplacian of Gaussian.
- Shape features. These features aim to characterise the morphological properties of the VOI. Common features in this category are the ratio between the volume and the surface of the VOI or the sphericity, which quantifies how sphere-like the volume is.

The full list of radiomics features and their formulas can be found in the image biomarker standardisation initiative (IBSI).[10]

## How to get started with radiomics

There are several software packages and libraries that allow the extraction of radiomics features, and most of them can be downloaded free of charge. The most important aspect to verify before choosing software is its compliance with the IBSI guidelines[10], in order to guarantee the results. Apart from this aspect, the choice of software can be motivated by other considerations such as the programming language, an open-source solution, a user interface, the supported image formats, the ability to compute radiomics from batches of images, the possibility of integration with other tools such as segmentation, or the output formats used to store the results.

The following is a brief overview of three software packages validated by the IBSI.

Pyradiomics (www.radiomics.io) is an open-source solution for radiomics written in python. It can be used in command lines to extract features for single images, or in batch mode. All image formats recognised

by ITK (DICOM, NRRD, NII, Analyzed, etc.) can be read by this package. By default, results are displayed on a console window but there is an option to save the results in a CSV-structured text file. Pyradiomics is a good option for people who are conducting research on radiomics, but the command-line interface may dissuade medical professionals from using it.

However, this package is also available as an extension for 3D Slicer (https://www.slicer.org/), which provides a nice user interface and the possibility to perform other image processing before features extraction.

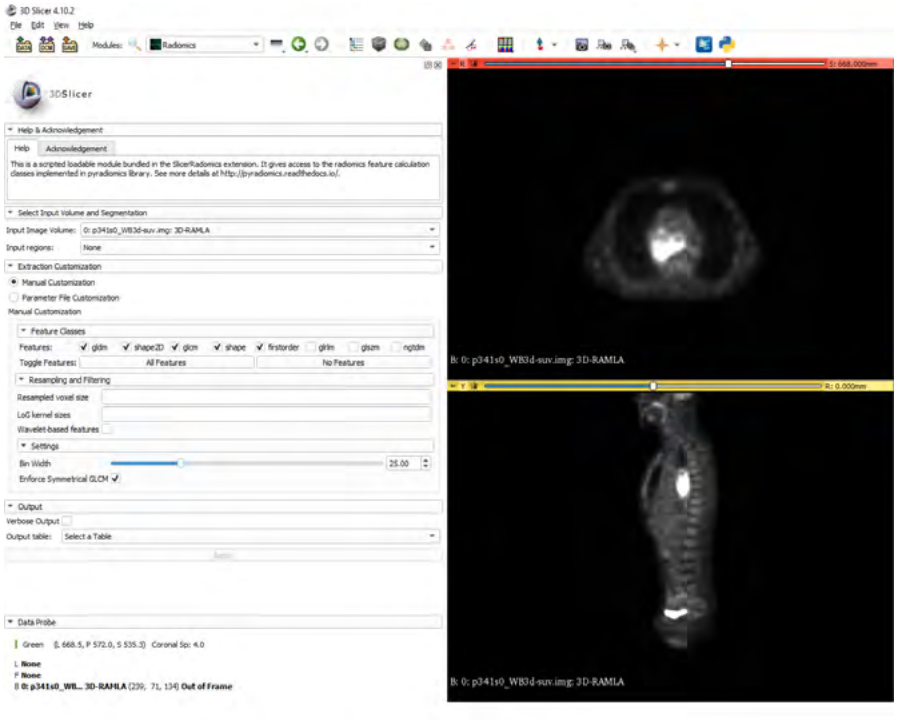


*Figure 3: Graphic interface of Pyradiomics integrated into 3D Slicer*









MIRAS (http://mirasoft.fr/) is a software based on ITK-SNAP with additional modules for segmentation (such as FLAB7) and radiomics. This software and its plugins are written in C++. The source code of MIRAS is available, but not the code used in the plugins, which are libraries (.dll for Windows or .so for Linux version). This software also works with all image formats supported by ITK and allows the extraction of features from a batch of images. Results are stored in CSV-structured text files. In comparison with Pyradiomics integrated into 3D Slicer, this solution has the advantage of being lighter and is more tailored for use by clinicians.

CERR (https://github.com/cerr/CERR) is a computational environment for radiotherapy research written in Matlab that includes code to extract radiomics features. Such an environment can be very convenient when the objective is to extract radiomics features from structures used in radiotherapy treatment planning.

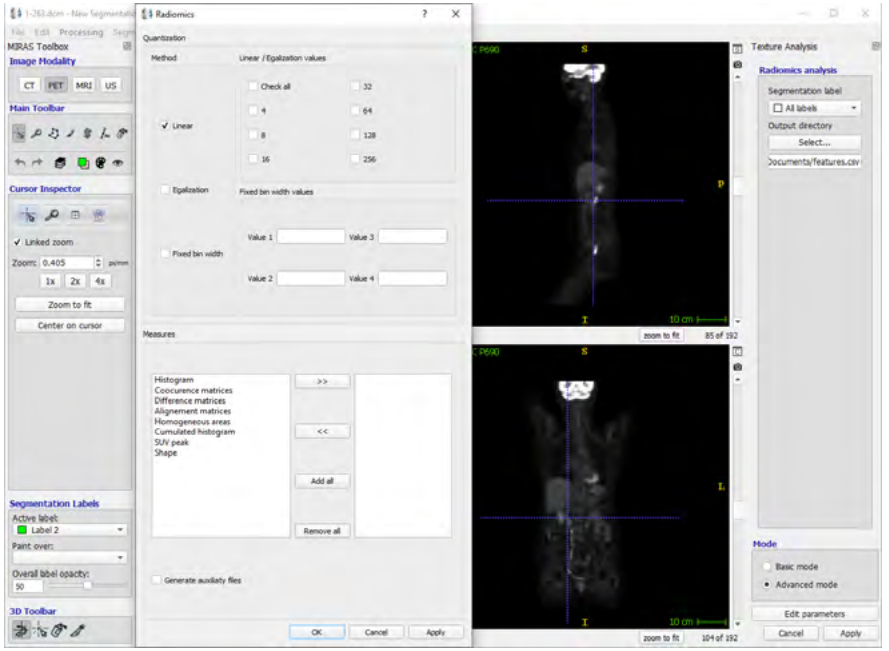


*Figure 4: Graphic interface of MIRAS*

## REFERENCES


1. Lambin, P. et al. Radiomics: Extracting more information from medical images using advanced feature analysis. Eur. J. Cancer 48, 441–446 (2012).
2. Hatt, M., Tixier, F., Visvikis, D. & Rest, C. C. L. Radiomics in PET/CT: More Than Meets the Eye? J. Nucl. Med. 58, 365–366 (2017).
3. El Naqa, I. et al. Exploring feature-based approaches in PET images for predicting cancer treatment outcomes. Pattern Recognit. 42, 1162–1171 (2009).
4. Tixier, F. et al. Intratumor Heterogeneity Characterized by Textural Features on Baseline 18F-FDG PET Images Predicts Response to Concomitant Radiochemotherapy in Esophageal Cancer. J. Nucl. Med. 52, 369–378 (2011).
5. Tixier, F. et al. Visual Versus Quantitative Assessment of Intratumor 18F-FDG PET Uptake Heterogeneity: Prognostic Value in Non–Small Cell Lung Cancer. J. Nucl. Med. 55, 1235–1241 (2014).
6. Hatt, M. et al. Radiomics: Data Are Also Images. J. Nucl. Med. 60, 38S-44S (2019).
7. Hatt, M., Rest, C. C. le, Turzo, A., Roux, C. & Visvikis, D. A Fuzzy Locally Adaptive Bayesian Segmentation Approach for Volume Determination in PET. IEEE Trans. Med. Imaging 28, 881–893 (2009).
8. Gonzalez, R. C. & Woods, R. E. Digital Image Processing. (2006).
9. Da-ano, R., Visvikis, D. & Hatt, M. Harmonization strategies for multicenter radiomics investigations. Phys. Med. Biol. (2020) doi:10.1088/1361-6560/aba798.
10. Zwanenburg, A., Leger, S., Vallières, M., Löck, S. & Initiative, for the I. B. S. Image biomarker standardisation initiative. ArXiv161207003 Cs (2016).






DOI: *** *** ***

**Publisher:**
European Association of Nuclear Medicine
Schmalzhofgasse 26, 1060 Vienna, Austria
Phone: +43 1 890 44 27 | +43 1 890 44 27-9
Email: office@eanm.org | URL: www.eanm.org

**Main-Editor:**
Agata Pietrzak

**Co-Editors:**
Luca Camoni
Christelle Terwinghe
David Bogovic

**English Language Editing:**
Angela Parker

**Project Management:**
Núria Serra Serra, EANM Executive Office
Banin Hosseini, EANM Executive Office

**Layout & Design:**
Olga Dogadina, EANM Executive Office

**Content:**
*No responsibility is taken for the correctness of this information.*
*Information as per date of printing September 2021.*

**FIND MORE EANM TECHNOLOGISTS' GUIDE HERE**

http://www.eanm.org/publications/technologists-guide/